Modelling the early development of cartilage and bone in Mseleni Joint Disease using induced pluripotent stem cells

By

Thulisa Mkatazo

Submitted to the University of Cape Town

In fulfilment of the requirements for the degree

MSc (Med) in Medical Cell Biology

Primary Supervisors

Dr Robea Ballo

Emeritus Professor Susan Kidson

Administrative Supervisor

Dr Mubeen Goolam

2025

DECLARATION

I, *…Thulisa Mkatazo (MKTTHU002)……*, hereby declare that the work on which this dissertation/thesis is based is my original work (except where acknowledgements indicate otherwise) and that neither the whole work nor any part of it has been, is being, or is to be submitted for another degree in this or any other university.

I empower the university to reproduce for the purpose of research either the whole or any portion of the contents in any manner whatsoever.

Signature: ….Signed by candidate..

Date: …10 February 2025……..

Acknowledgments

Without Jehovah God none of this would be possible. He gave me strength and love and support to make it through till the end. Thank you.

A special thank you to Dr. Robea Ballo—my mentor, supervisor, and friend. You truly embody what a teacher should be. I am very grateful for your dedication and willingness to teach me stem cell research. You went above and beyond to provide me with a platform to learn while listening, supporting, and guiding me. Thank you!

To Professor Susan Kidson, thank you for your patience and support. I feel incredibly privileged to have been under your supervision. You dedicated so much of your time in retirement to sharing your knowledge with me, teaching me the skill of writing like a scientist, and I can never thank you enough for that and so much more. Both you and Dr. Robea Ballo have had an invaluable impact on my journey. To Dr Mubeen Goolam, thank you for being a very supportive administrative supervisor and for your valuable input during discussions on this project.

I would like to express my sincere gratitude to Professor Gibbon for initiating this study and for traveling to the Mseleni region to collect the samples used in this project. Together with Dr. Fredlund, who raised awareness of the disease, I owe an immense debt of gratitude to both, as this project would not have been possible without them. A special thank you to Dr. Elizabeth Dinkele for her invaluable contribution to the early phases of this study, in which we attempted to reprogram the samples into iPSCs; your efforts were both enormous and deeply appreciated. I also want to extend my thanks to Dr. Janine Scholefield for generating the iPSCs from the Mseleni fibroblast.

I am deeply grateful to the Mseleni patients and control participants. Their willingness to share their samples was essential to the success of this research, and without them, this MSc would not have been possible. It is my hope that one day we will be able to give back to this community in a meaningful way as we continue our efforts to find solutions for this debilitating disease.

My deepest gratitude to my colleagues Mrs. Desiree Bowers - for being an awesome ex-line manager and always being willing to provide a helpful hand when everything just got overwhelming; Dr Ashwin Isaacs - for being an awesome current line manager and for the Histology training, Ms. Nuraan Ismail, Mrs. Mieatah Masha thank you for being such great cheerleaders.

Special thanks to Dr Karabo Serala and Dr Thato Medupe for their endless support, encouragement and comfort through this journey. The bonding session in TC will always be the highlight. Dr Hapiloe Maranyana and Dr Lucy Macharia for the consistent, unwavering love and encouragement.

Thank you to the Prince Lab, Goolam Lab and Hockman Lab for their support and assistance provided when needed.

I would like to thank the NRF and UCT Postgraduate fund for the financial support and as well as Emeritus Greenberg for providing a helping hand towards the end of this project.

A special thank you to my spiritual family and friends, Unathi, Wewe, Zlush and mamu Mbali (Thembi Mbali), nabanye nabanye, you guys have been a great support to me ngendlela yenu. Your motivation, prayers and encouragement were greatly appreciated.

A special thank you to my family, especially my mother, Nomnono Catherine Mkatazo for the support, prayers, love and sacrifices.

Table of Contents

Chapter 2: Materials and Methods

Chapter 3: Results

List of Tables

List of Figures

List of abbreviations

2D	**Two-dimension**
3D	**Three-dimension**
AFP	**Alpha-fetoprotein**
ALP/AP	**Alkaline phosphatase**
b-FGF	**Basic fibroblast growth factor**
CD	**Cluster of differentiation**
cDNA	**Complementary DNA**
c-MYC	**Myelocytomatosis oncogene**
CO2	**Carbon dioxide**
COL	**Collagen**
COL10A1	**Collagen type 10α1 gene**
COL2A1	**Collagen type 2α1 gene**
CSIR	**Council for Scientific and Industrial Research**
DMEM	**Dulbecco's Modified Eagle Medium**
dNTP	**Deoxyribonucleotide triphosphate**
DPBS	**Dulbecco's Phosphate Buffered Saline**
EB	**Embryoid body**
ECM	**Extracellular matrix**
EDTA	**Ethylenediaminetetraacetic acid**
EMT	**Epithelial-mesenchymal transition**
ESC	**Embryonic stem cell**
FBS	**Foetal bovine serum**
FGF-2	**Fibroblast Growth Factor 2**
FOXA2	**Forkhead box A2**
hESC	**Human embryonic stem cell**
hESC	**Human Embryonic Stem Cells Culture Medium**
ICC	**Immunocytochemistry**
iMEFs	**Inactivated mouse embryonic fibroblasts**
iMSC	**Induced mesenchymal stem cells**
iPSC derived MSCs	**iPSC-derived mesenchymal stem cells**
iPSCs	**Induced pluripotent stem cells**
KLF4	**Kruppel-like factor 4**
KODMEM	**Knockout Dulbecco's Modified Eagle Medium**

KOSR	**Knockout serum replacement**
MEFs	**Mouse embryonic fibroblasts**
MET	**mesenchymal-Epithelial transition**
ml	**mililitre**
mRNA	**messenger RNA**
NEAA	**Non-essential amino acids**
ng	**nanograms**
OCT	**Octomer**
OCT3/4	**POU domain class 5 transcription factor 1**
P	**Passage number**
PBS	**Phosphate buffered saline**
PCR	**Polymerase chain reaction**
Pen-Strep	**Penicillin-streptomycin**
PFA	**Paraformaldehyde**
PG	**Prerna Gowreesunker's Samples**
qRT-PCR	**Quantitative real time Polymerase chain reaction**
RNA	**Ribonucleic acid**
ROCK inhibitor	**Rho-associated protein kinase inhibitor**
rpm	**Revolutions per minute**
RT	**Room Temperature**
RUNX2	**Runt-related transcription factor 2**
SeVdp	**Replication-defective and persistent Sendai virus vector**
SeVdp	**Sendai virus**
SOX2	**SRY (sex determining region Y)-box containing gene 2**
TBE	**Tris/Borate/EDTA**
TE	**Trypsin EDTA(Ethylenediaminetetraacetic acid)**
TGF-β	**Transforming growth factor-beta**
UCT	**University of Cape Town**
V	**Volts**
α-SMA	**Alpha smooth muscle actin**
β-III tubulin	**Beta 3 class III tubulin**
µl	**microlitre**
µM	**micro-molar/micromole per litre**

Abstract:

Mseleni joint disease (MJD) is an unusual crippling osteoarthropathy that occurs in significant numbers of the indigenous population in a remote rural region of Northern KwaZulu Natal, South Africa. The most affected joints are the hip, and early developmental abnormalities lead to secondary osteoarthropathy. Autoradiographs show irregularities and fragmentation of the joint epiphyses in the early stage of MJD. Over time, erosion of the articular cartilage leads to fibrillation and flaking that ultimately exposes the bone. Despite extensive epidemiological, anthropological and genetic investigations, and studies on the local environment, diet and mineral deficiencies, the cause of MJD is still unknown.

The present study is built on the hypothesis that there are abnormalities in early joint cartilage and bone development, leading to functional abnormalities, which over time result in early onset arthritis. The aim of the present study is to create an *in vitro* model of embryonic cartilage and bone to determine whether there are intrinsic disturbances in the early differentiation of these tissues.

This study is part of a collaboration with Prof V. Gibbon (HREC: 822/2015). Skin fibroblasts from two MJD patients, one unaffected person from Mseleni and one unaffected non-Mseleni control, were reprogrammed into induced pluripotent cells (iPSC) by a collaborator. Pluripotency was confirmed by (qRT-PCR) gene expression analysis of the reprogramming genes OCT3/4, NANOG and SOX2 and immunocytochemical staining for their proteins. In vitro differentiation into the three germ layers was confirmed by ICC. To generate iPSC-derived mesenchymal stem cells (iMSC) from the iPSCs, two differentiation protocols were tested: one with low glucose medium and one with standard glucose medium. Changes in the morphology, growth characteristics and expression of relevant CD markers were determined. The mesenchymal phenotype was confirmed by the positive qRT-PCR expression of CD73, 105 and 90.

Induced MSC from one MJD and one control cell line were differentiated into adipose, bone and cartilage tissues. Two specific differentiation media were used for each specific tissue type. The first medium included basal medium supplemented with the reagents and chemicals appropriate for the particular tissue type (adipose, bone or cartilage). The second medium was the commercially available StemPro™ differentiation medium specific for either adipogenesis or osteogenesis or chondrogenesis.

The trilineage differentiation was monitored by qRT-PCR and tissue specific stains. Oil Red O staining revealed differentiation into adipose phenotype. Alizarin Red staining and qRT-PCR for Osteocalcin

and Alkaline Phosphatase confirmed the presence of bone tissues in cells cultured in both media types. For chondrogenic differentiation, cells were grown as micro-masses which were harvested and stained with toluidine blue. Only the experiments using the commercial StemPro™ kit were positive for chondrogenesis.

To determine what type of cartilage had been produced (articular or endochondral hypertrophic) in these experiments, chondrogenic micromasses were removed for gene expression analysis at various intervals over a 21-day period. qRT-PCR analyses revealed the presence of both COL2A1 and COL10A1, gene markers typical of hypertrophic cartilage.

In conclusion, the results of this study indicate that both the MJD and control iMSC cell lines were able to differentiate along adipogenic, chondrogenic and osteogenic pathways. The chondrogenic cells had differentiated into hypertrophic endochondral cartilage. A different culture approach would be needed to develop a protocol for differentiation into an articular cartilage phenotype which would, in turn, facilitate a further study for potential intrinsic disturbances underlying MJD.

[546 words]

Chapter 1: Introduction

1.1 Background.

Mseleni Joint disease (MJD) is an unusual bilateral crippling osteoarthropathy. It is rare in the world but occurs in large numbers in the indigenous people in a remote rural region of Northern KwaZulu Natal, South Africa (Du Toit, 1979; see Figure 1.1). It causes serious disabilities at different stages of life. When first described by Du Toit, 1979 it was first reported that in young adults, approximately 11% of men and 39% of women are seriously disabled (Du Toit 1979). Some patients with MJD also manifest a form of dwarfism with characteristics of brachydactyly and shortened long bones (Du Toit 1979; Lockitch et al. 1973; Lockitch, Fellingham, and Elphinstone 1973).

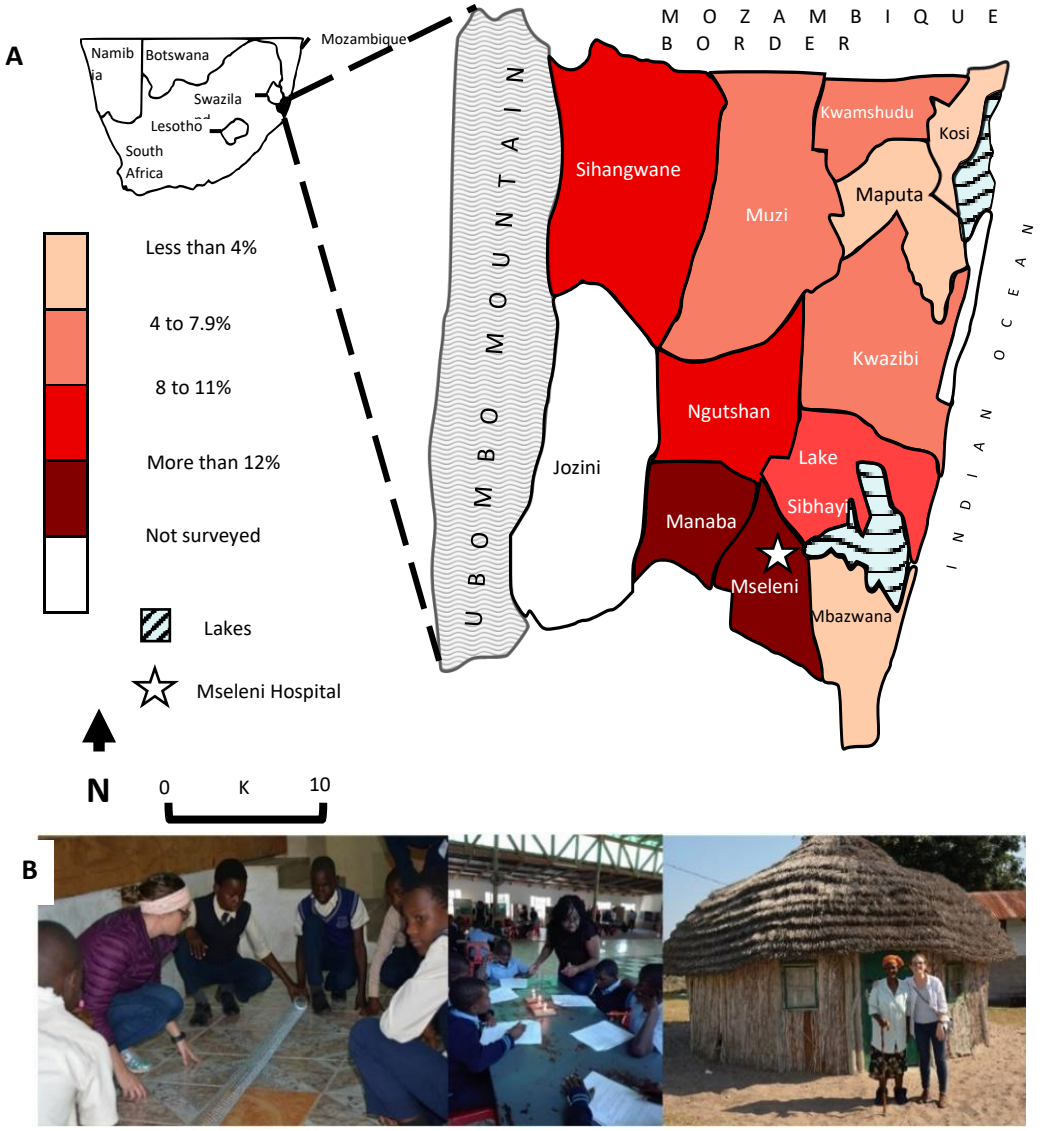

Figure 1.1. (A) Map of Maputaland in South Africa, showing prevalence rates of MJD per district. [Data from Yach and Botha (1981)]. (B) Visit of the University of Cape Town, Department of Human Biology, to the Mseleni Hospital. Dr Elizabeth Dinkele on the right in the right-hand side photo.

In one of the first reports, (Lockitch et al. 1973), along with the Division of Medical Statistics and Epidemiology of the National Research Institute for Nutritional Diseases, observed that individuals affected by MJD initially experienced pain in their hip and knee joints. The affected individuals, primarily in their early twenties, experienced increasing pain intensity and joint stiffness. As the disease progressed, they later needed a walking stick to help them move around. Originally, MJD was thought to impact only hip and knee joints, but subsequent studies by Fellingham, Elphinstone and Wittmann, (1973) revealed that it also affected other synovial joints. It primarily affected the hip joint, with evidence of epiphyseal dysplasia in some people (Lockitch, Fellingham, and Elphinstone 1973). They did a prevalence/epidemiological study and interviewed people in and around in the Mseleni region to identify patterns of MJD susceptibility. Their findings revealed that the prevalence of MJD was higher among females than males, particularly in the age range of 11 to 20 years. They postulated that this uneven distribution was possibly due to the difficulty in getting accurate measurements because of male migration from the region in search of employment at that time. An alternative hypothesis was the fact that men typically have a less active lifestyle compared to women, who often engaged in tasks such as tilling the soil, fetching water, and managing household activities which could exert significant strain on joints. A more recent study by Elizabeth Dinkele, (PhD thesis, 2024) supports a higher prevalence in females than in males but indicates a later age of onset, over 35 years of age, than previously reported.

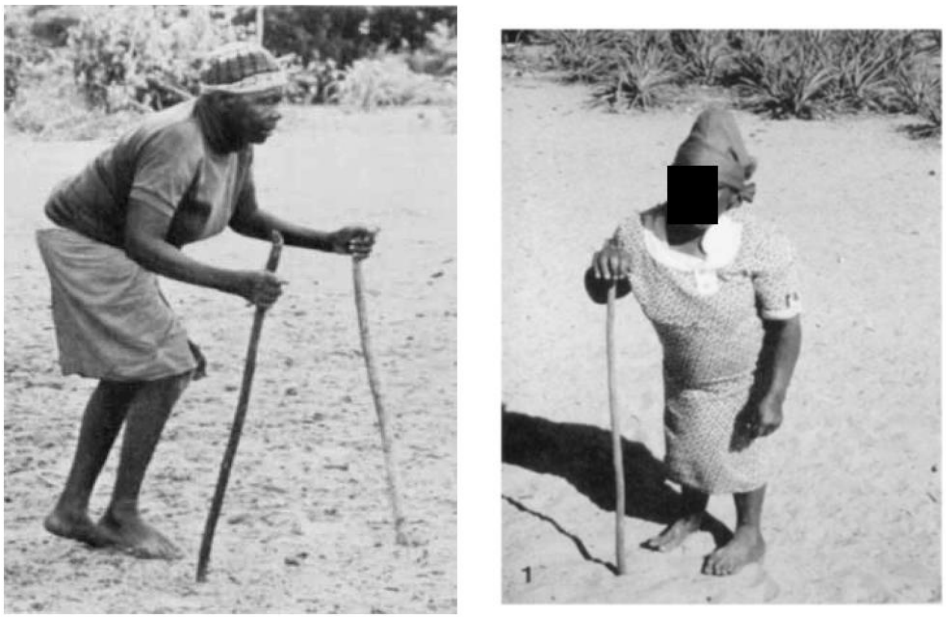

Figure 1.2. Typical deformities of individuals with Mseleni joint disease of normal stature and with dwarfism. (Viljoen et al. 1993)

1.1.1 Pathology:

In order to investigate the cause of this condition, various clinical studies and images were conducted (Lockitch, Fellingham, and Elphinstone 1973). MJD only affects synovial joints but most severely the hip. Clinical examination revealed a narrowing of the joint space, with osteoarthritis, and subarticular sclerosis.

Furthermore, autoradiographic findings support the observation that the disease starts at an early age, and may also be suggestive of prenatal development, with symptoms emerging when the condition becomes severe. X-ray assessments were conducted on all available family members, primarily to identify abnormalities in individuals that didn't present any symptoms. They also determined the earliest age of visible abnormalities seen by X-ray, explored the various types or patterns of abnormalities within families, and investigated potential inheritance patterns (Lockitch, Fellingham, and Elphinstone 1973).

Interestingly, they found that age didn't necessarily correlate directly with how severe the symptoms were. For instance, individuals aged 18 and 28 with significant hip and knee abnormalities were asymptomatic, while a 12-year-old boy experienced pain in hips, knees, and ankles joints for over a year. The youngest child with evident epiphyseal dysplasia in all X-rayed joints was 8 years old. In some cases, a mushrooming of the femoral head was seen, correlating to a femoral dysplasia. Spinal X-ray studies revealed a range of variations, from minor to moderate vertebral flattening and compression to unevenness on the vertebrae surfaces. In one case, a moderate presence of changes related to joint arthritis, like bony growths and lumps were detected. Significantly, Du Toit, (1979a) found that of 162 patients that were examined, 60 % of those with hip disease had bilateral and symmetrical *protrusio acetabuli* (Figure 1.3 B) (Du Toit 1979). Other dysplasias seen include a form of multiple epiphyseal dysplasia (Figure 1.3A) (Lockitch, Fellingham, and Elphinstone 1973), polyarticular steoarthritis (Du Toit 1979; Sweet, Schnitzler, and Hough 1987).

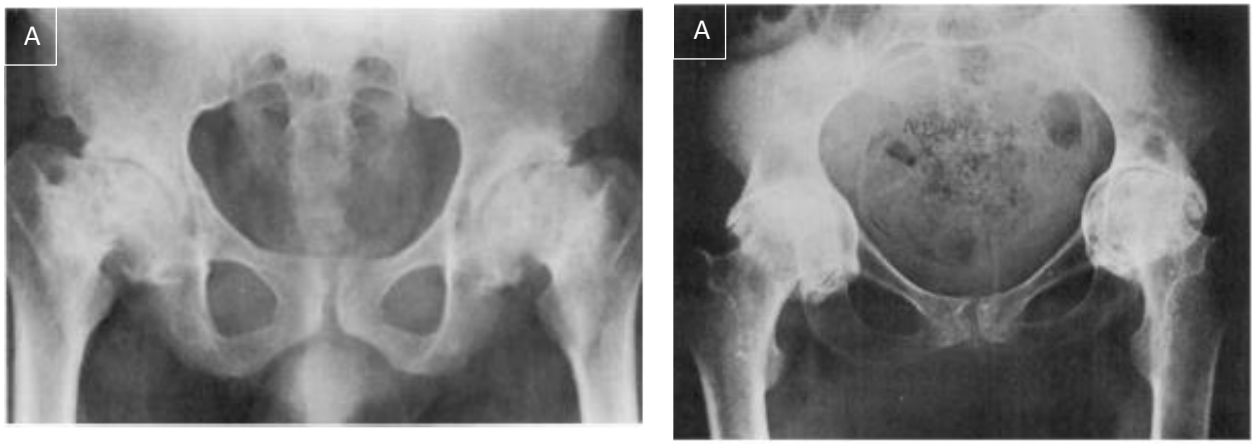

Figure 1.3. A) Coxa vara of MJD, a type of dysplasia epiphyseal (Du Toit 1979). B) Immobile protrusio acetabulae of a woman at 55 years of age (Solomon et al. 1986).

Analysis of femoral head samples taken after hip replacement surgery revealed cartilage degeneration, fragmentation, and thinning, with subarticular bone taking over the weight-bearing function because of the cartilage damage. Microscopic examinations by pathologists further revealed fibrotic changes in the bone marrow, suggesting a low-grade inflammatory process (Du Toit 1979).

In order to search for possible causes for the disease, Schnitzler *et al.*, (1988) carried out an analysis of iliac bone biopsies from MJD patients, and the bone mineralisation was measured. They found that there was a calcium deficiency and that might be the cause of MJD. There has been no further evidence to support this (Schnitzler et al. 1988).

1.1.2 Aetiology

Despite over 50 years of research, the cause of the disease is still a mystery. Little has been revealed from the many studies on the local environment, diet, nutrition, bone mineral deficiencies and composition of cooking utensils (Burger et al. 1973; Lubbe, Elphinstone, and Fellingham 1973; Fincham 1986; Fincham et al. 1986a; Gibbon et al. 2010). In 2010, Gibbon *et al.*, (2010) conducted a review on the MJD research including studies on autoimmune conditions, infectious agents and genetic factors, but no single cause has been identified. This suggested that the cause could be both multifactorial involving genetic and environmental factors.

In search of the **environmental** causes, the following factors have been considered. Firstly, the confined geographic distribution of MJD could suggest the possibility that some extraneous environmental factor might be involved in MJD (Wittmann and Fellingham 1970). Studies on water, soil and plants, diet, composition of cooking utensils and nutrition, have yielded little information (Burger et al. 1973; Lubbe, Elphinstone, and Fellingham 1973; Fellingham, Elphinstone, and Wittmann 1973; Fincham 1986; Fincham et al. 1986b; Gibbon et al. 2010). Testing for extractable Nitrogen (N), Phosphorus (P), Potassium (K), Calcium (Ca), Copper (Cu), Zinc (Zn), and Boron (B) from the topsoil (0-25cm) taken from the highly affected MJD region revealed deficiencies in these key elements in the Mseleni region's soil (Ceruti, Frey, and Pooley 1999). However, the pattern of deficiencies in these elements did not seem to correlate with specific locations of MJD household gardens.

In order to search for the **genetic** cause of the disease, Solomon *et al.*, (1986) proposed that MJD might share a common factor with other arthropathies. For example, he suggested that comparison of MJD to Namaqualand Hip Dysplasia, and Beukes Familial Hip Dysplasia, both of which have collagen abnormalities, (Agarwal et al. 1997a) might be instructive. This prompted Ballo *et al.*, (1996) to

investigate the link between MJD and COL2A1. These authors did not find a link between MJD and COL2A1. Furthermore, their familial studies revealed that MJD does not appear to be inherited in a simple Mendelian pattern. However, the presence of familial clustering within a specific geographical area implied that genetic factors might be involved in the aetiology of MJD. This also suggests the possibility for gene-environment interactions, that could be taking place during early development (Nurse, Jenkins and Elphinstone, 1974; Agarwal *et al.*, 1997).

Similarly, Handigodu disease in India showed potential similarities to MJD. This is a familial osteoarthropathy affecting primarily the hip joint. In Handigodu disease, which primarily affects the hips, environmental factors related to subtropical climate, low animal protein intake, and consumption of potentially toxic plant-based substances have been shown to play a role (Du Toit, 1979; Agarwal *et al.*, 1997). However, Du Toit, (1979) pointed out that the stored groundnuts in Mseleni did not show the presence of a fungus toxin that could be causing the disease (Du Toit 1979).

1.2. The Hip Joint

Since the hip is the joint most severely affected in MJD patients, and since it seems evident that the disease is initiated in foetal life or early postnatal development, it is necessary to have a fuller understanding of the morphological and molecular events that occur during early hip embryogenesis before the hypothesis in this project can be explained.

1.2.1 Anatomical Structure

The hip joint is a weight bearing ball and socket joint that is the connection between the legs and the torso. It allows for a wide range of movement. It is made up of the epiphysis of the femur (femoral head) which articulates with the acetabulum of the pelvis (Figure 1.4). The acetabulum is made up of the ilium, ischium and pubis which fuse during early development, forming a cup shaped socket (Figure 1.4).

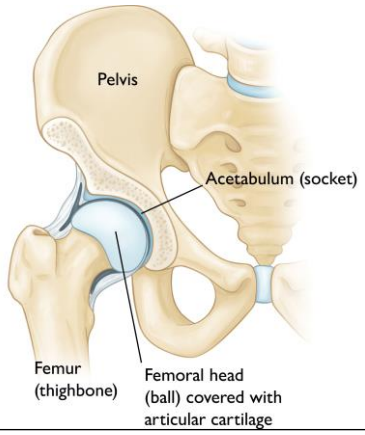

Figure 1.4. The structure of a Hip Joint. Image taken from https://orthoinfo.aaos.org/en/diseases--conditions/osteoarthritis-of-the-hip/.

Both the acetabulum and femoral epiphysis are lined with articular cartilage which is a highly specialized type of hyaline cartilage that has a smooth, lubricated surface that serves to reduce friction between the two bones during movement. It is constantly lubricated by lubricin, a glycoprotein, secreted by the superficial layer of the articular cartilage. The acetabulum is deepened by a fibrocartilage structure, the labrum, which provides stability to the femoral head. Between the acetabulum and the femoral head is a synovial cavity filled with synovial fluid, which is produced by synoviocytes. The synoviocytes make up the synovial membrane, which lines the inner surface of the joint capsule. The synovial fluid contains many different proteins and carbohydrates including phospholipids, hyaluronic acid and glycoproteins (reviewed by Salva and Merrill, 2017) and it provides lubrication and nourishment of the articular cartilage. The joint and the synovial cavity is enclosed by a fibrous capsule that further provides stability to the joint. Ligaments on the outside of the capsule also serve to support the joint, and in addition to that, they limit bone and joint movement to appropriate moving motions.

1.2.2 The development of the hip joint

The development of the human pelvis starts at 4 weeks, and this occurs in association with the development of the hind limb, along the ventro-lateral region of an embryo. As the limb grows out at about 6 weeks, the mesenchymal cells at the future site of the pelvis start to condense forming tight cell-cell interactions through mechanisms that include the cell adhesion molecule, N-cadherin. The condensation of the ischium, ilium and pubis occurs as the mesenchymal condensation forming the femoral head also progresses. The cells that lie between the condensing cells make up the interzone of the developing synovial hip joint and they will go on to form components such as the articular cartilage, synovial membrane and as well as the capsule.

The role of the interzone cells and how these cells create a functional hip joint with the correct shape of the femoral head and acetabulum remains unclear. (This is an important point because in MJD patients the hip joint morphological shape is dysplastic-refer to the section 1.4). However, some insight can be found in the reciprocal interaction between cells of the femoral head and acetabulum. Although studies on hip joint development have received less attention compared to other synovial joints (e.g. knee), there has been recent progress, particularly on the joint progenitor cells, their diversity and the signalling factors that play a critical role in the interaction between the acetabulum and the femoral head during early development (see review by Pacifici, Decker and Koyama, 2018). Some valuable experimental findings using mice and chick will be described here (Figure 1.5).

As can be seen in Figure 1.5 A, there are a number of cells (coloured red and green in the diagram) that are the progenitor cells in the joint. Holder, (1977) was among the first to investigate the fate of the interzone cells and thus deduce their function. They removed the interzone tissue of chick embryos at stages 24 and 25 through micro-dissection and this resulted in no joint development. Instead, the cartilaginous bones remained fused. The deduction was that the cells in the distal epiphyseal region were responsible for creating the space between the two developing bones, and thus the ultimate joint articulation. More recently, using the method of genetic cell lineage tracing, Pacifici, Decker and Koyama, (2018) conducted studies to understand the contributions to and relationships between cells of the lateral mesoderm plate during mouse hip joint development. They noted that in E12.5-E13 mouse embryos, the area where the future femoral head would form was surrounded by a group of mesenchymal progenitor cells (Figure 1.5 A). These mesenchymal progenitor cells together with some cells in the femoral head all expressed Sox9 and a subpopulation of these cells also express Gdf5. In the postnatal stage, the cartilaginous ilium took on an elongated shape.

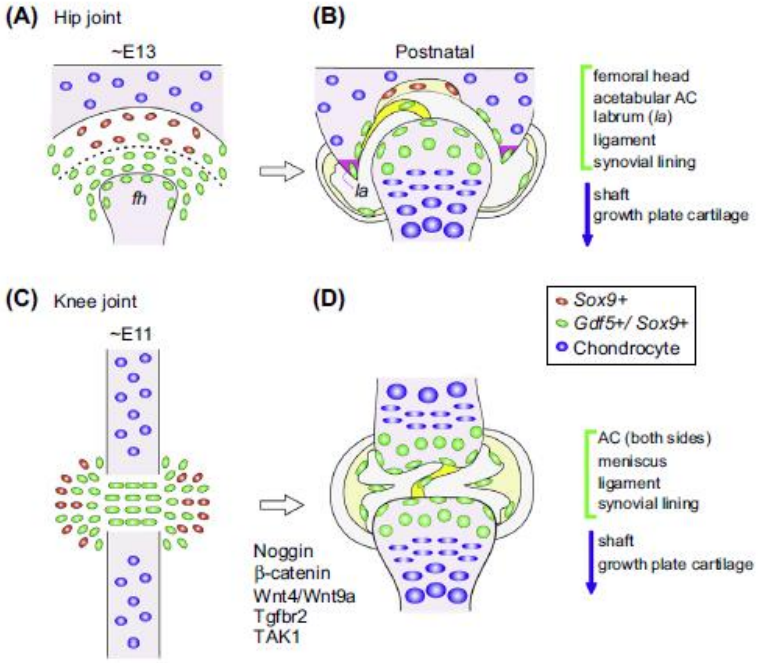

Figure 1.5. Schematic model summarizing and comparing major features and players in hip and knee joint development and growth. (A) At mid-gestation stages around approximately E13.0, the developing hip joint is characterized by the following: a prominent Gdf5/Sox9- expressing interzone-like mesenchymal cell population (green-coloured cells) surrounding the nascent femoral head (fh); and a population of Sox9-expressing progenitor cells (red-coloured cells) located in closer proximity to the ilium cartilaginous primordium (blue-coloured cells). (B) During postnatal stages, Gdf5/Sox9 lineage cells (green) would give rise to the entire femoral articular cartilage, teres, labrum (la) synovial lining, and inner capsule, while they would produce only articular cartilage located around the peripheral half of acetabulum. The tissues located in the central portion of acetabular fossa- and possibly including fat pad and accessory components - would originate from Sox9 lineage cells (red). (C) In the incipient embryonic knee joints starting around E11.0, Gdf5/Sox9-expressing cells would constitute the interzone and associated population (green-coloured cells), while additional Sox9-expressing cells (red-coloured cells) would be induced in, and recruited from, the immediate surroundings. The formation, functioning, fate, and roles of these cells would be dictated by an array of critical signalling proteins and transcription factors, including Noggin, b-catenin, Wnt4/Wnt9a, Tgfbr2, and TAK1 in addition to important others such as Gdf5, Gdf6, BMPs, Erg, and c-Jun (see text for details). (D) During postnatal development and growth, those progenitor populations would give rise to all the tissues present on the opposing femoral and tibial sides of knee joints, including articular cartilage, intra-joint ligaments, synovial lining, and inner portions of capsule and meniscus. Taken directly from (Pacifici, Decker and Koyama, 2018).

At E13.5, as the hip joint grows significantly, the Gdf5 expressing mesenchymal cells become tightly packed and connected to the femoral head. In contrast, the cells projecting towards the developing pelvis exhibit a more diverse shape, indicating the start of cavitation. Cells from this region go on to form other components of the joint, including the labrum, ligaments and the synovial lining. The Gdf5 positive cells in the femoral head remain densely packed (a process necessary to trigger cartilage formation) during the development of the articular cartilage.

Studies in normal hip development and developmental dysplasias in humans are largely based in imaging techniques including ultrasound, radiographs and X-rays. As with the mouse, the hip arises from a collection of flattened, condensed mesenchymal cells located at future hip sites. The acetabulum begins to form at about 6 weeks of gestation as a shallow depression to the femoral head. The normal growth and deepening of the hip rely in reciprocal interactions between the femoral head and the acetabulum. The pressure generated from this interaction inhibits appositional growth and ensure joint congruence. The acetabulum and the femoral head continue to shape each other and create the synovial space through appositional growth. The femoral head plays a significant role in determining the shape and geometry of the acetabulum (Harrison 1961; Chijimatsu and Saito 2019). By 11 weeks, all parts of the hip joint are visible. The presence and the correct shape of the femur head, including the articular cartilage is critical as any abnormalities in them could result in early abnormalities that later lead to early arthritis and seen in MJD. After birth, the growth of the hip joint continues to be a complex process. The acetabulum grows bigger because the triradiate cartilage contributes about 70% of its enlargement. This triradiate cartilage allows the acetabulum to become wider, in order to fit the growing femoral head. In addition to this, growth plates extend beneath the articular surface of each pelvic bone [(For reviews, see Decker *et al.*, 2017; Barrera *et al.*, 2019)].

The development of the femoral head is even more complicated. There are different stages in its growth, and the two essential features are the continuous cartilage along the neck and the path of the blood vessels inside the hip joint. All of these processes work together to form a fully functional hip joint that allows us to move and walk properly.

1.2.3 Articular cartilage

The epiphyseal end of the femoral head, which articulates with the acetabulum of the pelvic bone, is covered by a highly specialised articular cartilage and is made up of specifically arranged collagen type II and aggrecans to provide resilience during movement (See Figure 1.6). It is made up of only one cell type, the chondrocyte, which makes up about 10% of the tissue (Amin et al. 2009). The chondrocytes

that make up this tissue have a different origin compared to the transient chondrocytes that form the long bone, as mentioned above (Pacifici et al. 2006). Articular chondrocytes are fully differentiated cells responsible for the turnover of the various ECM components including type II, IX and X collagen fibres, proteoglycans, glycoproteins, and non-collagenous proteins. Sulphated glycosaminoglycan molecules provide resistance to compressive forces. Nutrients and oxygen are supplied to the articular cartilage through the heavily vascularised perichondrium. The articular cartilage is 2 to 4 mm thick and is divided into 3 layers:

- Layer 1 is the outermost superficial zone. It is a thin layer in contact with the synovial fluid. The arrangement and number of chondrocytes present in this layer protect the articular cartilage (AC) from shear stress. The glycosaminoglycan secretions, hyaluronan and lubricin (Seror et al. 2015; Salva and Merrill 2017) contribute to the lubrication and protection of the articular cartilage.
- Layer 2 is a middle transitional zone that consists of a high concentration of aggrecan that attracts water and makes the overall structure suitable for shock absorption.
- Layer 3 is an innermost deep zone that has a defined structural arrangement of chondrocytes relative to collagen fibres. This feature together with the high deposition of proteoglycans provides the articular cartilage with resistance to compressive forces and mechanical pressures (Fox, Bedi, and Rodeo 2009). The calcified region of the deep zone merges the articular cartilage to the underlying bone, giving the structure a stable and gradual transition to the mechanical stiffness of bone (Poole 1997).

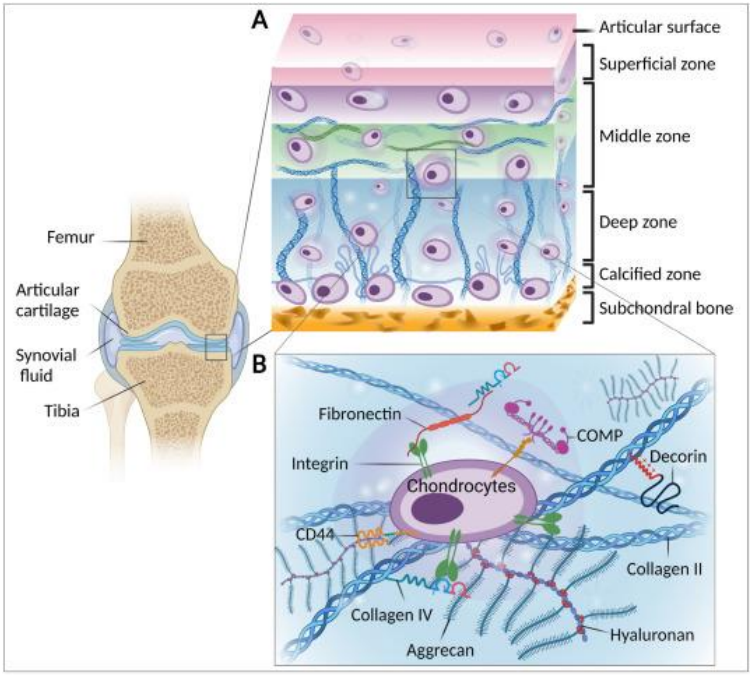

Figure 1.6 (A) The histo-morphology of articular cartilage. Image taken from Ulrich-Vinther et al., (2003) and (B) molecular components of the cartilage stroma (https://www.sciencedirect.com/topics/engineering/articular-chondrocytes)

1.3 Understanding the molecular pathways involved in chondrogenesis and osteogenesis

Chondrogenesis and osteogenesis occur through a series of events regulated by key signalling molecules and transcription factors during development and differentiation of mesenchymal cells into cartilage and bone. These include SRY (sex determining region Y)-box 9 (SOX9), growth factors such as Wnt/b- Catenin, fibroblast growth factors (FGF), hypoxia-inducible factor 1-alpha (HiF1alpha) and structural proteins including aggrecan and collagen types II, 1X, X and XI. Qualitative or quantitative changes may occur in the expression and levels of these molecules and/or genes that render the resulting cartilage and/or bone vulnerable to subsequent degeneration (reviewed by (Li and Dong 2016)).

1.3.1 In chondrogenesis

SOX9 is a master regulator of chondrocyte differentiation, playing an important role in both the development and maturation of cartilage (Li and Dong 2016). It is expressed by the mesenchymal progenitor cells (Wright et al. 1995) and by mature healthy chondrocytes in the body and in articular cartilage (Lefebvre and Dvir-Ginzberg 2017). During mesenchymal condensation, SOX9 helps direct the differentiation of the mesenchymal cells towards a cartilage lineage and in chondrocytes. SOX9 directly influences transcriptional activity of type II collagen, aggrecan and sulphated proteoglycans, thus regulating the structural genes responsible for chondrogenesis [As reviewed by (Marín-Llera, Garciadiego-Cázares, and Chimal-Monroy 2019; Lefebvre and Dvir-Ginzberg 2017)].

Prolonged mechanical stress and inflammation in a joint results in an increase in the release of cytokines, aggrecans and collagenases which degrade the core of the aggrecan, ultimately leading to impaired articular cartilage (Roughley and Mort 2014). Sox9 also regulates Type II collagen, along with proteoglycans, which plays an important role in maintaining the structure and strength of cartilage (Mayne 1989). Collagen type II, alpha 1 is encoded by the type II procollagen gene (COL2A1). Mutations in the COL2A1 gene have been associated with premature osteoarthritis and variant forms of spondyloepiphyseal dysplasia, a rare genetic disorder that results in abnormal growth and development of spine and limb bones in children and adults (Bonafe et al. 2015).

The minor collagens, including types IX, X and XI, are less abundant molecular components of articular cartilage. They play essential roles in maintaining the mechanical properties, organization, and shape of AC and have been associated with degenerative joint disease. Type IX collagen turnover by proteases is an early event in degenerative joint disease (Mayne 1989) and a COL9A1 gene mutation has been found in a patient with multiple epiphyseal dysplasia (Czarny-Ratajczak et al. 2001). Type X

collagen is expressed in human osteoarthritic cartilage but not in healthy articular cartilage (Brew et al. 2010). The upregulation of the COL10A1 gene is associated with hypertrophic chondrocytes and endochondral ossification (Q. Zheng et al. 2003). COL10A1 gene mutations have been detected in a human cartilage disorder accompanied by short stature (Kuivaniemi, Tromp, and Prockop 1997). Type XI collagen is thought to play a role in regulating articular cartilage formation (Xu et al. 2008) and COL11A1 gene has been associated with developmental dysplasia of the hip and secondary osteoarthritis (Jacobsen et al. 2024).

1.3.2 In osteogenesis

In addition to its role in chondrogenesis, SOX9 also plays a vital role in endochondral ossification through the activation and expression of Runt-related transcription factor 2 (RUNX2). RUNX2 is expressed in pre-hypertrophic and early hypertrophic chondrocytes found in the perichondrium of cartilage. It has been found to regulate molecules that promote hypertrophic differentiation in chondrocytes and include protein such as matrix metalloproteinase 13 (MMP13) (Selvamurugan et al. 2000; Takeda et al. 2001), Indian hedgehog (IHH) (Yoshida et al. 2004), COL10A1 (Drissi et al. 2003) and Vascular Endothelial Growth Factor A (VEGFA) (Zelzer et al. 2001). When RUNX2 is activated, it inhibits SOX 9 expression(G. Zhou et al. 2006), thereby, downregulating the production of aggrecan and collagen type II and chondrogenesis. Other factors that promote chondrocyte hypertrophy towards bone formation and mineralisation are myocyte enhancer factor 2 (MEF2), osterix (OSX) and osteocalcin (OCN) which are produced by osteoblasts (Arnold et al. 2007; Patti et al. 2013). COL10A1 is expressed in chondrocytes that will become hypertrophic: that is, chondrocytes that play a role in endochondral ossification. COL10A1 is therefore not expressed in articular cartilage.

1.4 Several separate skeletal joint disorders related to MJD

1.4.1 Protrusio Acetabulae

This condition was originally recognised and described by Otto in 1824 who called it an Otto pelvis (Pomeranz 2007). He described this abnormality as a "non-traumatic, chronic progressive arthritis of the hip joint, characterized by intrapelvic protrusion of the acetabulum and head of the femur." He characterized specific deformities in the pelvic region, especially involving the femoral heads and acetabula. The affected pelvis is normal in size and build but with deeper insertion of femoral heads into the acetabular. Later investigations further classified the condition, distinguishing between cases with underlying diseases or conditions (secondary) and those without (primary). The secondary protrusion can be caused by various factors like infection, trauma, metabolic, neoplastic, and genetic diseases while the primary protrusio typically manifests bilaterally and is more common in females

(Gilmour 1936; Alexander 1965). The consequence of acetabular Protrusio is secondary osteoarthritis (OA): Even minimal primary protrusio causes the femoral head to gradually migrate medially just like in MJD (Du Toit, 1979).

Based on his studies on MJD patients, Du Toit, (1979) proposed a developmental cause for primary protrusion. He raised the question of whether the degree of calcium depletion during pregnancy and lactation could be related to the development of osteomalacic protrusio acetabuli. Similarly, Solomon *et al.*, 1986) further discussed the pathogenesis of protrusio acetabuli in MJD affected individuals to be related to nutritional deficiency and metabolism. However, he noted that the absence of similar symptoms in other bones of patients presenting with protrusio acetabuli does not support this theory. While comparing the pelvis of 92 people, (79 women and 13 men) he reported that the observed depression of the acetabular floor might result from mechanical stress during puberty, especially when children in rural communities are known and proven to participate in doing heavy duty household chores like carrying water, firewood and other heavy loads.

1.4.2 Multiple epiphyseal dysplasia

As discussed by Lockitch, Fellingham and Elphinstone, (1973), the term "multiple epiphyseal dysplasia" was introduced by Fairbank, and since then, extensive literature on epiphyseal dysplasia has emerged. Clinically, it presents in early childhood. Pain in the hips and / or in knees after exercise are usually first affected, followed by waddling gait (Briggs, Wright, and Geert 2019). The affected adults are usually short in height, and as they get older, the progression of pain and joint deformity increases, which results in early-onset osteoarthritis, particularly in the hip and knee joints (Briggs, Wright, and Geert 2019).

1.4.3 Dwarfism

Researchers have also suggested that both MJD and brachydactylous dwarfism are different variants of the same condition, with dwarfism representing an extreme form of MJD (Viljoen et al. 1993). Homozygosity for the putative determinant gene would have been an obvious explanation, however, parents were unaffected or at least one parent would have been affected with the condition (Agarwal et al. 1997b).

1.5 Embryonic Stem (ES) Cells and induced Pluripotent Stem (iPS) Cells

Pluripotent stem cells are cells with the ability to develop into all tissues of an organism originating from the three embryonic germ layers, the ectoderm, endoderm, and mesoderm (Figure 1.7).

Pluripotent cells are usually found in the inner cell mass of a mammalian blastocyst. In 1988, Thomson and colleagues were the first to successfully isolate and culture human embryonic stem cells from human blastocysts. The cells had a normal karyotype with high levels of telomerase activity and displayed the stage-specific cell surface markers including embryonic antigens 3, 4, Tra-1-60, Tra-1-81 and alkaline phosphatase. These cells were successfully differentiated into tissues of the three embryonic germ layers: ectoderm, endoderm, and mesoderm (Thomson 1998). This led to a world-wide surge in the study of ES cells. However, despite the evident use of these cells and cell lines to study development and disease processes, the ethical issues related to the harvesting of cells from human embryos was very controversial and challenging, and furthermore, patient specific stem cells could not easily be obtained (Y. L. Zheng 2016).

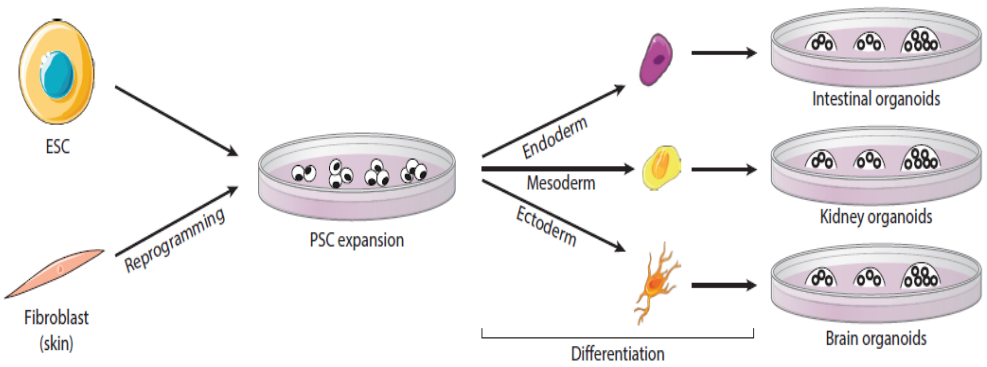

Figure 1.7. Pluripotent stem cell (PSC)–derived organoids use induced PSCs derived from cells such as reprogrammed skin fibroblasts or embryonic stem cells (ESCs), and these are then differentiated toward each of the three germ layers (endoderm, mesoderm, and ectoderm). Specific differentiation protocols are used to obtain the tissue of interest, such as intestine, kidney, and brain. Adaptation of (Schutgens and Clevers 2020)

It was therefore with great excitement that the generation of mouse induced pluripotent stem cells (iPSCs) was carried announced by Takahashi and Yamanaka, in 2006. They had been searching for and testing many embryonic transcription factor genes for the ability to turn adult differentiated cells into pluripotent stem cells. They finally found that the combination of four key transfection factors, POU domain class 5 transcription factor 1 (Oct3/4), SRY-box containing gene 2 (Sox2), Kruppel-like factor 4 (Klf4), and myelocytomatosis oncogene (c-myc), (OSKM) were able to reprogramme mouse fibroblasts into a pluripotent state, as determined by their ability to differentiation along all three germ line lineages. They then used the same four key transcription factors to generate human iPSCs from human dermal fibroblasts (Takahashi et al. 2007). The resulting iPSC cells were reported to be similar to ES cells by morphology, gene expression and their ability to differentiate into three germ layers (Takahashi and Yamanaka 2006; Takahashi et al. 2007). This discovery earned Yamanaka the Nobel

Prize in 2012 and has since been used by many groups across the world in advancing and understanding regenerative medicine and disease modelling (see(Cerneckis, Cai and Shi, (2024) for review). The reprogramming genes have come to be called “Yamanaka Factors”.

Since the development of human iPSCs, modifications to the delivery of the Yamanaka factors have been developed, including the use of integrating or non-integrating viral vectors. Lentiviral and retroviral vectors integrate with the host genome and this can cause an instability of the genome, which could lead to changes in the genetic organization as a result of gene silencing or fusion with endogenous genes (Mitalipov and Wolf 2015). It has also been shown for example, that genome instability caused tumour formation in mice that were injected with iPSCs (Pasi et al. 2011). In contrast, Sendai viruses do not integrate into the host genome. Expression of the reprogramming factors from the viral genome results in the activation of embryonic stem cell genes while switching off the expression of the somatic (differentiation) genes (Wen et al. 2016). Somatic cells have now also been shown to be reprogrammed into iPSC without the Yamanaka factors, including for example, the use of a combination of miRNAs (Anokye-Danso et al. 2011; Miyoshi et al. 2011), the use of small molecules (J. Kim, Koo, and Knoblich 2020), or transcription factors combined with small molecules (See (Cerneckis, Cai, and Shi 2024) for updates on direct and indirect approaches for iPSC reprogramming; and (Y. Kim, Kim, and Shin 2023) on the development and advance on blastoids formation and synthetic embryos)).

1.5.1 The use of iPS Cells

The use of induced pluripotent cells (iPSCs) has enabled many scientists to use patient specific cells to model aspects of specific diseases or conditions. They can be differentiated into specific lineages to study and trace different developmental stages and tissue formation, enabling one to investigate the relationship between cellular events and disease aetiology at molecular, cellular and tissues levels. They have also provided powerful platforms for drug development and novel treatments. The progress made in iPSCs has paved the way for personalised medicine and provided a deeper understanding of a number of complex events associated with progress. Methods for the derivation and study of iPSCs are continually being modified, with the aim of providing a consistent supply of high-quality and consistent iPSCs. These cells can proliferate and generate patient specific cells, which then reduces ethical constraints which would arise by using human embryonic stem cells (Castro-Viñuelas et al. 2018; Cerneckis, Cai, and Shi 2024).

One of the most valuable applications of iPSCs is disease modelling because somatic cells can be obtained from individuals affected by a condition, turned into iPS cells, then differentiated *in vitro* into the particular cell lineage of interest. In one of the earliest examples, brain organoid differentiation helped reveal some of the transcriptional and epigenetic regulators that controlled brain development (Camp et al. 2015). The first clinical trial using human iPSCs was the transplantation of iPSC-derived retinal pigment epithelial cells to treat macular degeneration in 2014 (Kimbrel and Lanza 2015). Even though the research was stopped because of tumour formation in the second patient, the results obtained from the first patient, who had improved vision because of the transplant, supported the progress of iPSC research.

The use of iPS cells has been further advanced by the creating of tissue "organoids" which can be made up of different tissues/cell types and could possibly help mimic the complexity of human tissues and aspects of early human development. For example, organoids were used to study the effect Zika virus (ZIKV) in pregnant women and how it caused microcephaly in infants (Qian et al. 2016). The researchers formed 3D brain organoids from iPSC's, exposed these organoids to ZIKV and observed the virus infect not only the newly formed neurons but also the neural stem cells. This led to a decrease in the number and volume of the neurons formed and layered in the cortex of the brain resulting in microcephaly in babies.

Early studies on human embryonic stem cells (ESCs) cultured in vitro, reported the formation of teratomas containing skeletal elements (Thomson, 1998). Between 1998 and 2015, key developments toward the generation of endochondral cartilage and bone included the use of mouse and human models from ESCs and later from iPSCs through mesenchymal intermediates (reviewed by (Humphreys *et al.*, 2022)). These were important steps that contributed towards the understanding of stem cell differentiation. Notably, Craft *et al.*, (2015) carried out studies that was aimed at generating articular chondrocytes from human iPSCs by first deriving the paraxial mesoderm lineage through embryoid body formation and supplementing the cultures with FGF and TGFβ3, following the protocol summarized in Figure 1.8. High density micromasses formed on the culture dishes had low expression of markers typical for endochondral bone such as, RUNX2, alkaline phosphatase and COL10A1. These micromasses did, however, express the normal cartilage markers (COL2A1 and ACAN). This result gives great promise in advancing the production of articular cartilage.

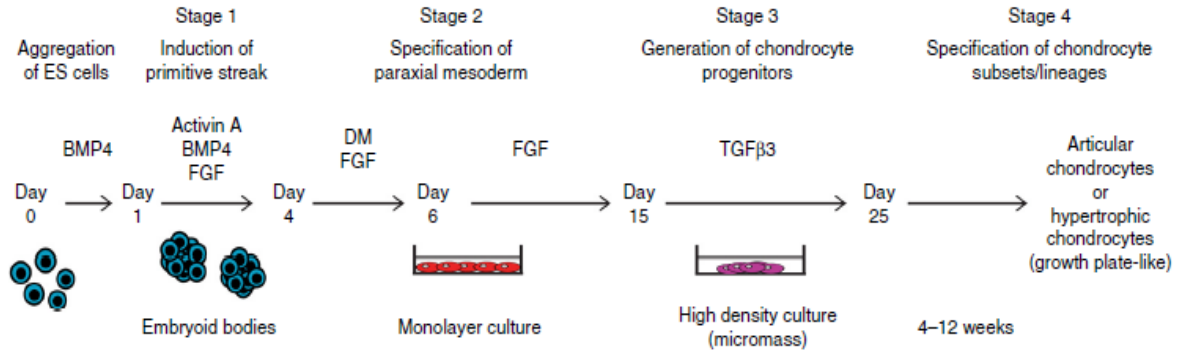

Figure 1.8. Generation of paraxial mesoderm and chondrocyte progenitors from hPSCs. Schematic representation of the protocol used for chondrogenic differentiation of hPSCs. The protocol consists of four stages: (1) induction of a primitive streak-like mesoderm population from days 1–4 as embryoid bodies; (2) specification to a paraxial mesoderm fate in monolayer culture by treatment with DM, days 4–6 and bFGF, days 4–15; (3) generation of chondrocyte progenitors in a high-density micromass culture in the presence of TGFβ3; and (4) specification to the articular chondrocyte or hypertrophic chondrocyte fate. (Craft *et al.*, 2015)

In an advance on joint "organoid" development *in vitro*, Limraksasin *et al.*, (2020) took the view that since synovial joint structures involve the concurrent development and differentiation of the cartilage and bone components it should be possible to develop a three-dimensional (3D) organoid *in vitro*. They therefore carried out a series of experiments developing a method for creating 3D hybrid bone and cartilage spheres using mouse iPSCs. They seeded the iPSCs into ultra-low-attachment 24-well micro-space cell culture plates with U-shaped-bottoms. The micromasses were cultured in a shaker in medium that contained trans-retinoic acid to induce mesenchymal precursor cells. After a few days, they replaced the medium with osteogenic medium containing β -glycerophosphate, ascorbate-2-phosphate. After 22 days, the medium was changed to osteochondral medium with TGFβ3. Following this process, they managed to obtain spheres that highly expressed chondrogenic markers (Sox9, Col2a1, aggrecan, and Ncam), as well as osteogenic markers Col1a1 and Osx (Limraksasin et al. 2020).

Recently, Pothiawala *et al.*, (2022) differentiated human iPSCs using chemically defined medium to generate embryoid bodies. From these cultures, they selected for $SOX9^{-/low}$ /$GDF5^{+}$ cells and formed 3D pellets which expressed gene markers of stable chondrocytes, possibly resembling those of articular cartilage or even intervertebral disk cartilage.

1.5.2 Modelling human development and diseases with iPSC derived cells.

1.5.2.1 Research question and approach

In this study we employed the disease modelling approach using iPSCs to investigate molecular signatures in cartilage development using cells obtained from people from the Mseleni region who were affected with the MJD condition. Specifically, it is hypothesized that the joint abnormalities in MJD arise from a disturbance of either cellular proliferation or differentiation processes during articular cartilage pre- or postnatal development. Abnormalities in cartilage formation and/or homeostasis may influence the joint surface and influence the growth of long bones and thus, link to dwarfism and joint pathology.

1.5.2.2 The broad OBJECTIVE of the present study

As described, MJD is an early onset severe arthropathy affecting synovial joints, especially the hip. The cause of the disease remains unknown, but early studies have revealed key information about the aetiology pathology. In brief it would appear that the relationship between the developing acetabulum and proximal femur is disturbed, resulting in conditions similar to protrusio acetabuli and other hip dysplasias. These abnormalities start to manifest as hip pathology when a child starts to walk and grows into an adult, this leads to very severe osteoarthritis early in life, particularly in females.

Having hypothesized that early embryonic stages are disturbed, the strategy was to look at the tissues involved in early embryogenesis. This would include the integrity of mesenchymal cells and their ability to differentiate into articular cartilage and bone. The aim of the present study was to create iPSCs from patients with MJD and Control subjects and then derive mesenchymal cells from the iPSCs and differentiate them into chondrocytes and osteocytes. This project focused on the technical steps needed to get to the point where MJD and control subjects can be compared.

The **AIM** was to generate iPSC-derived chondrogenic organoids from people with MJD disease (normal height and dwarfed) and people without MJD disease from the Mseleni region, and to investigate the molecular changes that occur during chondrogenic differentiation using iPS cells.

Specific aims:

NOTE: *Prior to the initiation of the present master's project, the following aims were achieved by colleagues*.

- **Aim 1**: To obtain skin samples from MJD patients and control samples (achieved by Prof Victoria Gibbon) and culture skin fibroblasts from the samples (achieved by Mrs Desiree Bowers).
- **Aim 2**: To reprogramme iPSCs from the culture fibroblasts (achieved by Dr Janine Scholefield)

NOTE: T*he following four aims (aims 3 to 6) formed part of the present project.*

- **Aim 3:** To expand and culture iPSCs from two patients and two control lines and fully characterise them using gene expression analysis of pluripotency markers by qRT-PCR, expression of pluripotency protein markers using immunocytochemistry and using *In vitro* differentiation to confirm their ability to generate the three germ layers.
- **Aim 4:** To derive mesenchymal cells from the iPSCs and characterise their phenotype using morphological criteria and qRT-PCR of CD cell surface markers.
- **Aim 5:** To determine whether the iMSCs were able to form adipose, bone and cartilage *in vitro*.
- **Aim 6:** To determine, using molecular markers, whether there were any differences in expression of osteogenic and chondrogenic genes between the patient and the control samples.

Chapter 2: Materials and Methods

2.1 Ethics approval

The current study forms part of a larger study initiated by Professor Victoria Gibbon in the Division of Clinical Anatomy & Bio Anthropology, Department of Human Biology, University of Cape Town (UCT). The primary study received ethics approval from the (UCT) Faculty of Health Sciences Human Research Ethics Committee (HREC) REF HREC: 822/2015, and the current study was approved on 31 October 2020 (REF HREC: 618\2020) which was annually renewed.

2.2 Cell culture

All cell culture was performed in a Class II Biosafety Cabinet and the cells were incubated in a 37^{o}C water jacketed 5% CO incubator, at 65% humidity, and 95% atmosphere air (ThermoFisher Scientific, Waltham, MA, USA). Before and after use, the Bio-Safety cabinet hood was cleaned and wiped with 70% ethanol, including the plastic consumables and all the other equipment used, such as the EVOS XL Core Cell Imaging System Microscope (Life Technologies, USA) which was used to view the cells. A lab coat and gloves were always worn inside the tissue culture unit. The cells were stored in liquid nitrogen tanks at a temperature of -190^{O}C.

2.2.1 Derivation of human dermal fibroblasts

Skin biopsies were obtained from the inner thigh of consenting individuals by a clinician under sterile conditions. The biopsies were kept at 4^{o}C in tissue culture medium (Dulbecco's Modified Eagle Medium (ThermoFisher Scientific, Waltham, MA, USA) supplemented with 10% heat-inactivated foetal bovine serum (FBS) and 100µg/ml Penicillin and 100µg/ml Streptomycin (1% Pen-Strep) until they could be transported to the UCT laboratory. The biopsies were processed within 2-3 days by Mrs Desiree Bowers in the Department of Cell Biology, using the (Normand and Karasek 1995) method to derive and isolate skin fibroblasts.

Briefly, skin biopsies were shredded with scalpel blades and placed between coverslips and submerged in medium. Over a period of a 1-2 weeks cellular outgrowths were tracked and the medium refreshed. The coverslips were separated into two separate dishes when skin fibroblasts became the dominant cell population.

2.2.1.1 Passaging cells

Cells were routinely examined under the EVOS microscope to observe morphology, cell growth, and for signs of bacterial contamination. The culture medium was refreshed every 4 days. The cells were passaged into increasing dish sizes by trypsinisation. At 80 – 90 % detachment, pre- warmed culture medium was added to the cells at an equal or double volume of Trypsin-EDTA (T/E) added, transferred to a 15 ml tube and centrifuged at 1 500 rpm for 5 minutes. The skin fibroblasts were passaged weekly and frozen down at passage number 3 (P3).

2.2.1.2 Thawing

In order to re-culture frozen cells, a vial of cells was removed from the liquid nitrogen and transported to the tissue culture laboratory in paper towel sprayed with 70% ethanol. The vial was rapidly swirled in a 37^{O}C water bath until 70-80% of the contents were thawed. The vial was sprayed with 70% ethanol, dried completely, and transferred to the Class II Biosafety Cabinet. The thawed cells were transferred dropwise to a 15 ml tube containing 4 ml of pre-warmed complete medium, to dilute the toxic effects of the DMSO in the cryopreserving solution.

The cells were centrifuged at 1000 rpm for 5 minutes and the supernatant removed. Complete medium, (1 ml), was added and the pellet triturated a few times to get a single cell suspension. The cells were seeded into a 10 cm dish (or smaller, depending on the size of the cell pellet) with 9 ml of complete medium, evenly distributed and cultured at 37^{O}C. Medium was changed every second or third day until the culture dish was 80% confluent.

2.2.1.3 Growth Curves

To determine cellular proliferation rate of the cells, a growth curve was performed. Fibroblasts (50,000 cells per well) were seeded in duplicate in a 6 well plate. They were cultured for a period of 7 days, and samples removed and counted on days 2, 3, 5 and 7 using a haemocytometer (see Appendix B). Cells were trypsinised and the cell pellet resuspended in 1 ml of fresh complete DMEM culture medium (DMEM^{++}). The cells were mixed 1:1 with Trypan blue and counted using a haemocytometer. Cell counts were plotted on a graph to determine growth patterns. The doubling time of the cells was counted using this equation: PDT = T ln2/ln (Xe/Xb) where T represents the hours of incubation, Xb represents the cell number at the start of the incubation time and Xe represents the cell number at the end of the incubation time (Aliborzi et al. 2016).

2.2.2 Mouse Embryonic Fibroblasts (MEFs).

The inactivated MEF feeder layers play a vital role in maintaining pluripotency in iPSCs and their quality and integrity is critical for maintaining healthy iPSCs. For that reason, utmost care is taken with the preparation of the feeder layers and their long-term storage to ensure that the cells are healthy and mycoplasma free.

2.2.2.1 Culture of ATCC MEFs

Mouse embryonic fibroblasts (MEFS) (ATCC SCRC- 1040) at passage 3 were purchased from the American Type Culture Collection (ATCC, Rockville, MD, USA) and stored in liquid nitrogen. For inactivation, a cryovial of MEFs was thawed as described in section 2.2.1.2. and seeded into 15ml of prewarmed MEF medium (DMEM supplemented with 10% FBS, 1% Pen-Strep, 1% GlutaMAX and 0.1% 2-mercaptoethanol) in a T75 Flask (all plastic consumables were purchased from BioSmart, South Africa) and incubated at 37 ^{O}C for 7 days. Medium was changed every second or third day until the cultures were about 80% confluent. At each medium change the cells were checked under the microscope to see if they were healthy, and to look for any signs of bacterial, yeast or fungal infections. Once the cultures reached 80% confluency, the cells were passaged and counted as described under section 2.2.1.3. With each new passage the cells were seeded at a cell density of 1x 10^5 cells/cm^2. At every passage, a few drops of cell suspension were removed to perform a Mycoplasma test to ensure that the frozen cells were Mycoplasma free.

2.2.2.2 Preparation of the Feeder layer: Inactivation of MEFs and preparation of frozen stocks

Inactivation of MEFs

At passage 6, MEF cultures were allowed to grow to 100% confluency before being treated with Mitomycin C derived from Streptomyces caespitosus (MIT C, Sigma, Germany). Culture medium was removed, and the cells incubated in MEF medium containing 10µg/ml of MIT C for 2.5 hours at 37 ^{O}C. The cells were washed carefully three times with 1x PBS to make sure all the excess MIT C was completely removed. Liquid waste was disposed of in biohazard waste containers and contaminated plasticware discarded in sealed plastic bags according to UCT regulations.

Freezing inactivated MEFs

The preparation of inactivated MEF aliquots for freezing down required a team of 3-4 people as it was labour intensive and usually took 4-5 hrs to complete. The team identified functions for each member including tube labelling, maintaining stocks of reagents and consumables, washing and trypsinising

inactivated cells, topping up ice boxes, preparing freezer storage boxes, waste removal and very importantly, counting cells and calculating cell densities.

The first step was to label cryovials according to the MEF densities regularly required by the stem cell users such as 0.15x 10^6, 0.3x 10^6, 1x 10^6, 2x 10^6 cells. The number of vials for each density varied at each inactivation, depending on the total number of cells inactivated.

Washed Mit C-treated MEFs, (now called inactivated MEFs/ iMEFs), were trypsinised with Trypsin/EDTA, inactivated with fresh warm MEF medium and pelleted in 50ml sterile tubes at 1500 rpm for 5 minutes. The cell pellet was resuspended and triturated in fresh MEF medium then counted using a haemocytometer. Working on ice, the cell suspension was mixed with ice cold 2x freeze down medium (Appendix A), and the cells frozen down in the different densities in a final concentration of 20% FBS and 10% DMSO.

2.3 Human Induced Pluripotent Stem Cells (iPSCs)

2.3.1 Source of iPSCs for this study

To derive iPSCs, frozen primary fibroblasts were reprogrammed using the Yamanaka four factor protocol (Takahashi and Yamanaka 2006). In preparation for stem cells studies including the current study, members of the UCT laboratory attempted the reprogramming process for the MJD fibroblasts in 2018. Briefly, skin fibroblasts from the patient and control cells were transfected with a replication-defective and persistent Sendai virus (SeVdp) vector (Miyoshi et al. 2011) containing the Yamanaka four factors, POU domain class 5 transcription factor 1 (OCT3/4), SRY-box containing gene 2 (SOX2), Kruppel-like factor 4 (KLF4) and Cellular-Myelocytomatosis oncogene (C-MYC) (Takahashi et al. 2007). Over a period of 21 to 30 days, emerging iPSC colonies were picked by manual dissection using insulin injection needles and transferred to 35mm gelatine-coated dishes pre-seeded with 0.3x10^6 feeder layers. Clones with specific iPSC characteristics were picked, enriched and expanded on feeder layers. After three attempts at the UCT laboratory, it was found that the iPSC colonies were fragile and could not be passaged successfully. Fibroblasts were therefore sent to Dr Janine Scholefield, a collaborator at the CSIR, in Pretoria for reprogramming (MTA Ref 27595) who used the CytoTune™-iPS 2.0 Sendai Reprogramming Kit (Invitrogen) to deliver the Yamanaka-four factors. After successfully reprogramming the fibroblasts to passage 3 (P3) over a period of 2-3 months they ascertained that the Sendai virus had been silenced and that there were no chromosomal abnormalities in the iPSCs (Scholefield, personal comm). Frozen iPSCs were transported to the UCT laboratory for the present study.

2.3.2 Culturing iPSCs on inactivated Feeder Layers: Thawing and Passaging

Thawing of iPSCs

In preparation for seeding iPSCs, iMEF feeder layers were plated on gelatin-coated dishes two days in advance. Routinely, 35 mm dishes were coated evenly with 1 mL of 0.1% gelatin (Sigma) (Appendix A) and incubated at 37°C for 1 hour. The excess gelatin solution was removed, and 1ml of MEF medium was added to the dish. A 1ml cell suspension containing $0.15x10^6$ iMEFs in MEF medium was seeded as outlined in section 2.2.1.2. The cells were allowed to settle over 48hrs before plating the iPSCs.
All iPSC grown on iMEFs layers were cultured in human embryonic stem cells culture medium (hESC). The hESC complete medium was made up of KnockOut™ DMEM supplemented with 20% KnockOut™ Serum Replacement (KOSR), 1% Non-Essential Amino Acid (NEAA), 1% GlutaMax, 1% Pen-Strep, 0.1% 2-Mercaptoethanol (all products of Gibco and Invitrogen, ThermoFisher) and 10 ng/ml of basic Fibroblast Growth Factor (bFGF/FGF-2) (Miltenyi Biotec).

iPSCs were thawed as described in section 2.2.1.3 with minor modifications. The cells were centrifuged at 1000 rpm for 5 minutes and the cell pellet gently resuspended in 1ml of hESC culture medium. The cell suspension was plated dropwise into two wells of feeder layers in a 80:20 ratio. The hESC medium was topped up to a total of 2ml and 10µM of Rho-associated protein kinase (ROCK) inhibitor (Y-27632) (Sigma, St Louis, MO) was added to prevent dissociation-induced cell death of iPSC cell. The plate was gently rocked to spread the cells evenly over the dish then transferred to the back of the 37 ^{O}C incubator to avoid disturbances.

After 48 hours in culture, the medium was changed and the cells viewed under the EVOS microscope to look for developing colonies. Thereafter, 50% medium changes were performed daily. The iPSCs colonies were allowed to form and expand in culture for between 5 and 8 days (a window of growth, established in the UCT laboratory) until they became large enough to passage.

Passaging iPSC colonies

Feeder layers were plated onto newly coated gelatinised wells as mentioned in section 2.3.2 (Thawing of iPSCs). On the day of passage, medium on the feeders was replaced with hESC medium two or more hours before the iPSC would be transferred to the new well to condition the hESC medium with growth factors produced by the iMEFs. The hESC medium on the iPSC plate was refreshed and the colonies manually dissected using a 1 ml insulin syringe needle to cut the colony from side to side, forming a grid of small patches of similar sizes as shown in figure 2.1. Using a white tip that was attached to a scalpel for easy handling, each patch was lifted off the dish by loosening up the edges and gently

flicking the patch into the medium. A pipette with a cut/widebore 1ml tip was used to transfer the floating patches to the new dish of iMEFs. The number of undifferentiated colonies in a well determined how many new wells were needed for the next passage. On average, 10 good colonies would be cut into 60-120 patches and transferred to 1-2 new 35mm well of iMEFs. Any additional colonies were either frozen down or passaged for a planned experiment. The newly passaged colonies were evenly distributed on the iMEF layer ensuring that they did not stick to each other or clump in parts of the dish, and the dish placed at the back of the 37 ^{O}C incubator. After 48hrs, the medium was replaced with fresh hESC medium and over the following 5-8 days 50% medium changes were performed daily until the colonies were big enough for another passage or freezing down.

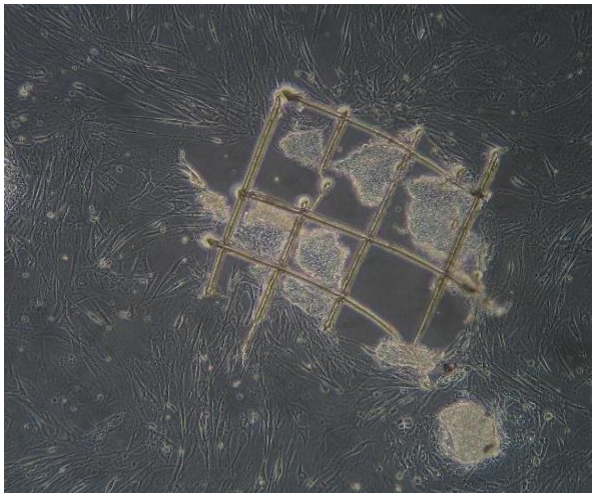

Figure 2.1. A cut iPSC colony during a passage. Small equal size patches are formed from the grid lines made using the 1ml insulin syringe. Image taken by an EVOS microscope at 40x Objective.

2.3.3 Culturing iPSCs on Feeder Free culture

Passaging iPSC colonies from iMEF feeder layers to feeder free conditions

The transfer of iPSC from iMEFs to feeder free conditions was done with an intermediate step in which iPSCs were first transferred to another dish of iMEFs using EDTA as the method of passaging instead of manual passaging (Beers et al. 2012). Bad or differentiated colonies were first manually removed from the iPSC culture plate and only good or undifferentiated colonies were left behind on the iMEF feeders. The colonies were loosened with 0.5 mM EDTA. The EDTA was carefully removed and 2ml of hESC medium added to suspend the cell clusters. The cell suspension was transferred directly to the wells in a 1:1 ratio of a 6 well plate containing an iMEF feeder layer. 10 µM of ROCK inhibitor was added to the medium and the cells evenly distributed. After the first 48 hours, the medium was changed completely. Thereafter, for 4 - 5 days, 50% culture medium was replaced daily. Using the

non-enzymatic EDTA passage method, the cultures became confluent more rapidly than they did with manual passaging and were therefore passaged much earlier.

In preparation for feeder free conditions, 1-2 wells of a 6 well plate was coated with Geltrex™ LDEV-Free, hESC-Qualified, Reduced Growth Factor Basement Membrane Matrix (Geltrex) (Gibco). To prepare the Geltrex solution, 1 ml of Geltrex was thawed overnight at 4 ^{O}C, then mixed thoroughly with 1 ml of cold KODMEM in a 15 ml tube on ice. Care was taken not to introduce bubbles into the solution. Aliquots of 100 and 200 µl were stored at -20 ^{O}C. To coat the wells, a fresh 100 µl aliquot was thawed on ice and mixed with 4.9ml of cold KODMEM. Two wells of a 6 well plate were covered with 2.5ml each of the Geltrex solution and incubated at 37 ^{O}C for an hour. The plate was returned to the Biosafety hood, for 1 hour at room temperature.

The culture medium for feeder free cell culture had to be prepared on the day of the passage. Essential 8™ supplemented medium (E8 medium) (A1517001, Gibco,) was made up by adding 1 ml of 50X E8 supplement to 49ml of E8 basal medium and incubated for 2 hours at room temperature before being used in an experiment.

The 4–5-day old iPSC cultures were treated with 0.5 mM EDTA and incubated for 5 minutes at 37 ^{O}C. The EDTA was removed, and 2ml of E8 supplemented medium added to suspend the cell clusters. The cell suspension was transferred directly to the two Geltrex - coated wells in a 1:1 ratio, with the addition of 10uM ROCK-inhibitor. The cell suspension was distributed evenly in the wells or dishes and transferred to the back of the incubator for 48hrs.

The E8 medium was changed completely for the first time after 48 hours and thereafter every day until day 4 or 5 when the colonies grew confluent.

Passaging iPSC colonies under feeder-free conditions.

After 3-5 days in E8 medium, iPSC cultures were ready to be passaged. In preparation for a passage, Geltrex coated wells were prepared as described above, section 2.3.3 (Passaging iPSC colonies from a feeder layer to feeder free conditions). The iPSC cells were dissociated with 0.5mM EDTA and resuspended in E8 supplemented medium. Once all the cells were collected from the well(s), they were split equally in a 1:2 or 1:3 ratio in Geltrex-coated wells and E8 supplemented medium. The E8 medium was changed after 48 hours followed by daily changes until day 4 or 5 when the cultures became confluent.

2.3.4 Freezing down iPSC colonies

After day 5, when the colonies were big enough, medium was removed, and the cells were washed twice with 1x PBS. iPSC colonies were lifted with 0.5mls TryplE express (Gibco, ThermoFisher) and incubated for 5 minutes at 37 ^{O}C. Following that, the TrypLE was inactivated by the addition of 4.5 mls of 1x PBS. The iPSC cell suspension was then transferred to a 15ml tube for centrifugation at 1 000 rpm for 5 minutes. While working on ice, the supernatant was removed and the cell pellet resuspended in 1 ml of ice cold 1x freeze down medium (30% KODMEM, 60% FBS, 10% DMSO). The cell suspension was then transferred to a cryovial and stored at -80 ^{O}C for up to one month before being transferred to liquid nitrogen for longer storage. (refer to freeze down section in Appendix A).

2.3.5 Characterisation of iPSC to confirm pluripotency

Pluripotency is typically confirmed through several methods: Immunocytochemistry (ICC) to detect reprogramming proteins, *In vitro* differentiation to show that the cells are able to differentiate into all three germ layers and gene expression analysis to confirm the expression of the reprogramming genes in the cells.

2.3.5.1 Immunocytochemistry (ICC)

Immunocytochemistry (ICC) was used to determine the expression and location of pluripotency markers in iPSC cells cultured on inactivated MEF feeder cells. It was also used to detect differentiation markers of *in vitro* differentiated samples.

In preparation for ICC, iPSC colonies were cultured on inactivated MEF feeders as described in section 2.3.2, with the following change: the iMEFs were layered onto 20 mm gelatine-coated coverslips before seeding the iPSCs.

When good colonies formed, they were fixed in 4% paraformaldehyde (PFA) (Sigma, Germany) for 15 minutes at room temperature. The PFA was removed, and the cells were washed three times with 1x PBS, for 5-minute intervals. For nuclear stains (NANOG and OCT3/4, ABCAM) the last PBS wash was done using ice cold 1x PBS so not to shock the cells upon the addition of methanol. Ice cold methanol was added to the cells to permeabilise the membrane and was incubated for 15 minutes at room temperature. The permeabilization step was omitted for cells that were going to be used to detect cell membrane bound pluripotent proteins (TRA1-60 conjugated with ALEXA-Fluor 488, MAB4360A4, Millipore, Germany).

Permeabilized cells were rinsed three times with 1x PBS, at 10-minute intervals then blocked for 1 hour at room temperature using a blocking buffer made up of 3% Bovine Serum Albumin (BSA) solution, 1% Triton X-100 (Sigma, Germany) made in 1x PBS. After blocking, the primary antibody was added, and the plates incubated overnight at $4^{O}C$. The primary antibody was prepared in the blocking buffer as listed in Table 2.1

Table 2.1: Primary and Secondary antibodies of Pluripotency and in vitro differentiation markers

Primary antibody	Host species	Antibody dilution	Secondary antibody
NANOG (Nuclear localisation)	Rabbit pAb	1:100	Cy3-Fluor (Donkey anti-rabbit) (1:1000)
OCT 3/4 (Nuclear Localisation)	Rabbit pAb	1:500	Cy3-Fluor (Donkey anti-rabbit) (1:1000)
TRA-1-60 (Localised in the cell membrane)	Mouse pAb	1:500	Alexa-Fluor 488 conjugate
Alpha SMA (myofibroblasts/Mesoderm)	Mouse mAb	1:100	Alexa Fluor-488 (Goat anti-mouse) (1:500)
β-III tubulin (microtubules/Ectoderm)	Mouse mAb	1:300	Alexa Fluor-488 (Goat anti-mouse) (1:500)
FOXA2 (Endoderm)	Rabbit pAb	1:1000	Cy3-Fluor (Donkey anti-rabbit) (1:1000)

The following day, cells were washed twice with 1x PBS for 15 minutes. The secondary antibody, Cy3 donkey anti-rabbit 1:1000r (for NANOG and OCT 3/4; Molecular probes, USA) was added to the respective wells as in Table 2.1 and incubated for 2 hours in the dark. Cells incubated with TRA1-60 required no secondary antibody as it was Alexa 488 conjugated. After 2-hours the cells were rinsed with 1x PBS twice and incubated in 0.1 mg/ml of Hoechst 3342 (Life ThermoFisher Scientific) for 15 minutes in the dark to stain the cellular DNA. After washing twice with 1x PBS, the coverslips with the cells were removed from the wells and dried with paper towel, to make sure the 1x PBS did not

crystalise. 0.1 g of Antifade (Sigma, Germany) was added to 1ml Mowiol mounting fluid and heated at 60 ^{O}C for 5 minutes. The Mowiol was briefly microfuged to pellet flocculence and a drop of the clear Mowiol added to a glass slide. The coverslip with the cells was mounted onto the Mowiol with cells facing down. The prepared slides were stored in the dark at room temperature or overnight at 4^{O}C, if they were not viewed immediately. The inverted Zeiss fluorescence microscope (Zeiss Axiovert 200M Fluorescence microscope, Axiocam HR camera, Axiovison 4.7 software) was used to visualise the cells. Secondary-only controls were used as negative controls and used to correct for background fluorescence.

2.3.5.2 Embryoid Body (EB) formation and *In vitro* differentiation

For embryoid body (EB) culture, day 5-8 iPSC colonies on inactivated MEF feeder layers were manually dissected into patches slightly bigger than those prepared for routine passaging (Figure 2.1). The patches were transferred to non-adherent 10cm dishes in hESC medium to allow the iPSCs spheres to grow in suspension and form EBs. For *in vitro* differentiation for each of the three - germ layers cultures, endodermal, mesodermal and ectodermal cultures, three separate 10 cm petri dish with at least 20 patches in suspension were prepared.

After the first 24 hours, hESC medium was removed gently to avoid disturbing the EBs. Lineage specific differentiation medium was carefully added to each 10 cm dish and the EBs cultured for 4 days.

For **endoderm differentiation**, the EBs were maintained in EB culture medium (Knock-out DMEM supplemented with 10% FBS, 1% NEAA, 1% Pen-Strep 1% GlutaMAX and 0.1% 2-mercaptoethanol - all reagents from Gibco/Invitrogen). After 4 days, 4-5 EBs were transferred to 12 well plates containing gelatin-coated coverslips. The cultures were maintained in EB culture medium for 10-16 days with medium changes every second or third day. The coverslips were then removed and processed for the immunocytochemical analysis as described in section 2.3.5.1.

For **mesoderm differentiation** the EB cultures were treated the same as for endodermal differentiation, with mesoderm differention medium (endodermal culture medium supplemented with 0.5mM ascorbic acid (Merck)).

To **ectoderm differentiation**, EBs were cultured in PA6 conditioned ectoderm differentiation medium, which included 48ml Neural basal medium and 48ml DMEM/F12 (Gibco), supplemented with 0.5% N2 and 1% B27 supplements, 1% GlutaMAX and 1% Pen-Strep. (PA6 cells are bone marrow stromal cells

that secrete neural differentiation factors - for PA6 cells preparation, please see Appendix B). The EBs were seeded into wells containing 0.1% gelatine coated coverslips and maintained in the PA6 conditioned ectoderm differentiation medium for 16 days. Medium was changed every second or third day until immunocytochemistry analysis.

2.3.5.3 Gene expression analysis using qRT-PCR

All gene expression analysis preparations were conducted in a clean and semi sterile environment dedicated for the process. The work bench was cleaned before and after use with 10% bleach and wiped down with single distilled water and sprayed twice with 70% ethanol. All pipettes and tip boxes were cleaned in the same manner before and after use. A "PCR" lab coat and new gloves were worn when the experiments were done and when handling the reagents to prevent contamination.

For qRT-PCR, the room was treated as above. Lab coats dedicated to the room were worn to prevent bringing in amplicons from previous PCR work. The UV light in the hood was switched on for 15 minutes before and after use, with all the pipettes, tube rack, tips, and Eppendorf tubes placed in the hood. Following the UV light sterilisation, the hood, pipettes, tube rack, tips, and Eppendorf tubes were wiped with 10% bleach, and rinsed with single distilled water and sprayed twice with 70% ethanol.

2.3.5.3.1 RNA extraction

For all cell lines and nodules, total RNA was extracted using the TriPure™ Isolation Reagent (Roche, Switzerland), according to the manufacturer's instructions (Appendix B). This method utilises a single phenol-chloroform step to separate DNA, RNA and proteins from each other (Chomczynski and Sacchi 2006). Briefly, the cells or nodules were lysed by triturating in TriPure reagent and the RNA isolated from the homogenised cells by chloroform extraction followed by precipitation with ice cold isopropanol (Appendix B).

2.3.5.3.2 Nanodrop Quantification

The RNA pellet was resuspended in 20 µl of sterile RNase free water and dissolved by passing the solution through a pipette tip several times. This step was followed by incubating the RNA solution at 60 ^{O}C for 10 to 15 minutes. Total RNA concentration was measured using a nanodrop ND - 1000 spectrophotometer (ND-1000, ThermoFisher) and the samples stored at -80 ^{O}C. The nanodrop ND - 1000 spectrophotometer also displayed the total RNA purity through the A260/A280 and A260/230 ratio readings.

2.3.5.3.3 Assessing mRNA integrity and quality

RNA integrity and quality was assessed by electrophoresis through a 1% agarose gel (SeaKem LE Agarose (Lonza, USA) in 1x Tris/Borate/EDTA (TBE) buffer (Appendix A) at 100 V for 1 hour. Ethidium bromide (Sigma Aldrich) was added to the agarose to visualise the 28S and 18S bands of the ribosomal proteins. 2 µl of 6x loading dye (Fermentas) was mixed with 0.5-1 µg of RNA and loaded on the gel. The GeneRuler 1 kb Plus DNA Ladder (Fermentas) was used as the molecular weight marker. Samples were visualized using the Spectroline Transilluminator (Spectroline, USA) and KODAK EDAS 290 camera system (KODAK, USA).

2.3.5.3.4 Complementary DNA (cDNA) synthesis

Complementary cDNA was synthesised using the Maloney-Murine Leukaemia Virus (M-MLV) RT (Promega, Madison, WI, USA) according to the manufacturer instructions. In the first step, working in 200ul PCR tubes, 1µl of 61 µM oligo dT was added to 0,5-1 µg of RNA, and then topped up with RNase free water to a total of 8.5 µls. The sample was mixed gently by lightly tapping the tube then incubated in the MultiGene TM Gradient Thermal Cycler (Labnet International, Edison, NJ, USA) at 70 ^{O}C for 5 minutes. The tube was transferred to slushy ice for 10 minutes. For the second step, 11,5ul of a PCR MasterMix was added to the denatured RNA. The MasterMix contained 1 mM dNTPs (Bioline Limited, UK), 2.5 mM $MgCl_2$ (Bioline Limited, UK), 1x RT buffer (Promega, Madison, WI, USA) and 1 U/µl RNase inhibitor (New England Biolabs, UK). Finally, 1 µl of 50,000 50U M-MLV RT (Promega, Madison, WI, USA) was added to the test samples (+RT) or 1ul of Sabax water was used for the negative control samples (-RT). Each tube had a final volume of 20 µl. The samples were gently mixed, briefly centrifuged, and incubated at 42 ^{O}C for 1 hour in the Thermal Cycler (Biorad Thermal Cycler C1000). The cDNA product was stored at -20 ^{O}C if not used immediately.

2.3.5.3.5 Quantitative Reverse Transcription polymerase chain reaction (qRT-PCR) (With Primer sequences)

For all qRT-PCR reactions, reagents were kept on ice to reduce degradation of the nucleotides and enzymes. Following cDNA synthesis, the cDNA was diluted to a 1:5 ratio, 1µl of cDNA with 4 µl of DNase/RNase free water (for iPSC and iMSCs). From this dilution, 2µl of cDNA was used for the qRT-PCR reaction. For each gene of interest, the reaction mix was prepared as shown in Table 2.2. This mixture was added to the wells of a 96-well plate (MicroAmp™ Fast Optical 96-Well Reaction Plate with Barcode, 0.1 mL, 4346906, Applied Biosystems, ThermoFisher). Following that, cDNA was added to the respective wells, resulting in a total reaction volume of 10 µl per well.

Table 2.2: qRT-PCR reaction mix

Reagent	Volume in µl
Sabax Water	2.6
Forward Primer	0.2
Reverse Primer	0.2
MasterMix SYBR green	5

The primers that were used and their specifications are tabulated in Table 2.3. These primers were either obtained from published research articles or the ORiGene website (https://www.origene.com/). To ensure that they were accurate, the SnapGene software program (https://www.snapgene.com/) was used to verify the correct primers placement within the target gene. In addition, the primers were checked to confirm that their melting temperatures were compatible, were between 55 and 65 ^{O}C, and that the GC content was within the acceptable range. Where possible, the primers were designed to span exon-exon junctions. They were then purchased from Integrated DNA Technologies (IDT WhiteSci, South Africa). The primers used in this study were designed to detect the endogenous version of the OCT3/4 and SOX2 (Mahito Nakanishi).

Glucuronidase Beta (GUSB) (QT00046046, Qiagen, Germany) and Glyceraldehyde 3-phosphate dehydrogenase (GAPDH) (Whitehead Scientific) were used for internal normalisation to correct for sample-to-sample variations within a PCR reaction. To confirm and validate pluripotency and the success of deriving MSCs from iPSCs, the Real-Time Quantitative Reverse Transcription (qRT-PCR) was used with GUSB as an internal control/housekeeping gene. GUSB expression was observed to be more or less constant in the transition from the iPSCs to the MSC stages/phenotypes. However, after testing a few samples of the chondro-differentiated CT1.5 samples, GUSB values were found to be ‘’undetermined” (StepOne terminology). Therefore, an alternative housekeeping gene, GAPDH, was selected. GAPDH has been found to be one of the most commonly used (Ong et al., 2022) and most stable housekeeping genes during chondrogenesis and osteogenesis (He et al., 2018) and was therefore used as an internal control during the validation of the trilineage differentiation. Ideally, two or more housekeeping genes should be used for normalisation.

Once all the wells were filled with sample, the 96 well plate was sealed with the MicroAmp™ Optical Adhesive Film (4311971, ThermoFisher), taking care to prevent cross contamination of the wells. SYBR Green Mastermix (Applied Biosystems™ Power SYBR™ Green PCR Master Mix, ThermoFisher) is light sensitive requiring the 96 well plate to be covered with foil when transferring to an Eppendorf 5180R

centrifuge (Eppendorf, Germany). The plates were centrifuged at 3000 rpm for 20 seconds to remove air bubbles and to collect the samples in the bottom of the wells.

Table 2.3. Table of Primer sequences for pluripotent, mesenchymal and trilineage differentiation.

Gene	Accession number	Primer sequence Forward (F) and Reverse (R)	Product Size
hOCT3/4 - F	NM_001285987.1	5'-GAC AGG GGG AGG GGA GGA GCT AGG-3’	144
hOCT3/4-R		5'-CTT CCC TCC AAC CAG TTG CCC CAA AC-3’	
hNANOG-F	XM_011520852.1	5'-CAG CCC CGA TTC TTC CAC CAG TCC C-3’	391
hNANOG-R		5'-CGG AAG ATT CCC AGT CGG GTT CAC C-3’	
hSOX2-F	NM_003106.3	5'-GGG AAA TGG GAG GGG TGC AAA AGA GG-3’	151
hSOX2-R		5'-TTG CGT GAG TGT GGA TGG GAT TGG TG-3’	
ALP-F	XM_006710546.3	5'-ATC TGA CCC TCC CAG TCT C-3’	165
ALP-R		5'-GAG TGA GTG AGT GAG CAA GG-3’	
hOC/BGLAP - F	NM_199173.5	5'-GGCAGCGAGGTAGTGAAGAG-3’	158
hOC/BGLAP-R		5'-CGATAGGCCTCCTGAAAGC-3’	
hACAN- F	NM_001135	F: 5’ AGG CAG CGT GAT CCT TAC C 3’	135
hACAN-R		R: 5’ GGC CTC TCC AGT CTC ATT CTC 3’	
hCOL2A1 - F	NM_001844	F: 5’ CGT CCA GAT GAC CTT CCT ACG 3’	121
hCOL2A1 - R		R: 5’ TGA GCA GGG CCT TCT TGA G 3’	
CD73 -F	NM_002526	AGTCCACTGGAGAGTTCCTGCA	132
CD73 -R		TGAGAGGGTCATAACTGGGCAC	
CD90 -F	NM_006288	GAAGGTCCTCTACTTATCCGCC	143
CD90 -R		TGATGCCCTCACACTTGACCAG	
CD105 -F	NM_000118.3	CGG TGG TCA ATA TCC TGT CGA G	109
CD105 -R		AGG AAG TGT GGG CTG AGG TAG A	

CD34 -F	NM_001025109	CCTCAGTGTCTACTGCTGGTCT	144
CD34 -R		GGAATAGCTCTGGTGGCTTGCA	
CD45 -F	NM_002838	CTTCAGTGGTCCCATTGTGGTG	107
CD45 -R		CCACTTTGTTCTCGGCTTCCAG	
CD14 -F	NM_000591	CTGGAACAGGTGCCTAAAGGAC	120
CD14 -R		GTCCAGTGTCAGGTTATCCACC	
COL2A1 - F	NM_001844	F: 5′ CGT CCA GAT GAC CTT CCT ACG 3′	121
COL2A1 - R		R: 5′ TGA GCA GGG CCT TCT TGA G 3′	
COL2A1_ - F	NM_001844	CGT CTA CCC CAA TCC AGC AA	269
COL2A1_ - R		R: 5′ TGA GCA GGG CCT TCT TGA G 3′	
COL10A1 - F	NM_000493.4	5′ ATG CTG CCA CAA ATA CCC TTT 3′	107
COL10A1 - R		5′ GGT AGT GGG CCT TTT ATG CCT 3′	

The plate was loaded in the StepOne Plus machine (Applied Biosystems, Life Technologies) on the comparative method programme with the following settings (Table 2.4): Run method was set at 10 µl, for 40 cycles; "continuous" option was selected to generate the Melt curve and C_t values. Each reaction sample was run in duplicate, with a minus (-) RT sample as a negative control. Each primer set had a non-template control (NTC) running alongside to monitor contamination. The data output was collected from a computer connected to the StepOne Plus machine and the $2^{-\Delta\Delta Ct}$ method (Schmittgen and Livak 2008) was used to analyse the data.

Table 2.4 qRT- PCR cycling conditions.

Step	Temperature (°C)	Duration	Cycle (depending on Primer settings)	Additional notes
Initial Denaturation	95	15 minutes	1	-
Denaturation	95	15 Seconds	40	-
Annealing	60 (or depending on primers)	1 minute	40	Optimised for primer settings
Amplification (Extension)	95	15 Seconds	40	-
Cooling	40	30 Seconds	1	-

Melt Curve Generation	Continuous	Automatic Ramp	-	Ramp changed from 0.3% to 2.8%

2.3.5.3.6 Visualisation of the qRT-PCR Product

The qRT-PCR product was visualised by electrophoresis through a 2% agarose gel as described in section 2.3.5.3.3 using the GeneRuler 100 bp Plus DNA Ladder (Fermentas) as the molecular weight marker to confirm the correct sizes of the qRT-PCR product.

2.4 Differentiation of iPSC clones into induced mesenchymal stem cells (iMSCs)

An important part of this study is to differentiate iPSCs into chondrocytes. Several methods for chondrogenesis have been described, the most frequently used method being through Embryoid Body (EB) intermediates (Doetschman, Eistetter, and Katz 1985). For the purposes of this study, the iPSCs were differentiated via a mesenchymal stem cell intermediate without going through an EB-stage. The resultant cells were called iPSC-derived MSCs or referred to in this thesis as iMSCs. This method is thought to yield a more homogeneous population of iMSCs. Two different protocols were tested as described below.

2.4.1 iMSC derivation Protocol I

In the first protocol, pluripotent iPS cells were grown in E8 medium under feeder free conditions and passaged onto Geltrex coated dishes. The medium was changed to low glucose iMSC medium (DMEM-low glucose (1 g/L) supplemented with 10% FBS, 1% Pen-Strep, 1% NEAA and 1% GlutaMAX) according to the method of Zhou *et al.*, (2018).

Cells were maintained in low glucose medium for 14 days and medium was changed every second day. On day 14, two wells were coated with 0.1% gelatine and incubated for an hour, in preparation for the iPSC-derived MSC passaging.

On Day 14, the iPSC derived MSC cells were over 100% confluent and were passaged as described in section 2.2.1.1, on pre-prepared 0.1% gelatine-coated wells. The cells were seeded at a ratio of 1:1, to improve their survival and growth. They were cultured in low glucose iMSC medium, followed by incubation at 37 ^{O}C. After 48 hours, not all the cells had adhered to the wells, thus the medium was changed carefully by tilting the dishes to aspirate the medium without removing the floating cells.

Fresh medium was replaced slowly along the side of the each well. Low glucose medium was changed every second day until about day 7, when the cells were 80 – 90% confluent. They were passaged with T/E, centrifuged, and counted using a haemocytometer to seed cells at a density of 1 x 10^4 cell/cm^2 on gelatine-coated wells. Medium was changed every other day and the cells were passaged until they reached 80-90% confluency (normally within 5-7 days.) Cells were then either frozen down using 1x Freezing medium or plated onto larger gelatine-coated vessels for further experiments. At passage 3, the cells were characterised for the presence of MSC markers (Dominici et al. 2006).

It is important to note that these cells were lifting off the wells as sheets after incubation in Tris/EDTA. To minimize this, a light force was placed on the cells by finger tapping the 6 well plates a few times. This helped to break the cell-cell bonds responsible for the formation of cell sheets. If they were left to lift as sheets, they would have formed clumps and made it difficult to seed single cells in subsequent passages.

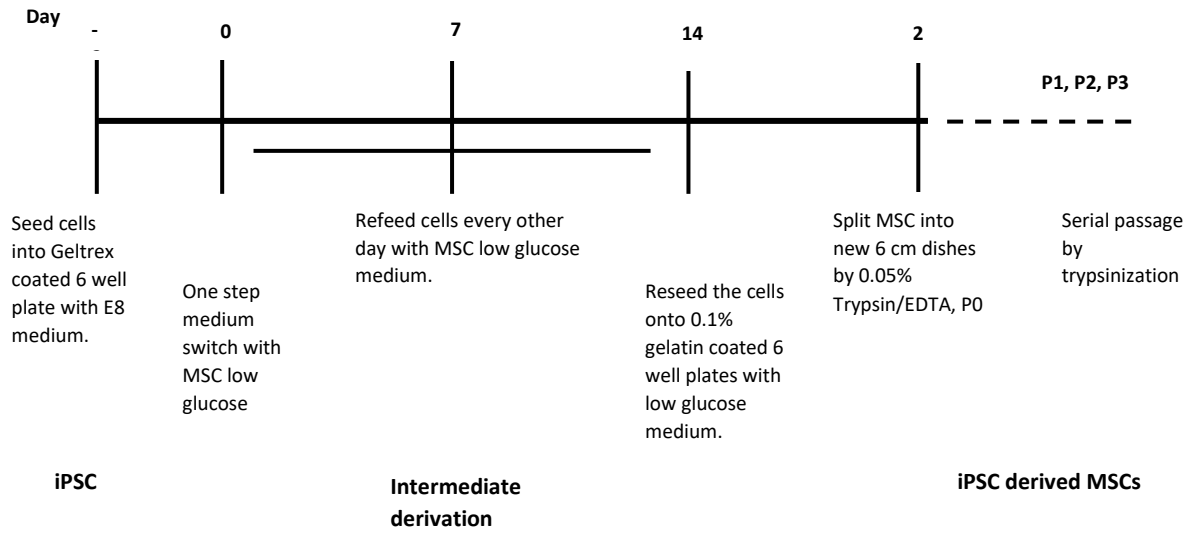

Figure 2.2. iMSC derivation Protocol timeline. The diagram displays steps taken for the one-step medium change protocol by Zhou *et al.*, (2018) for the derivation of iPSC-MSCs.

2.4.2 Bone, cartilage and adipose differentiation

To determine whether the iPSC-derived iMSCs were multipotent, they were cultured in osteogenic, chondrogenic, and adipogenic medium as follows.

2.4.2.1 Osteogenesis Differentiation

iPSC-derived MSCs, between passage 3 and 5, were thawed and passaged as described in sections 2.2.1.2 and 2.2.1.1 and were seeded at a density of 4×10^3 cells/cm^2 in 0.1% gelatine coated 12 wells in low glucose medium at 37 ^{O}C for 3 days or until 100% confluency. After day 3, medium was changed into osteogenesis differentiation medium, made by supplementing 50 µM ascorbate 2 phosphate, 10mM B-glycerophosphate, 1 µM dexamethasone in DMEM basal medium. Control cultures with cells that were not treated with osteogenic differentiation medium were cultured in low glucose iMSC medium. Cells were cultured for a further 21 days in the osteogenesis differentiation or control medium which was refreshed every second- or third day. The cells were checked under the EVOS microscope for morphological changes and general cell health. On day 21, RNA was harvested for RNA extraction and gene expression analysis, while some of the wells were reserved for the Alizarin Red S stain to view calcium deposited by osteocytes after the differentiation.

2.4.2.2 Chondrogenic differentiation

iPSC-derived MSCs were thawed between passages numbers 3-5 and passaged as described in sections 2.2.1.2 and 2.2.1.1. Cell numbers were expanded in T75 flasks and passaged to P8 when they were lifted with T/E. These cells were labelled P9. The cells were centrifuged at 1 5000 rpm for 5 minutes, and the supernatant was removed. One ml (1ml) of fresh low glucose iMSC medium was added to the pellet and resuspended 6-7 of times to obtain a single cell suspension. Using a haemocytometer, 10 µl was counted and the cell suspension adjusted to $0.8x\ 10^7$ cells/ml. The cell suspension was mixed carefully to reduce bubbles and, 5 µl pipetted onto the centre of a well. The developing cell clusters, now referred to as the micromasses, were incubated at 37°C to dry and aggregate the cells for 2 hours. Five hundred microlitres of chondrogenesis differentiation medium (DMEM basal medium containing 10 ng/ml TGFB3, 500 ng/ml BMP-2, 10^{-7} M dexamethasone, 50 mg/ml ascorbate-2-phosphate, 40 mg/ml proline, 100 mg/ml pyruvate, and 1:100 diluted ITS) was added to the wells, submerging the micromasses. For control cultures, micromasses were cultured in low glucose iMSC growth medium. Cells were cultured for a further 21 days in the chondrogenesis differentiation medium or control medium. Every second- or third-day medium was completely replaced, and the cell aggregates were checked under the EVOS microscope regularly. On day 21, cells were harvested for RNA extraction and gene expression analysis, while some of the wells were reserved for histological staining with Alcian Blue to view sulfated GAGs and glycoproteins which are found in cartilage after chondrogenic differentiation.

2.4.2.3 Adipogenic differentiation

iPSC derived iMSC cells were thawed and passaged as described in sections 2.2.2 and 2.2.3 and seeded at a density of 4×10^3 cells/cm^2 in a 0.1% gelatine coated 6 well plate. The passage number of cells was between 3 and 5, and low glucose medium was used to culture the iPSC-MSCs at 37 ^{O}C for 3 days, when they were 100% confluent. After day 3, medium was changed into adipogenesis differentiation medium, made by DMEM supplemented with 0.5 mM 3-Isobutyl-1-methylxantine (IBMX), 10 µg/ml insulin, 1 µM dexamethasone and 100 µM indomethacin while control wells were only treated with low glucose medium. The medium was changed every second or third day for a period of 21 days. On day 21, RNA was harvested for RNA extraction and gene expression analysis. Some of the wells were stained with Oil Red O stain for lipid droplets as a marker for adipogenesis.

2.4.3 iMSC derivation following Protocol II

In this protocol, DMEM with normal (25mM) glucose level (Cat#11965092, Gibco) was used instead of low glucose (5mM) iMSC growth medium.

iPSc cells were cultured on inactivated MEF feeder layers as described in section 2.3.2 and at day 5, the cell growth was checked under the EVOS microscope. The iPSCs were partially differentiated, just about 50% differentiated, which was not a problem for the protocol. Medium was removed from two wells using 0.5ml TrypLE™, followed by inactivating and washing with 4.5ml of 1x PBS. Cells were collected in 15 ml tubes, centrifuged at 1 500 rpm for 5 minutes. The supernatant was suctioned off and the cell pellet resuspended in complete DMEM growth medium (DMEM^{++}). One half of the cell suspension was seeded onto a 0.1% gelatine coated 35 mm dish and cultured further with complete DMEM growth medium. The other half of the cell suspension was also seeded on 0.1% gelatine coated 35 mm dishes but cultured in hESC medium and treated with 10 µM of (ROCK) inhibitor (Y-27632).

Cells were allowed to grow, as in protocol 1 (section 2.4.1), for 14 days without passaging. Medium was changed every second day with fresh DMEM^{++} and hESC media, respectively until day 14. The cells were passaged using TrypLE™ and transferred to 0.1% gelatine coated dishes at a ratio of 1:1. Cell culture was continued in either DMEM growth medium or in hESC medium until 80% confluency was reached. Cells were passaged and reseeded on gelatine-coated dishes at a density of $1x10^4$ cells/cm^2 -this passage was referred to as P1. All subsequent passages were performed at 80% confluency (not more than 7 days) and the cells replated at a density of $1x10^4$ cells/cm^2.

2.4.4 Trilineage differentiation (Using Commercially bought StemPro® Differentiation Kit)

2.4.4.1 Osteogenesis Differentiation

iPSC derived MSCs maintained in complete DMEM growth medium were passaged and used for this differentiation process. The cells were plated on 0.1% gelatine coated wells of a 12 well plate at a seeding density of 5×10^3 cells/cm^2. For four days, cells were cultured at 37 ^{O}C to allow them to reach 90 -100% confluency. Once they were 100% confluent, cells were rinsed twice with 1x PBS and fresh StemPro® Osteogenesis Differentiation supplemented medium (A10072-01 Gibco, USA) was added. Complete DMEM growth medium or hESC medium was used to maintain control samples. Cells were cultured for 21 days at 37 ^{O}C and medium was changed at every 3rd or 4th day until day 21.

StemPro® Osteogenesis Differentiation supplemented medium was made according to the manufacturer's instruction, where 1ml of the StemPro® Osteogenesis Supplement was added to 9mls of StemPro® Osteocyte/Chondrocyte Differentiation Basal Medium. Gentamicin reagent was added at 5 µg/mL to prevent infection during the 21 days of osteogenic induction.

2.4.4.2 Chondrogenesis differentiation

The iPSC-MSC cells that were maintained in complete DMEM medium were expanded in two T175 flasks and once they reached 85-90% confluency they were lifted off the flasks using TrypLE. After centrifugation the resuspended cells were counted using a hemocytometer. The desired number of 250,000-275,000 cells was pelleted in a 15 ml tube. For the chondrogenesis differentiation, cells were treated with 0.4 ml of StemPro® Chondrogenesis Differentiation medium (A10071-01, Gibco) and the control (non-induced) cell pellets were maintained in 0.4 ml of compete DMEM growth medium. The 15 ml tubes with the cell pellets were incubated with loosened caps at 37 ^{O}C for 21 days. Medium was changed every third day until day 21. The cell pellets, (nodules), were harvested for gene expression analysis and histological staining.

StemPro® Osteocyte/Chondrocyte Differentiation Medium was made according to the manufacturer's instructions, where 1ml of the StemPro® Chondrogenesis Supplement was added to 9mls of StemPro® Osteocyte/Chondrocyte Differentiation Basal Medium. Gentamicin was added at 5 µg/mL, to prevent infection during the 21 days of chondrogenic induction.

2.4.4.3 Adipogenesis differentiation

Cells maintained in complete DMEM growth medium were passaged and plated at a seeding density of 1×10^4 cells/cm^2 on 0.1% gelatine coated wells in a 12 well plate. For four days, cells were cultured at 37 ^{O}C to allow them to be 90 -100% confluent. The confluent cells were rinsed twice with 1x PBS

and fresh StemPro® Adipogenesis Differentiation supplemented medium (A10070-01, Gibco, USA) was added. Complete DMEM growth medium was used to maintain control samples. Cells were cultured for 21 days at 37 OC and medium was changed every 3rd or 4th day until day 21.

StemPro® Adipogenesis Differentiation supplemented medium was made according to the manufacturer's instruction, where 1ml of the StemPro® Adipogenesis Differentiation Supplement was added to 9mls of StemPro® Adipogenesis Differentiation Basal Medium. Gentamicin reagent was added at 5 µg/mL concentration, to prevent infection during the 21 days of adipogenic induction.

2.5 Mycoplasma tests

All cell lines were tested for mycoplasma as described in Appendix B.

2.6 Histological staining for trilineage differentiation of mesenchymal stem cells

2.6.1 Alizarin Red staining

After 21 days of osteogenic differentiation, the medium was removed, and the cells were washed once with 1x PBS then fixed in 4% PFA solution for 1 hour at room temperature, followed by two washed in 1x PBS (pH 4.2) for 5 minutes. 2g of Alizarin Red S powder was added to 100 ml of PBS (pH 4.2) and the mix filtered using a 0.2 µm syringe filter. This working Alizarin Red S stain was added to the cells and incubated for 20 minutes in the dark at room temperature. After the incubation, the cells were washed five times with double distilled water to remove excess stain. Alizarin Red S-stained cells were then viewed and imaged using the EVOS microscope at 20x objective.

2.6.2 Alcian Blue staining

Chondrocyte pellets were washed twice with 1× PBS, fixed in 4% PFA for 1 hour at room temperature, and then washed twice with distilled water. They were stained with haematoxylin before they were cryofrozen using the Optimal cutting temperature compound (OCT) before being sectioned using a microtome. Sections were cut in 0.3, 0.5 and 0.8 µm-thick slices. They were then stained with 1% Alcian blue solution for 30 min. The working solution was prepared by dissolving 1 g of Alcian blue 8GX powder in 100ml of 3% acetic acid. The pH was adjusted to 2.5 and filtered with a filter membrane.

2.6.3 Toluidine Blue Staining

After day 21 of chondrogenic differentiation, micromasses were washed twice with 1× PBS, fixed in 4% PFA for 1 hour at room temperature, and then washed twice with distilled water. They were then stained with Toluidine Blue solution for 30 minutes. The stock solution was prepared by dissolving 1g of Toluidine Blue powder in 100mL of 70% ethanol. The working solution was then prepared by diluting 5 ml of the stock solution in 45 mls of 1 % sodium chloride, with the pH adjusted to 2.5.

2.6.4 Oil Red O staining

After 21 days of adipogenic differentiation, cells were washed twice with 1x PBS and fixed for 1 hour in 4% PFA at room temperature and then washed twice with single distilled water. The stock solution of 0.5% Oil-Red-O was prepared in isopropanol and from that, the working solution was prepared by mixing three parts of the stock solution with two parts of single distilled water. The working solution was left to stand for 10 minutes before it was filtered using a 0.22 µm syringe filter (Pall, Separations). After removing the single distilled water from the cells, the Oil Red O working solution was added to the cells and the cells incubated for 30 minutes at room temperature. The cells were washed thoroughly with double distilled water to remove excess stain. The Oil-Red-O-stained cells were air-dried for 10 minutes and viewed using the EVOS microscope at 20x objective.

Chapter 3: Results

The current MSC project forms part of a broader study conducted in collaboration with Professor Victoria Gibbon (HREC: 822/2015). Skin biopsies were obtained by Prof Gibbon in 2017, and primary skin fibroblasts from four patient and four control individuals were isolated, cultured and cryopreserved at passage three as described in Material and Methods. Fibroblasts from two individuals affected with Mseleni Joint Disease (MJD) and one unaffected individual were selected for reprogramming and further culture and expansion.

3.1 Fibroblast cultures

To determine the proliferation rate of patient and control cells, they were seeded in duplicate at a density of 5x 10^4 cells per well, cultured in DMEM complete medium and manually counted using a haemocytometer on days 1, 2, 3, 5 and 7. The results are plotted in Figure 3.1a (control) and 3.1 b (patients). As can be seen, all eight cell lines proliferated sufficiently to continue with the reprogramming experiments. Two patient lines (MJD 5.3 and 8.5) and one control line (MJDC 3.4) were selected for further study.

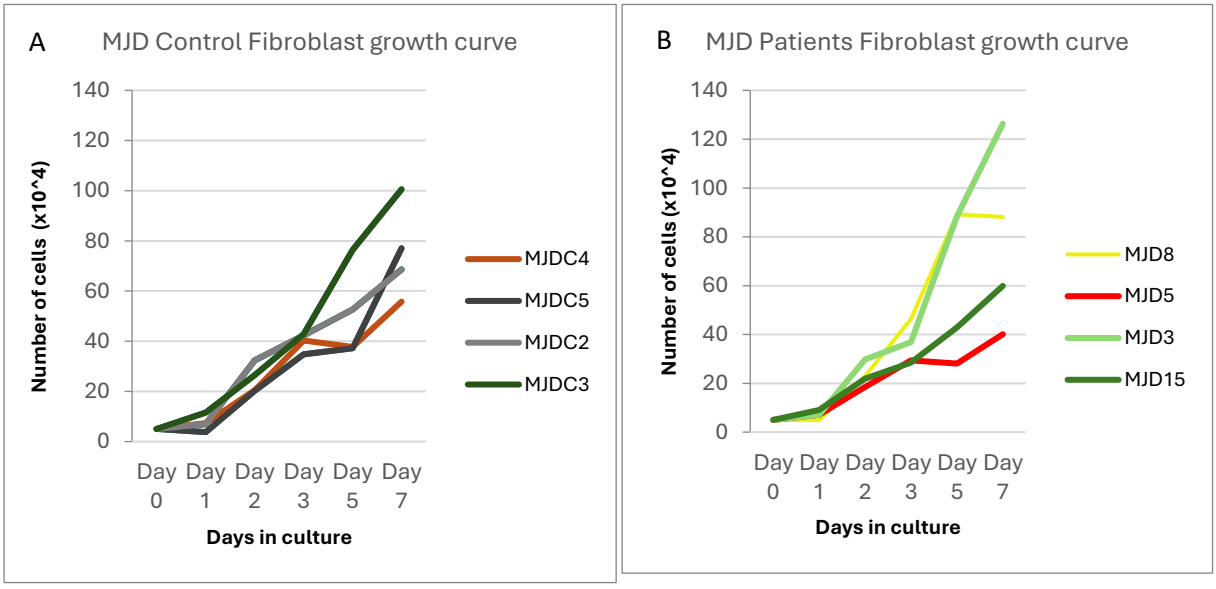

Figure 3.1. Growth curve of patient and control MJD fibroblasts. Patient and control fibroblasts from the Mseleni region were cultured for 7 days. The cells were counted on days 1 ,2, 3, 5 and 7 to determine their growth pattern.

3.2 iPSC derivation from fibroblast cultures

3.2.1 Cell lines used in this study.

Frozen primary skin fibroblasts were reprogrammed by Dr Janine Scholefield, at the CSIR in Pretoria. Pluripotency at P3 was confirmed and frozen clones were transported to the Cape Town laboratory for the present study.

One iPSC clone was selected from each of the study participants for this project. These samples were chosen because they represented the different categories of MJD phenotypes that are observed in the Mseleni area. In addition, we avoided the samples that had been difficult to reprogram in a previous UCT sub study. They will be referred to as:

1) **MJD5.3** - iPSCs derived from skin fibroblasts of an individual with MJD and dwarfism,
2) **MJD8.5** - iPSCs derived from skin fibroblasts of an individual with MJD of average height and
3) **MJDC3.4** – iPSCs derived from skin fibroblasts of an unaffected individual from the Mseleni district.
4) An additional control (from the foreskin of an unaffected individual from Cape Town, referred to as **CT1.5)** was included in the study.

3.2.2 Characterisation of the iPS cell lines:

3.2.2.1 Morphology on feeder layers

On receipt of the frozen cells in Cape Town, they were thawed, passaged to P10 on feeder layers in hESC medium supplemented with 10 ng/ml bFGF at 37^{O}C as described in Section 2.3. The control CT1.5 iPSCs were used to test the various protocols for this section of the study. Following the 5–8-day growth period they were cultured on feeder layers. They grew into the characteristically compact and rounded or ovoid shaped colonies with regular smooth and well-defined edges (Figure 3.2). Under the microscope the edges were bright and distinct and were easily distinguished from the feeder layer (indicated by the white arrows, Figure 3.2). The individual cells had a high nucleus-to-cytoplasm ratios.

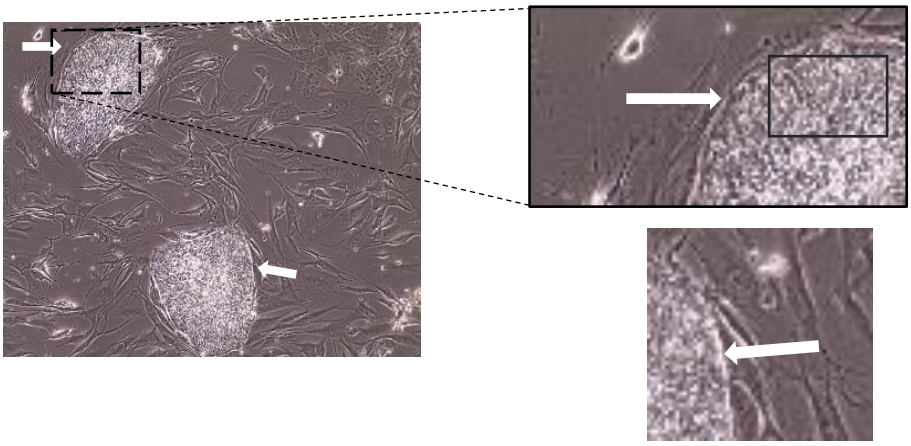

Figure 3.2. Morphology of iPSC colonies. CT1.5 iPSC colonies at passage 23, cultured on inactivated mouse embryonic fibroblasts. Images taken by an EVOS microscope at 10x objective magnification.

During manual passaging, the cut patches of cells were mostly similar in size and, depending on the size of the colony, 6-12 similarly sized patches were transferred to new feeder layers.

The MJD colonies took longer to develop the key iPSC morphological characteristics (8-10 days) compared to the CT1.5 Colonies (5-6 days). About 50% of the MJD 5.3 and MJD 8.5 colonies were fragile, with ill-defined and jagged borders (Figure 3.3B). In addition, some colonies with well-defined edges developed cavities within them (Figure 3.3A) after a few days in culture. Most of these latter colonies were "sticky" and tore as they were being passaged. When they were transferred to new feeder layers, these ragged patches either did not settle or lifted after a few days in culture.

The remaining 50% of the MJD 5.3, and MJD 8.5 colonies had the typical iPSC morphological features; they were compact with smooth well-defined edges and were packed with cells with a large nucleus to cytoplasm ratio. The colonies were easy to dissect microscopically, and the cell patches lifted easily when transferred to fresh iMEF feeder layers. However, after 2-3 passages, these colonies also developed jagged edges (Figure 3.3B, red arrows), and had unclear, hazy regions indicative of partial differentiation which initiated at the edges of the colonies (Figure 3.3C, inside the black box). By P6, these colonies also became "sticky" and adhered to the dish surface, making it very difficult to cut without tearing them. Of the few patches that were transferred to new feeder layers only about one third settled and the rest remained floating and were lost during medium changes (Figure 3.3B).

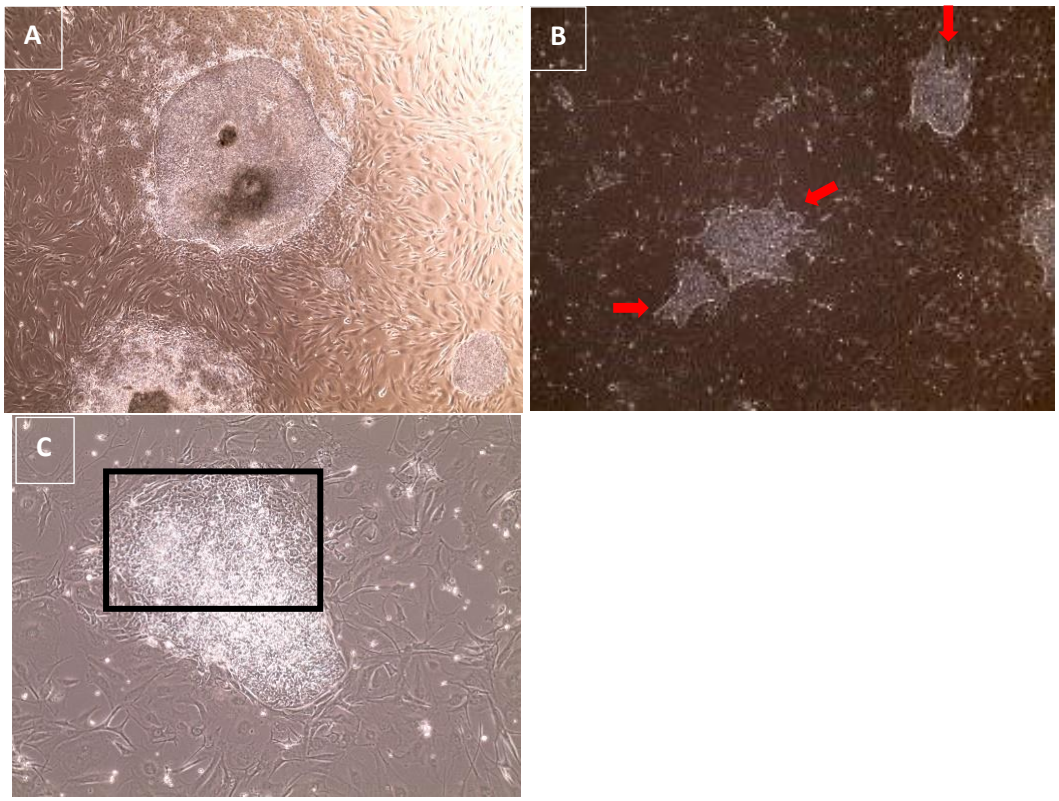

Figure 3.3. Ill-defined iPSCs. A- colony with a cavity, B- colonies that developed jagged and irregular edges (by red arrows), C- partial differentiation at the edge of a MJD5.3 colony. Images taken by an EVOS microscope at A) 4x and B-C) 10x objective magnification.

MJDC3.4 behaved differently compared to MJD5.3 and MJD8.5. When cultured with iMEFs, MJDC3.4 colonies were round, with bright well-defined edges but the size of the colonies was smaller than those of the other MJD samples. The MJDC3.4 colonies didn't grow any larger after further passaging and eventually started to differentiate by passage 6 (Figure 3.3C and Figure 3.4).

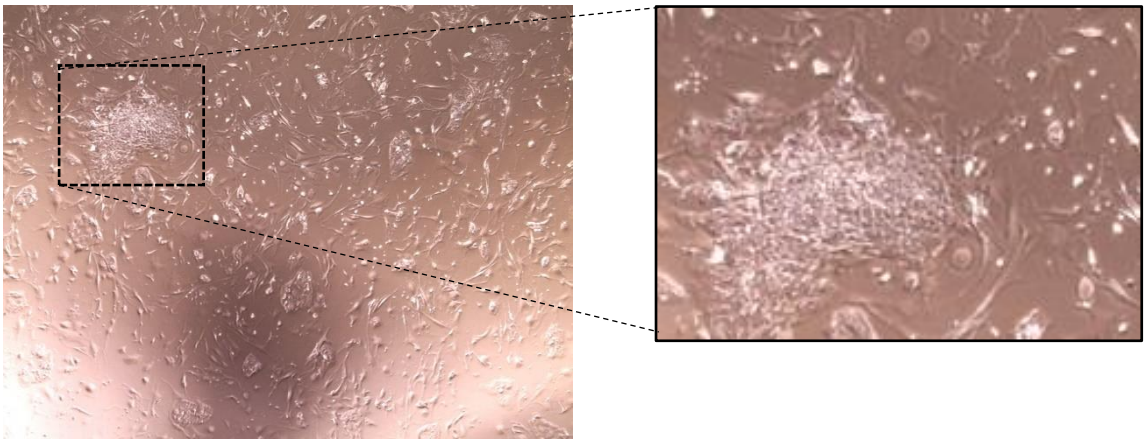

Figure 3.4. A partially differentiated MJDC3.4 colony at Passage 6. Images taken by an EVOS microscope at 4x objective magnification.

To address the problem of the unusual morphology and partial differentiation seen in the MJD cultures, increasing concentrations of bFGF in hESC medium were tested within the range of 10 ng/ml to 20 ng/ml. Concentrations of bFGF below 20 ng/ml did not appear to reduce the colony differentiation. However, the number of differentiated colonies were markedly reduced when 20 ng/ml bFGF was used. The edges of the colonies were more regular, and the colonies were less sticky and therefore easy to passage (Figure 3.5). The colonies formed with 20 ng/ml bFGF displayed typical, compact morphological features of iPSCs with well-defined bright edges (Figure 3.5A-D). These colonies were easily distinguished from the feeder layer. Figure 3.5 shows A) MJD5.3 at passage 8, B) MJD8.5 at passage 13, and C) MJDC3.4 at passage 16. All the colonies show the typical iPSC morphology, rounded with well-defined edges and a big nucleus-cytoplasm ratio, as seen in CT1.5 (Figure 3.1). Images were taken with an EVOS microscope at 10x objective magnification to obtain better images.

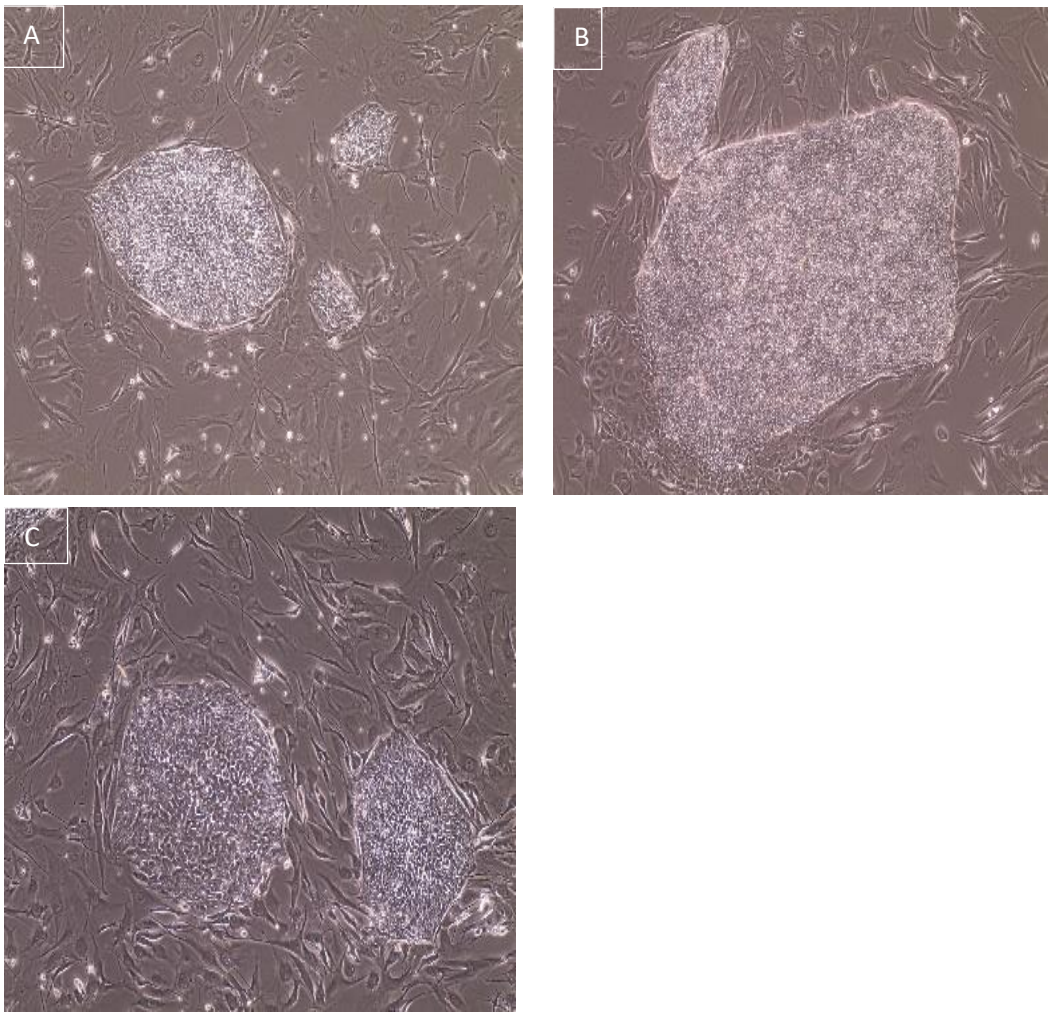

Figure 3.5. Morphology of MJD iPSC colonies. Improved MJD iPSC colonies after the increase in bFGF concentration. A) MJD5.3 at passage 8, B) MJD8.5 at passage 13, and C) MJDC3.4 at passage 16. Images taken by an EVOS microscope at 10x objective magnification.

3.2.2.2 Expression of pluripotency protein markers in iPSC colonies using immunocytochemistry.

To confirm pluripotency in the expanded iPSCs, immunocytochemical staining was used as described in section 2.3.5.1. This enabled the determination of the protein expression and localisation for NANOG, octamer-binding transcription factor 3/4 (OCT3/4) and TRA160. Briefly, iPSCs were cultured for 3-5 days on an iMEF feeder layer that had been grown on a 20 mm gelatine-coated coverslip and stained with the NANOG, OCT3/4 and TRA160 antibodies. All of the iPSC lines tested positive for these antibodies. The transcription factors NANOG (Figure 3.6 B, E, H, K) and OCT3/4 (Figure 3.7 B, E, H, K) were localised in the nucleus, indicated by the purple colour resulting from the merging of the blue Hoechst stain (nuclear indicator) with the red NANOG or OCT stain. The cell surface antigen, TRA-160 (Figures 3.8 C, F, I, L) was localised on the cell surface. This was reflected by the green stain surrounding the blue Hoechst stain. (See appendix C for secondary-only controls images).

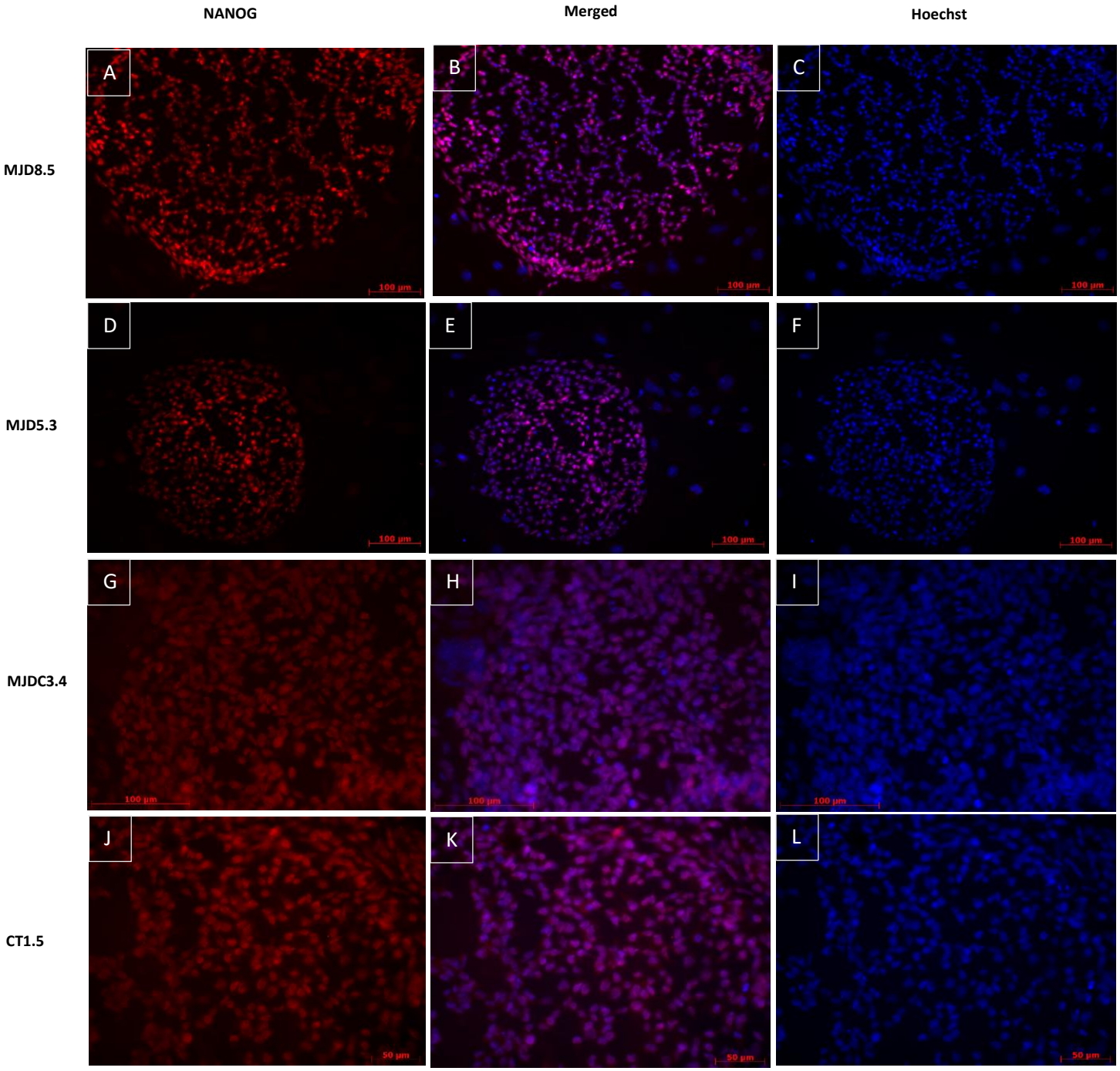

Figure 3.6. Immunocytochemistry staining showing iPSC colonies expressing the Nanog protein and its localization. Nanog was positively expressed by all iPSC lines (A, D, G & J). The merged, Nanog and Hoechst (B, E, H & K) displayed the nuclear localisation of Nanog. Figures C, F, I &L, show the positive Hoechst stain. Images were taken using an inverted Zeiss fluorescence microscope using a Cy 3 channel for Nanog and merged, DAPI channel for Hoechst.

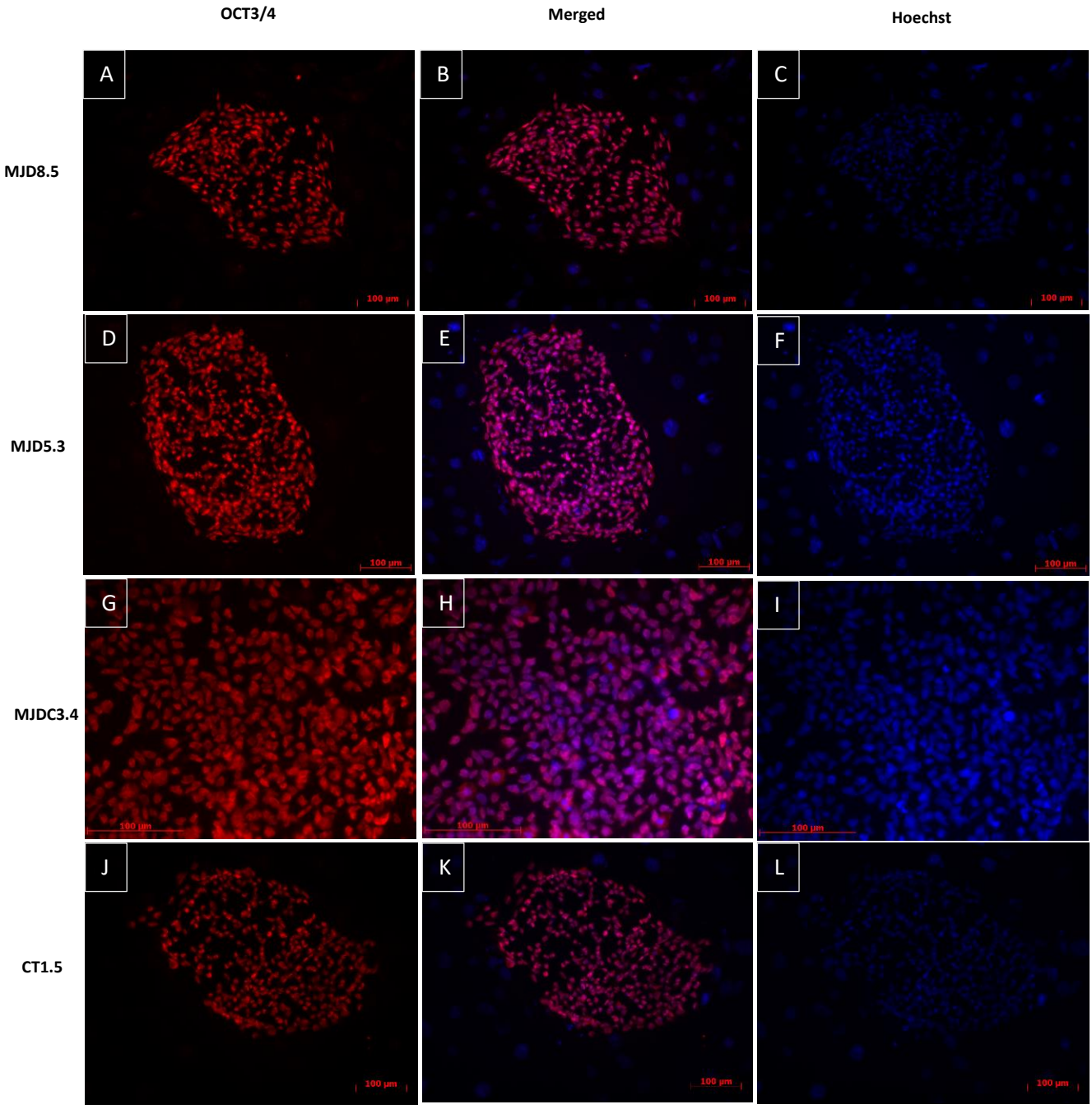

Figure 3.7. Immunocytochemistry staining showing iPSC colonies expressing the OCT3/4 protein and its localization. OCT3/4 was positively expressed by all iPSC lines (A, D, G & J). The merged, OCT3/4 and Hoechst (B, E, H & K) display the nuclear localisation of OCT3/4. Figures C, F, I &L, show Hoechst stain. Images were taken using an inverted Zeiss fluorescence microscope using a Cy 3 channel for Nanog and merged, DAPI channel for Hoechst.

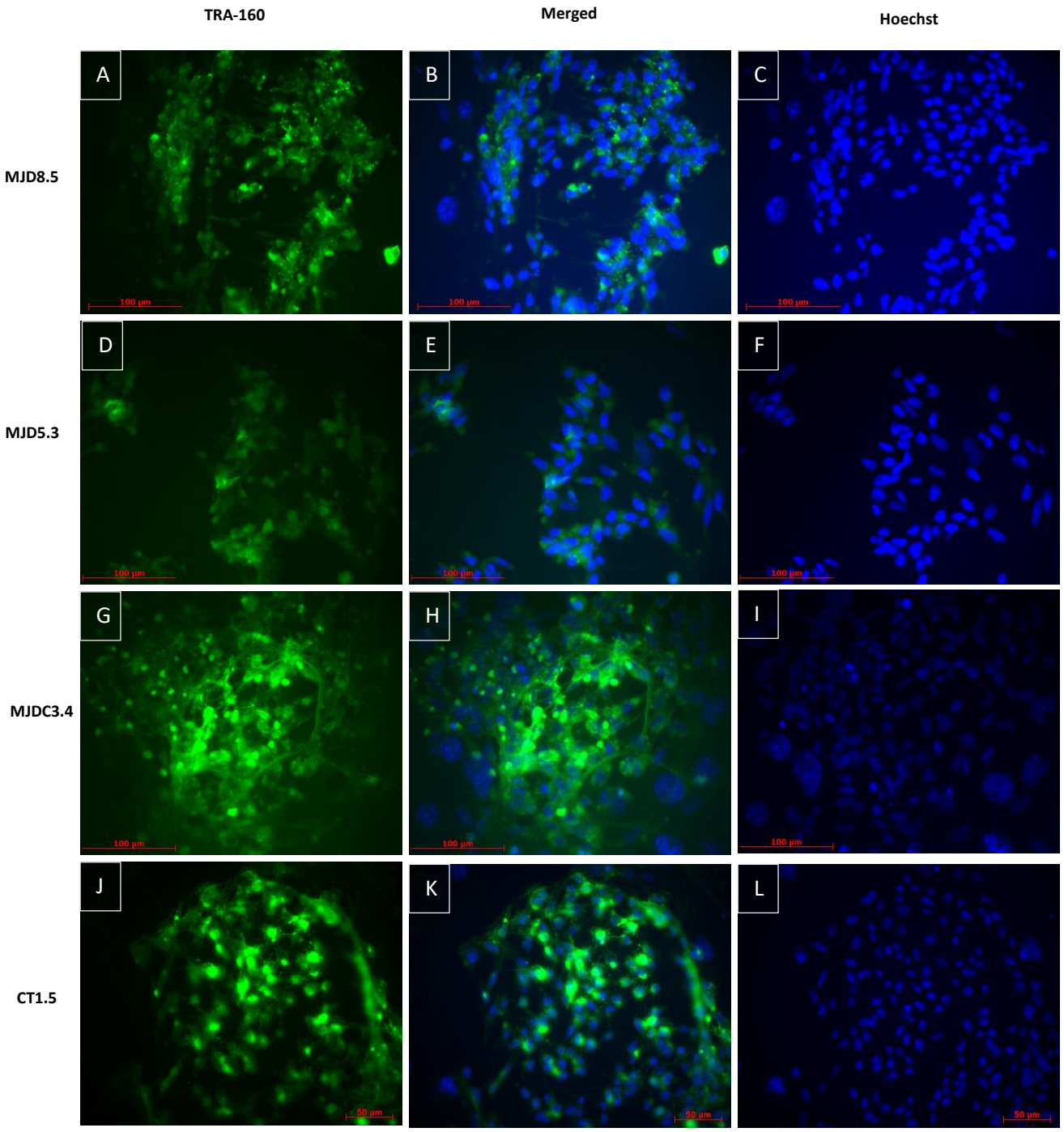

Figure 3.8. Immunocytochemistry staining showing iPSC colonies expressing the TRA160 protein and its localization. TRA160 was positively expressed by all iPSC lines (A,D,G,J). The merged, TRA160 and Hoechst (B, E, H & K) display the cell surface localisation of TRA160. Figures C, F, I &L, show Hoechst stain. Images were taken using an inverted Zeiss fluorescence microscope using a Alexa488 channel for TRA160 and merged, DAPI channel for Hoechst.

3.2.2.3 Expression of pluripotency gene markers in iPSC colonies using qRT-PCR.

The gene markers provide additional support for the pluripotent state. Expression of pluripotency markers was confirmed and validated using Real-Time Quantitative Reverse Transcription (qRT-PCR) as described in section 2.3.5.3. Briefly, iPSCs were cultured on Geltrex-coated dishes in E8-supplemented medium under feeder-free conditions. RNA was extracted from cell pellets, and MMLV-RT was used to synthesise cDNA. Thereafter, qRT-PCR analysis was performed to assess relative gene expression with β-glucuronidase (GUSβ) serving as a housekeeping gene. A non-iPSC control (CT1.5 iMSC) was used as a calibrator.

The analysis of the pluripotency gene markers on the iPSCs validated the immunocytochemistry results. iPSC cells exhibited positive and relatively higher expression levels of the stem cell markers NANOG, OCT3/4 and SOX2 compared to CT1.5 iMSC-sample (Figure 3.9). Overall, the expression level of SOX2 was higher in the control MJDC3.4, and patient iPSC samples, compared to NANOG and OCT3/4.

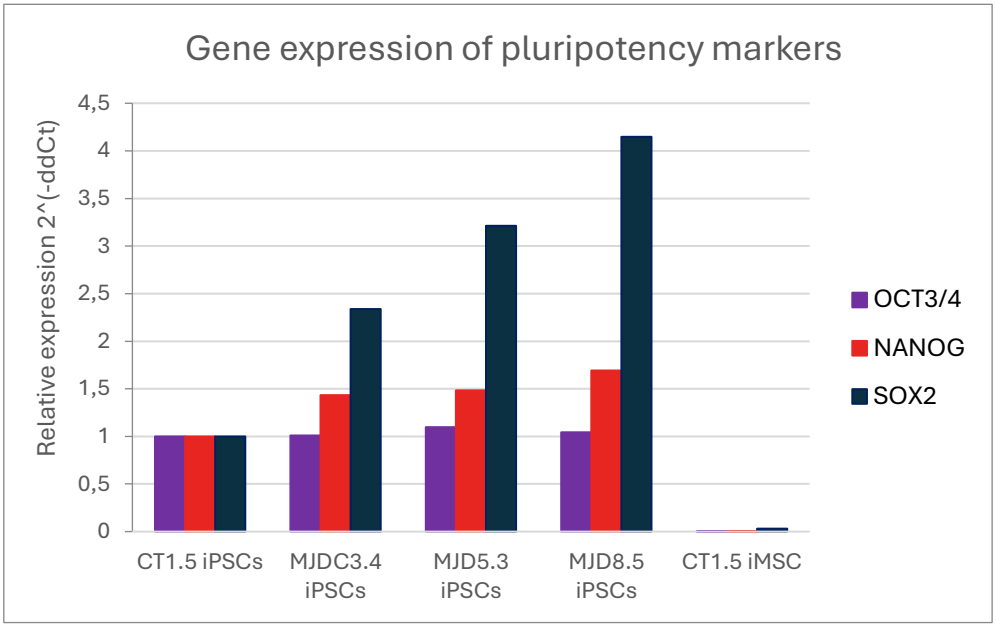

Figure 3.9. qRT-PCR analysis indicating the expression of pluripotency gene markers (NANOG, OCT3/4 and SOX2) in iPSC colonies compared to a non-iPSC line. All four iPSC lines showed relatively higher expression levels of stem cell markers compared to the control sample. Human GUSβ was used as a housekeeping gene and qRT-PCR performed using the StepOne instrument, using SYBR green. (n=1)

3.2.2.4 *In vitro* differentiation

One of the defining characteristics of iPSCs is their ability to differentiate into the three embryonic germ layers, mesoderm, endoderm and ectoderm. In brief, iPSCs were subjected to directed differentiation via embryoid body (EB) formation along the three lineages as described in the methods section 2.3.5.2. EBs formed from iPSC patches were differentiated in lineage specific medium. After 16-21 days of differentiation, cell outgrowths stemming from the EBs were observed in each of the three lineage-specific cultures (ectodermal (Figure 3.10), mesodermal (Figure 3.12), and endodermal (Figure 3.14).

3.2.2.4.1 Ectodermal differentiation

After 16 days in the ectodermal specific medium, cell outgrowths resembling dendritic or neuronal structures were observed when viewed under the EVOS Light microscope. They presented as long strings seen growing out of the EBs branching across the dish (Figure 3.10, black box). Cell clustering was observed immediately surrounding the EBs (Figure 3.10, black arrow).

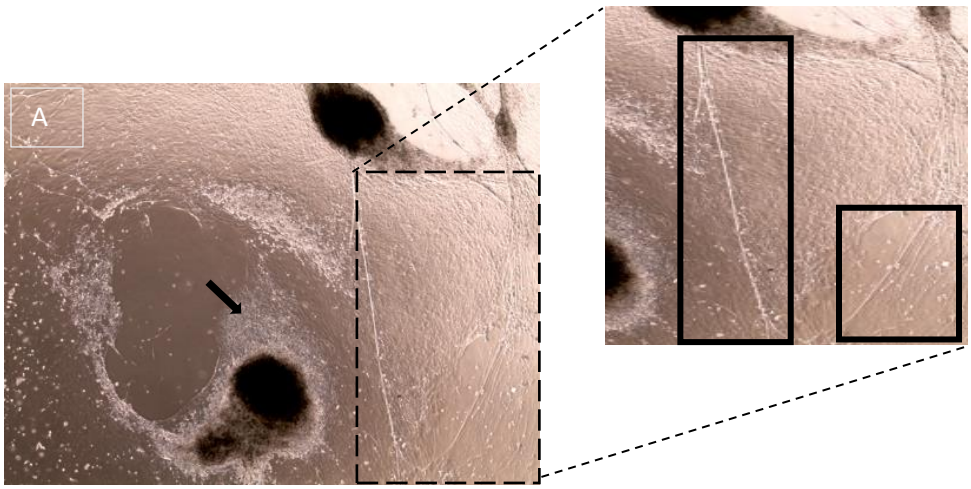

Figure 3.10. Visualisation of ectodermal cellular organisation after 16 days of *In vitro* differentiation. Cell outgrows were observed, with neuronal structure formation from the EBs. Images taken by an EVOS microscope at 4x objective magnification.

Immunocytochemical staining was used to determine protein expression and localisation specific to each lineage. Staining targeted the neuronal microtubule protein β class II tubulin (βIII-tubulin) which is a marker of an ectodermal lineage; Figures 3.11 A, D & G showed positive βIII-tubulin staining representing the ectodermal differentiation. The βIII-tubulin was also shown to be localised in the cell cytoplasm as reflected by the green stain surrounding the blue Hoechst stain, nuclear stain.

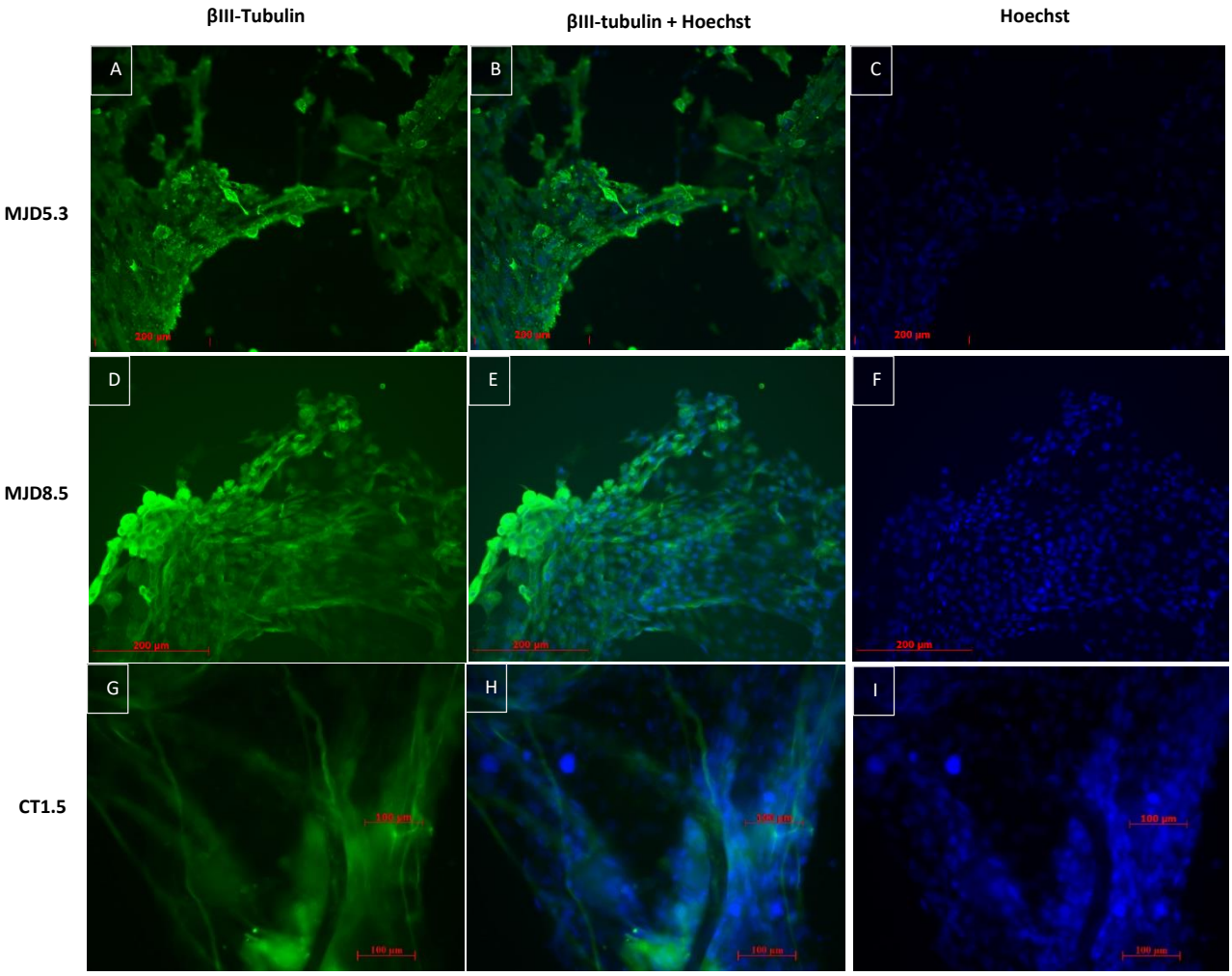

Figure 3.11. Immunocytochemistry staining displaying a successful *In vitro* differentiation of iPSCs towards the ectoderm lineage. The cells stained positive for neuronal microtubule protein β class II tubulin (βIII-tubulin) (A , D, G). The merged images (B, E, H) display the βIII-tubulin fibres arrangement in the cell cytoplasm. The Hoechst images (C, F, I) are displaying the cell nucleus. Images were taken using an inverted Zeiss fluorescence microscope using a Alexa488 channel for βIII-Tubulin and merged, and a DAPI channel for Hoechst.

3.2.2.4.2 Mesodermal differentiation

After 16 days in culture with mesodermal lineage-specific medium, small cells emerging from the EBs formed a densely packed monolayer which took on a mat-like appearance around the EBs (Figure 3.12). Images taken by an EVOS microscope at 4x objective magnification.

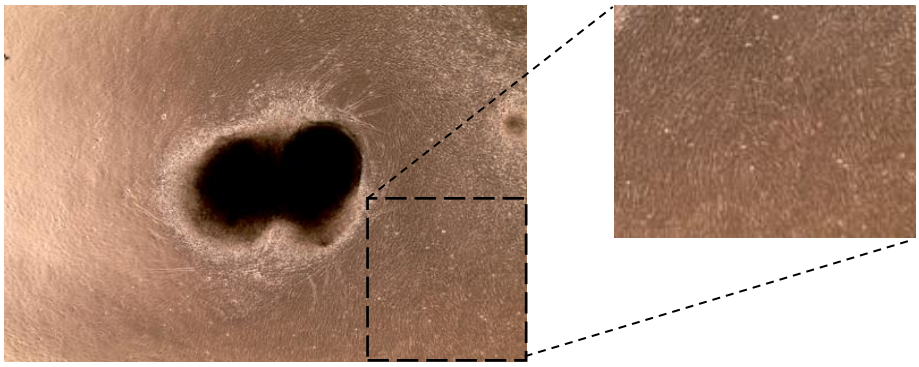

Figure 3.12. Visualisation of mesodermal cellular organisation after 16 days of In vitro differentiation. Cells cultured from the EBs were small and highly confluent. Images taken by an EVOS microscope at 4x objective magnification

Immunocytochemistry was performed to determine protein expression and localisation of the Alpha Smooth Muscle Actin (αSMA). The cells tested positive for αSMA (Figure 13 A, D). The merged images (Figure 13 B, E) showed how αSMA fibres were expressed in the cell cytoplasm, while the Hoechst images (Figure 13 C, F) showed the cell nuclei. Images were taken using an inverted fluorescent microscope. The Alexa488 channel was used to view and record the αSMA and merged images, and the DAPI channel was used to view and record the Hoechst images.

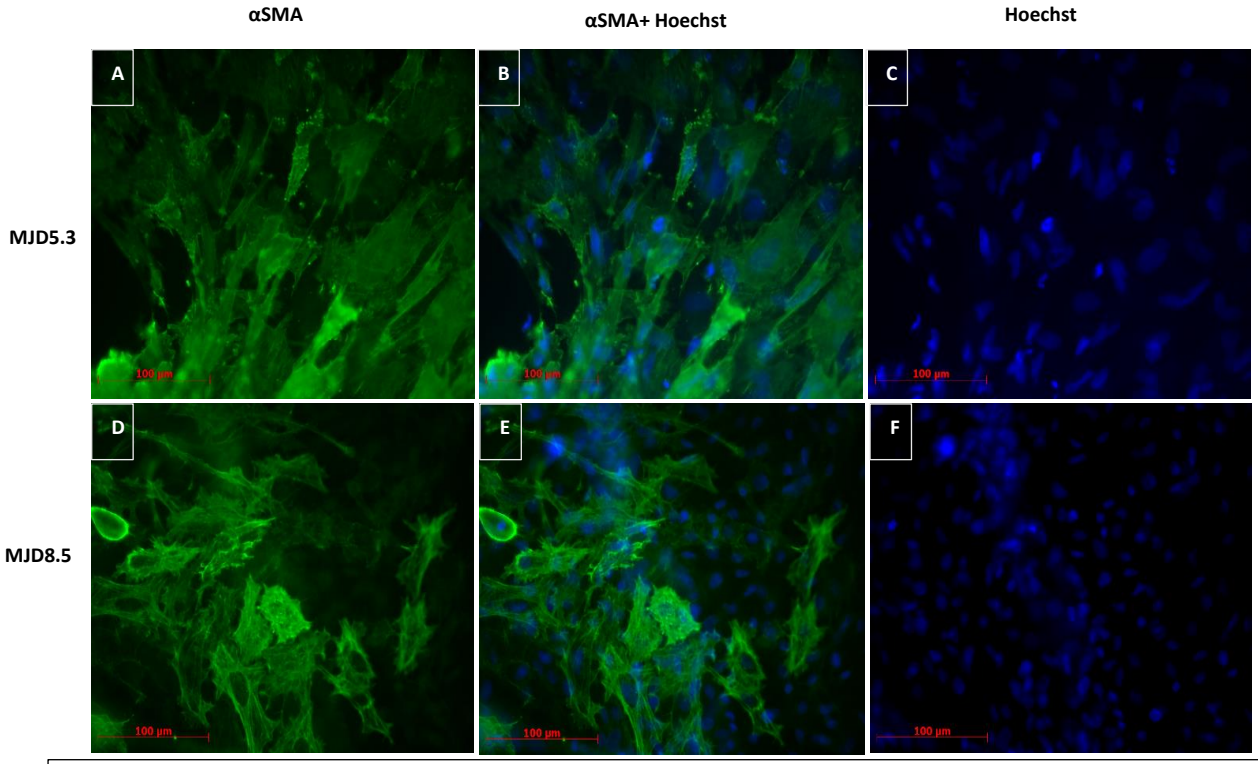

Figure 3.13. Immunocytochemistry staining displaying a successful *In vitro* differentiation of iPSCs towards the mesodermal lineage. The cells stained positive for Alpha Smooth Muscle Actin (αSMA) (A, D). The merged images (B, E) displaying the αSMA fibres arrangement in the cell cytoplasm. Hoechst images (C, F) showed the cell nuclei. Images were taken using an inverted Zeiss fluorescence microscope. The Alexa488 channel was used to view the αSMA and the DAPI channel was used for Hoechst.

3.2.2.4.3 Endodermal differentiation

After 21 days in the endodermal specific medium, cell outgrowths exhibiting a variety of cell types were observed when viewed under the EVOS Light microscope. Most prominent were layered sheets of flat, tightly packed cells adhering to the dish surface (Figure 3.14, Black block). Another observed feature was the loosely attached mesh-like layers comprising varying cell shapes (Figure 3.14, red block).

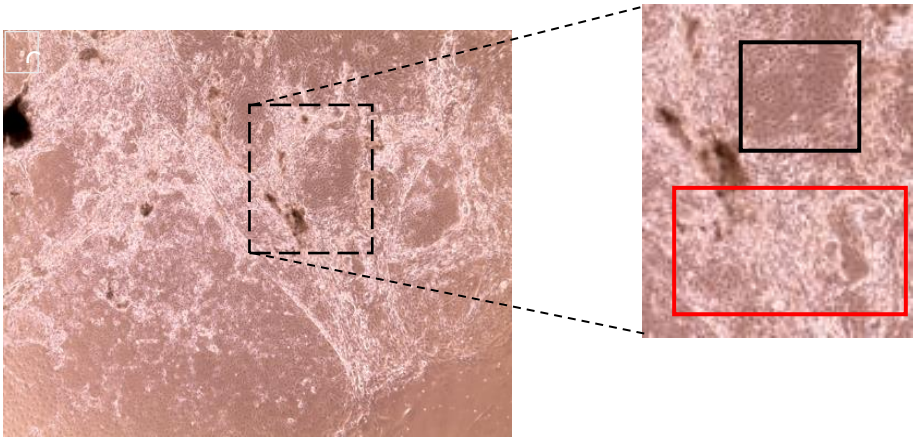

Figure 3.14. Images of endodermal cell morphology and organisation after 16 days of *In vitro* differentiation. A mixture of cell types was observed with layered sheets of flat tightly packed cells adhering all around the dish surface (Black block). Images taken by an EVOS microscope at 4x objective magnification

With immunocytochemistry staining, the transcription factor Forkhead box protein A2 (FOXA2) expressed in endodermal lineage was positively stained and was localised in the cell nuclei (Figure 3.15 A, D).

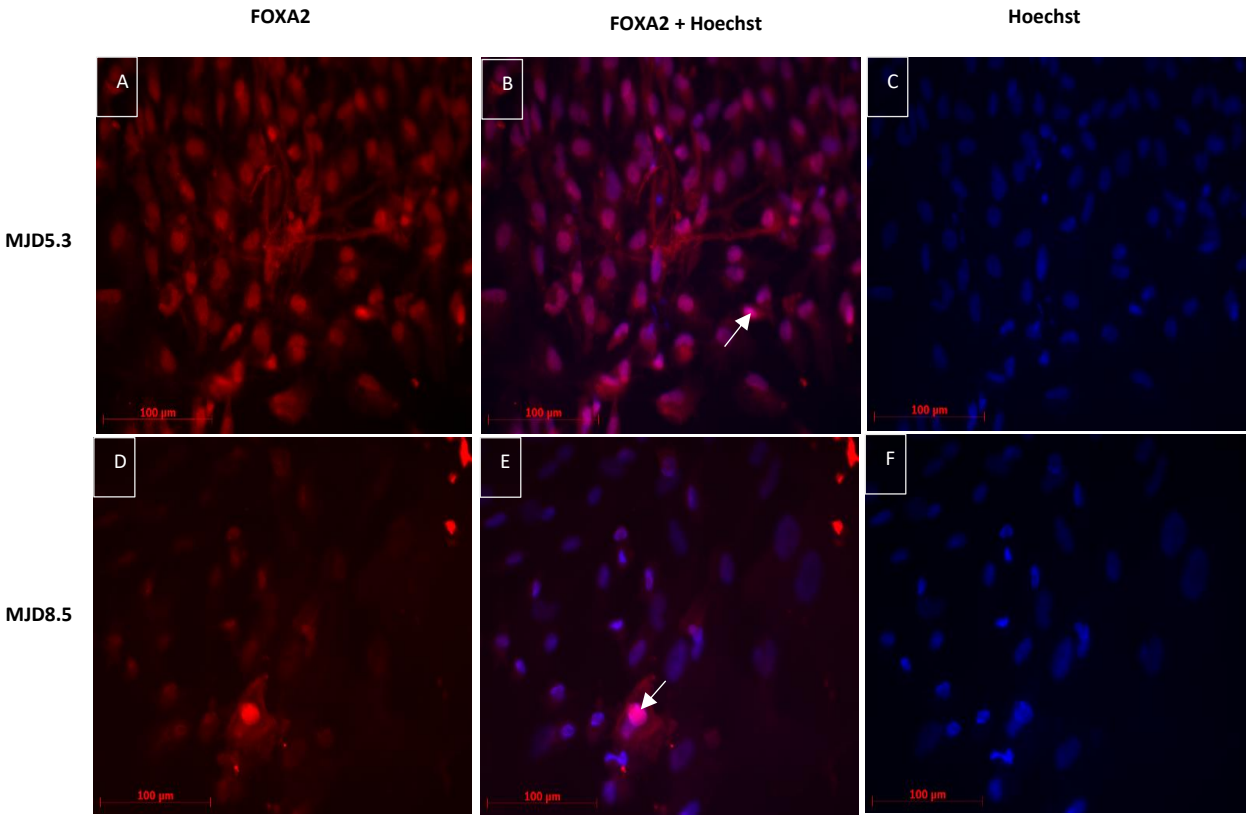

Figure 3.15. Immunocytochemistry staining showing a successful *In vitro* differentiation of iPSCs towards the endoderm lineage. After 16 days of differentiation, positive staining for the transcription factor Forkhead box protein A2 (FOXA2) (A, D) was observed. The merged images (B, E) displayed the nuclei localization of FOXA2. The Hoechst images (C, F) displayed the cell nucleus. Images were taken using an inverted Zeiss fluorescence microscope. The FOXA2 and merged images were viewed using the Cy3 channel, and the DAPI channel used for the Hoechst images.

3.2.3 Concluding remarks

All the colonies showed the typical iPSC morphological characteristics being rounded with well-defined edges with a big nucleus to cytoplasm ratio when cultured on feeder layers. These colonies expressed the pluripotency protein markers, NANOG, OCT3/4 and TRA-160. The mRNA levels of the pluripotency gene markers were validated using qRT-PCR. Lastly, after *in vitro* differentiation in lineage-specific media for the three germ layers, MJD5.3 and MJD8.5 iPSC lines exhibited positive expression for germline proteins, βIII-Tubulin, αSMA, and FOXA2. In contrast, MJDC3.4 did not grow well in the *in vitro* culture and most of the cells lifted and died before they could be expanded. Nevertheless, the results from the other pluripotency indicators based on morphology and the presence of the pluripotency protein markers and their genes, indicated that MJDC3.4 was indeed pluripotent. Overall, these results combined, summarised in Table 3.1, support the conclusion that the iPSC colonies cultured for further investigation in this study retained pluripotency over 10 or more passages.

Table 3.1: Expansion and characterisation of iPSCs summarised results:

Sample ID	iPSC characterization		
	Gene expression Characterization. Quantification: NANOG, OCT3/4 and TRA-160 (qRT-PCR)	Protein expression: Nanog, OCT3/4 and SOX2 (ICC)	*In vitro* differentiation: Mesoderm, Ectoderm and Endoderm (ICC)
CT1.5	√	√	√ Not all images are shown
MJD5.3	√	√	√
MJD8.5	√	√	√
MJDC3.4	√	√	excluded

3.3 The derivation of mesenchymal stem cells from IPSCs

Having successfully derived and characterised iPS cell lines from fibroblasts of MJD patients and unaffected controls, the next objective of this study was to differentiate them into iPSC derived mesenchymal stem cells (also referred to as iMSCs in this dissertation). According to a useful summary by Dominici *et al.*, (2006), the iMSCs must meet three criteria in order to be considered mesenchymal cells. These are 1) an ability to adhere to plastic vessels in culture, 2) a positive expression of a specific subset of cell surface antigens (Ags) and 3) a multipotent differentiation potential. The approach used in this study was to derive MSCs from iPSCs using the method of Zhou *et al.*, (2018) and the mesenchymal phenotype was validated by checking for the criteria proposed by Dominici *et al.*, (2006).

3.3.1 iMSC derivation Protocol I

As described in Materials and Methods (Section 2.4.1), iPS cells grown on inactivated MEFs were transferred to E8 medium on Geltrex coated dishes. The cells were sub-cultured several times in E8 medium until the inactivated MEFs were totally removed and a homogeneous iPSC culture remained.

Medium was switched to low-glucose DMEM supplemented with serum and antibiotics (MSC medium) to derive the iMSCs in a feeder free environment.

Using the method of Zhou *et al.*, (2018), MJD8.5 iPS cells growing in E8 medium were switched to MSC medium. Morphological changes were observed within 6 hours after the medium switch (Figure 3.16 A). The well-defined borders and compact colony morphology was lost, resulting in rough-edged formations and a colony structure that became less cohesive (red arrows shown in Figure 3.16 A). By day 2, the cells were becoming flatter and adhered tightly to each other, creating a continuous monolayer without any significant gaps or clustering and covering about 80% of the dish surface (Figure 3.16 B). By day 2 it was evident that the cells had lost their characteristic high nucleus-to-cytoplasm ratio typical of iPSCs.

By day 14, the MJD8.5 cultures were confluent with some cell clusters reaching over 100 % confluency. About 60% of the cells in the dish were hexagonal with clear, tight cell-to-cell interactions (Figure 3.16 C - expanded images indicated by yellow arrows). The cells remained adherent to the dish and showed no signs of detachment despite the high density of the culture. On day 14, the cells were sub-cultured at a ratio of 1:3. Seven days later (day 21), a visual evaluation (assessment) of the dish showed that about 30% of MJD8.5 cultures had formed tight cell-clusters with the remainder of the cells forming a monolayer as indicated by the white arrows (Figure 3.16 D).

As the cultures proliferated, consecutive passaging was performed to allow for the gradual maturation of the immature iMSCs and to promote the emergence of the mesenchymal phenotype. From P0 to P1, MJD8.5 cells were passaged onto gelatine-coated dishes at a seeding density of 1 x10^4 cells/cm^2. After 48 hours, only about 40% of the cells re-adhered. These cells were predominately flat and broader in shape and appeared to extend dendrites out to neighbouring/adjacent cells (Figure 3.16 E). The cells were less dense than expected and as a result, fewer cells were present on the dish at the end of the 7-day period for P1. The cells were passaged at the end of the 7-day timeframe despite the lower confluency.

Between P2 and P3, MJD8.5 cells continued to proliferate and mature, displaying four very distinct morphologies: some were spindle – shaped, broad and flat, some long and flat and some more round and flat (Figure 3.16 F). At P4, the MJD8.5 cells started to show morphological characteristics typical of mesenchymal stem cells (Figure 3.16 G). The majority of these cells were spindle shaped, elongated and uniform in both size and shape.

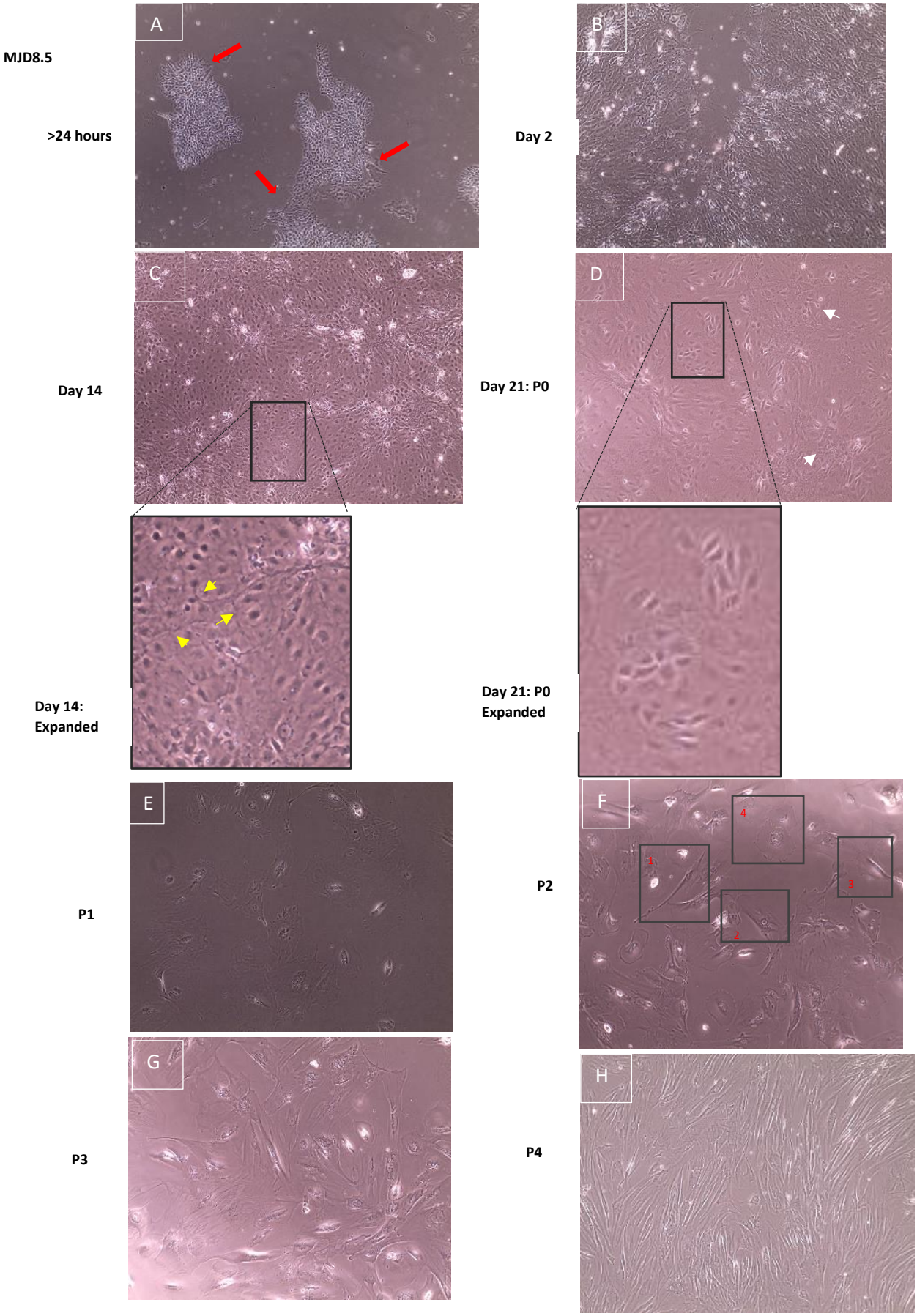

Figure 3.16. Morphological changes of MJD8.5 iPSC colonies during the derivation of iMSCs using Protocol I. Changes were observed A) - within 6 hours (day 0), B) on day 2, C) day 14, D) day 21 which is also referred to as P0, E) at passage 1, F) at passage 2, G) at passage 3, and H) at passage 4. Images taken by an EVOS microscope at 10x objective magnification

The MJD5.3 cells were switched onto MSC medium as done with MJD8.5. Similar changes were observed in MJD5.3 cells as they transitioned from an iPSC phenotype to an immature iMSC phenotype (Figure 3.17 A-D) with randomly dispersed spindle shaped cells observed on day 14 (Figure 3.17 C – white arrow). As observed in MJ8.5 cells, MJD5.3 cells displayed a hexagonal shape at P0 and presented with tight cell-cell interaction across the culture dish. Cells that did not take up the hexagonal shape were seen to be rounder in shape (Figure 3.17 D). The MJD5.3 cultures developed the four very distinct morphologies seen in MJD8.5 between P2 and P3 at P1 (Figure 3.17 E). These cells later developed more of a spindle/elongated shape by P2 (Figure 3.17 F). The mesenchymal phenotype became more pronounced by P3 and P4 (Figure 3.17 G and K).

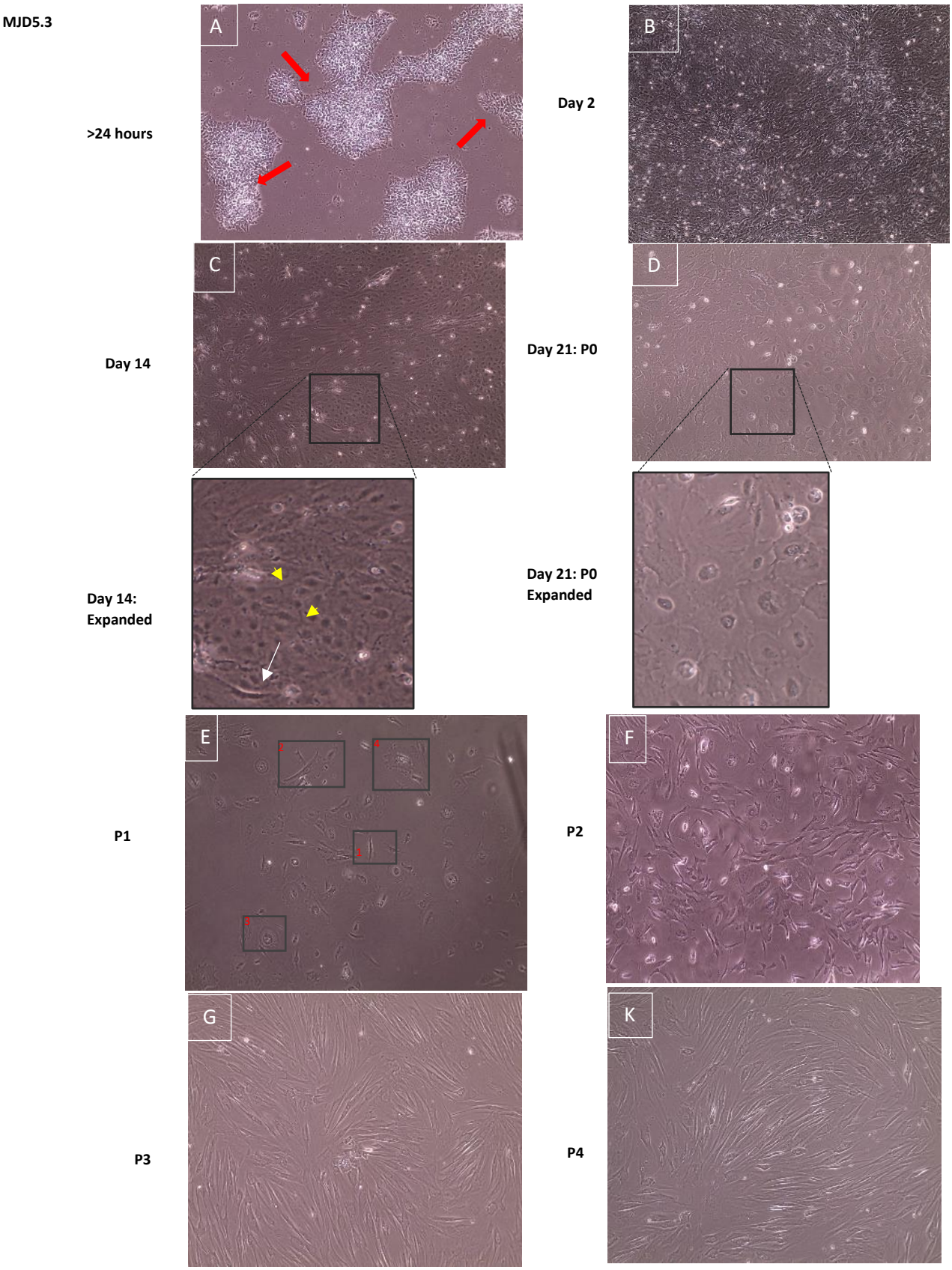

Figure 3.17. Morphological changes MJD5.3 iPSC colonies during the derivation of iMSCs using Protocol I. Changes were observed A) - within 6 hours (day 0), B) on day 2, C) day 14, D) day 21 which is also referred to as P0, E) at passage 1, F) at passage 2, G) at passage 3, and H) at passage 4. Images taken by an EVOS microscope at 10x objective magnification.

MJDC3.4 (Figure 3.18 A-C) shows a similar pattern of cell transition as was observed for MJD8.5. However, immediately after the medium change at D0, a significant number of cells detached and floated into the medium. By day 2, the remaining cells migrated slowly across the dish surface, covering approximately 70% of the dish. Following the 1:3 ratio split on day 14, the MJDC3.4 seeding efficiency was low, which then resulted in cultures reaching only 50-60% confluency by the end of P0 (7 day) culture.

The MJDC3.4 also displayed various cell morphologies across the passages, similar to both MJD5.3 and MJ8.5. However, some cells appeared slightly larger compared to those observed in MJD5.3 and MJD8.5 cultures. MJDC3.4 became spindle shaped at P1 and fully adopted the mesenchymal phenotype by P2 (Figure 3.18F) compared to MJD5.3 which displayed the mesenchymal phenotype at P3.

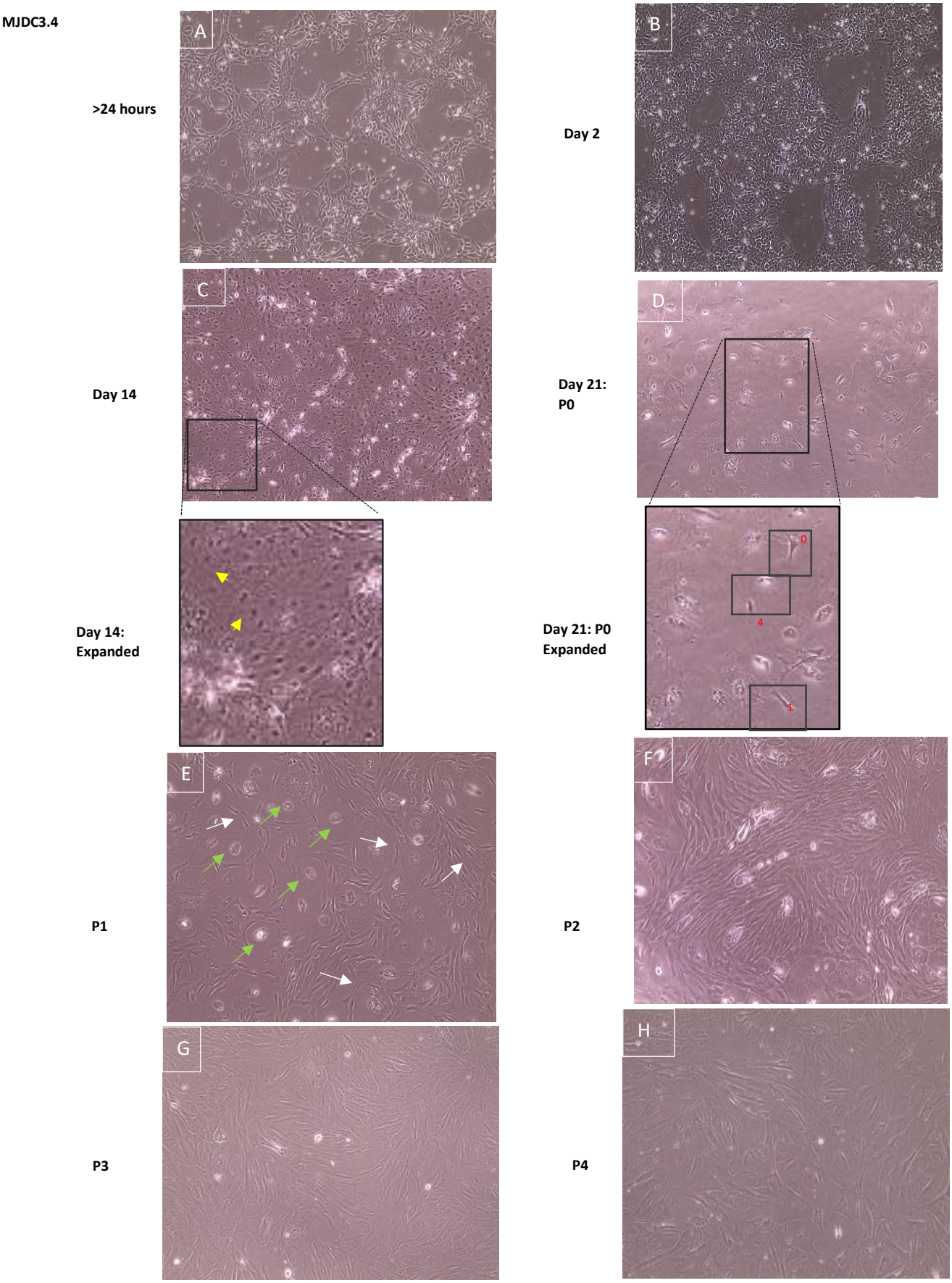

Figure 3.18. Morphological changes of MJDC3.4 iPSC colonies during the derivation of iMSCs using Protocol I. Changes were observed A) - within 6 hours (day 0), B) on day 2, C) day 14, D) day 21 which is also referred to as P0, E) at passage 1, F) at passage 2, G) at passage 3, and H) at passage 4. Images taken by an EVOS microscope at 10x objective magnification.

Culturing iPSCs in a feeder free environment was challenging and required several attempts before homogeneous iPSC cultures were obtained.

For example, as seen in Figure 3.16, the CT1.5 colonies exhibited differentiated cells within the colonies (Figure 3.19, area with the brown arrow). Similar issues occurred with the other MJD cell lines; however, successful colonies were eventually obtained (Will be discussed further in Discussion).

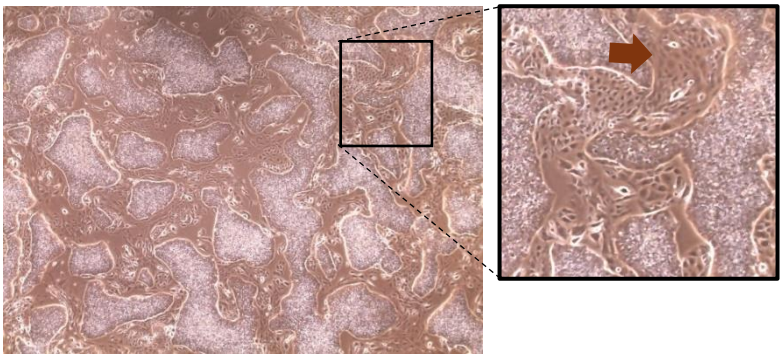

Figure 3.19. Feeder-free culture of CT1.5 showing differentiated cells between colonies. A typical feeder free iPSC-culture needing further optimization. Images captured by an EVOS microscope at 4x objective

Ultimately, similar mesenchymal morphological characteristics to those observed in the MJD8.5 trial sample were also displayed by the CT1.5 cell line at P3 (Figure 3.20).

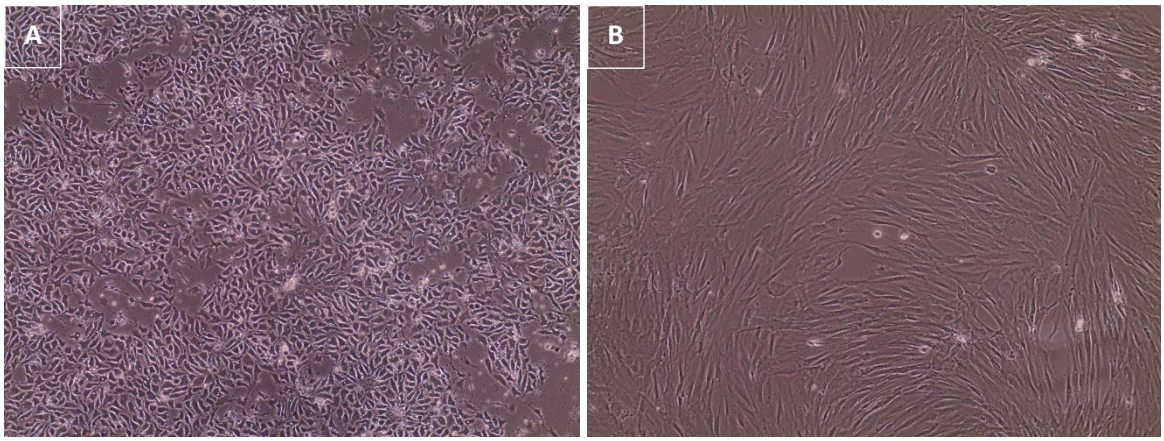

Figure 3.20. Morphological differences during iMSC derivation using Protocol I. A) CT1.5 at day 0, and B) at passage 3. Images taken by an EVOS microscope at 10x objective magnification.

3.3.1.1 Characterisation of iPSC induced mesenchymal stem cells (iMSCs)

Following the emergence of the mesenchymal phenotype, they were passaged, and RNA was extracted from cells at P3 and P4. qRT-PCR analyses were performed to determine the expression of pluripotent gene markers as well as the cluster of differentiation (CD) markers that are associated with mesenchymal stem cells.

The expression of the pluripotent gene markers, NANOG, SOX2 and OCT3/4, were evaluated for CT1.5, MJDC3.4 and MJD5.3 iMSC samples and compared with their expression in the iPSCs samples. The gene expression was calculated using the 2^{-DDCt} as described in section 2.3.5.3.5 and the results are presented in Figure 3.21. As can be seen, there is positive expression of all three pluripotency markers in the iPSCs in contrast to the iPSC-derived MSCs, where no expression was detected.

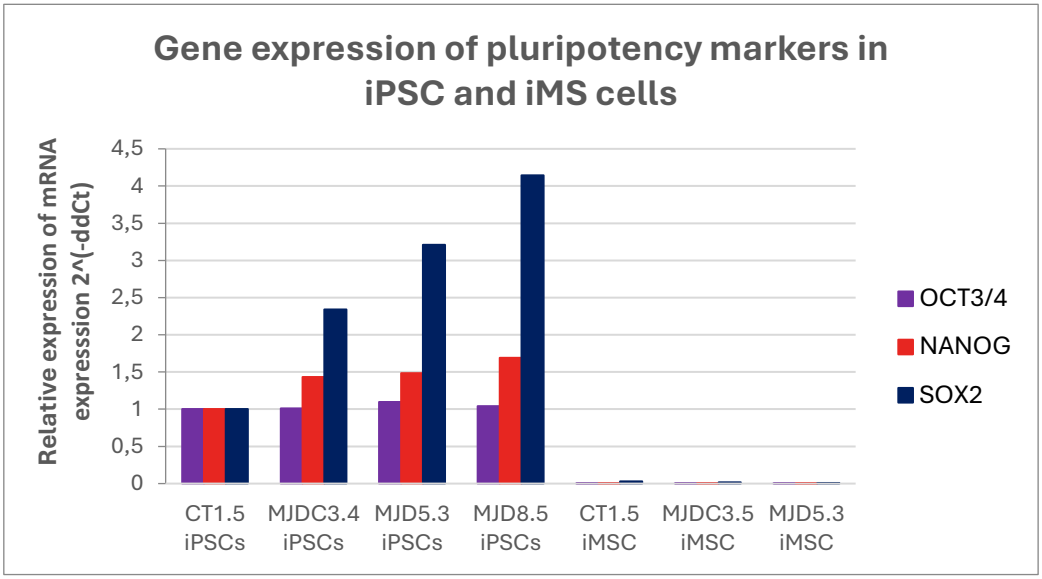

Figure 3.21. qRT-PCR analysis of pluripotency gene markers (NANOG, OCT3/4 and SOX2) in iPSC cells compared to iMSC derived iMSCs. Human GUSβ was used as housekeeping gene, and qRT-PCR performed using the StepOne instrument, using SYBR green. The CT1.5 iPSC sample was used as a calibrator. Technical repeats: 1 (n=1).

To determine whether the cells expressed the mesenchymal markers CD73 and CD90, qPCR analysis was conducted using appropriate primers. As can be seen in Figure 3.22, all three cell lines (CT1.5, MJDC3.4 and MJD5.3) expressed CD73.

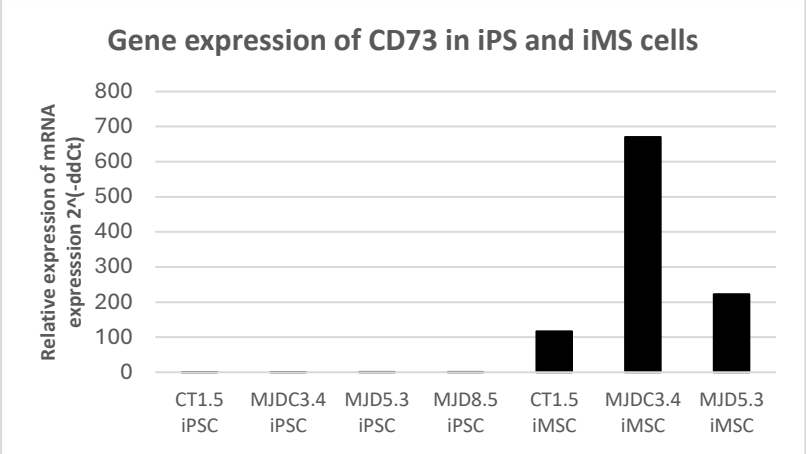

Figure 3.22. Expression levels of CD marker, CD73, in iPSC and iMSC cells using qRT-PCR analysis. Low levels of CD73 were observed in all the iPSC lines, while iMSCs exhibited relatively higher expression levels of CD73. Human GUSβ was used as a housekeeping gene, and qRT-PCR performed using the StepOne instrument, using SYBR green. The CT1.5 iPSC sample used as a calibrator. n=1.

CD90's results were inconclusive. Both the C_t values and expression levels displayed by the graph for the iMSC cells were similar to those expressed by the iPSC cells (Figure 3.23). C_t values are shown in the Table 3.2.

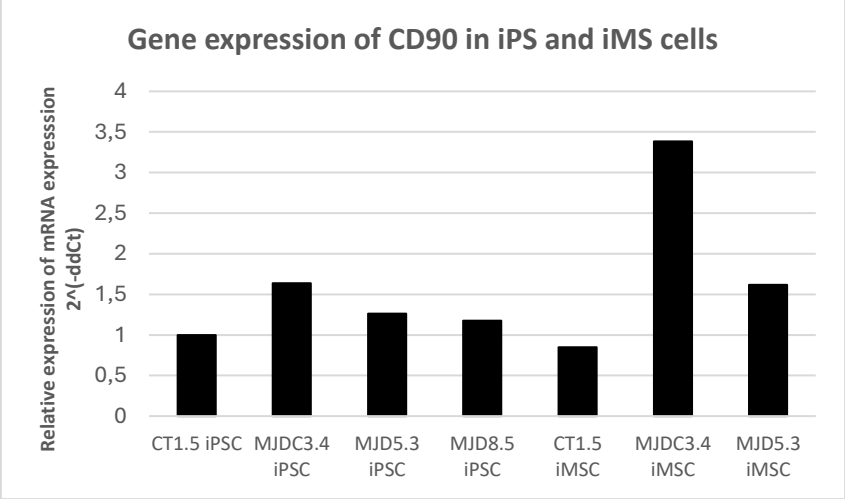

Figure 3.23. Expression levels of CD marker, CD90, in iPSC and iMSC cells using qRT-PCR analysis. The expression levels observed in CD90 were similar in both iPSCs and iMSCs. Human GUSβ was used as a housekeeping gene, and qRT-PCR performed using the StepOne instrument, using SYBR green. The CT1.5 iPSC sample used as a calibrator, n=1.

Table: 3.2: C_t values of CD90 of both iPSC and iMSC cells.

Sample	CD90 C_t mean values	GUSβ C_t mean values
MJDC3.4 iPSC	15,45072	23,105
CT1.5 iPSC	14,64672	21,77904
MJD5.3 iPSC	16,46507	24,25368
MJD8.5 iPSC	15,8964	23,14506
MJDC3.4 iMSC	15,78404	24,46862
CT1.5 iMSC	16,93322	23,8774
MJD5.3 iMSC	16,17139	23,86417

Subsequent to this finding, it was established that although CD90 is commonly used as a positive marker for MSCs it has been observed to be expressed in iPSCs (Wang et al., 2011).

A third CD marker, CD105, known as an endoglin, is a transmembrane glycoprotein that is expressed in MSCs was also tested. The results show higher levels of expression in iMSCs compared to iPSCs (Figure 3.24).

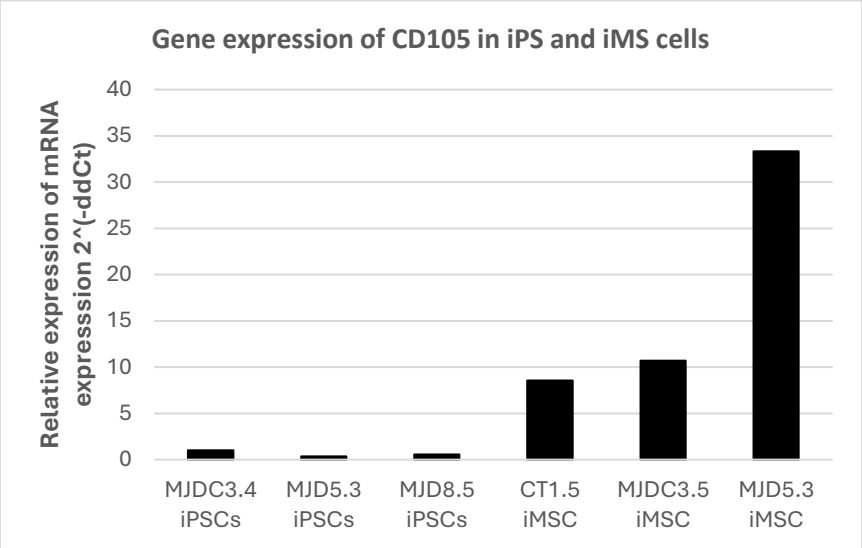

Figure 3.24. Expression levels of CD105 in iPSC and iMSC cells using qRT-PCR analysis. MJDC3.4 iPSC sample used as a calibrator and qRT-PCR was performed using the StepOne instrument, using SYBR green, n=1.

To accurately characterize iMSCs, Dominici *et al.*, (2006) indicated that to be mesenchyme stem cells, not only must they express CD105, CD73 and CD90, they must also not express the hematopoietic markers such as CD45, CD34 and CD14 or CD11b, CD79a or CD19 and HLA-DR. For this project, the expression of CD45, CD34 and CD14 was therefore assessed using qRT-PCR.

Figure 3.25 and Table 3.3 demonstrates a relative expression of CD45, CD34 and CD14. However, the Ct values of these genes, CD45 and CD14, were found to be , with values in their 30s and approaching 40 cycles. The very high C_t value range indicated that the expression of these genes was nearly absent in both cell types, suggesting a lack or very low level of hematopoietic marker expression, characteristic of mesenchymal stem cells. CD34 on the other hand, had lower C_t values between 25 and 29, for both iPSCs and iMSCs samples, which is indicative of expression of this gene.

Table 3.3: C_t values of CD45, CD34 and CD14 of both iPSC and iMSC cells.

Gene			
CD45			
	Sample	Gene C_t mean value	GUSβ C_t value
	MJDC3.4 iPSC	32,53	23,10
	CT1.5 iPSC	34,13	21,78
	MJD5.3 iPSC	35,34	24,25
	MJD8.5 iPSC	34,16	23,14
	MJDC3.4 iMSC	32,68	24,47
	CT1.5 iMSC	35,41	23,88
	MJD5.3 iMSC	33,67	23,86
CD34			
	MJDC3.4 iPSC	28,23	23,11
	CT1.5 iPSC	27,52	21,78
	MJD5.3 iPSC	29,90	24,25
	MJD8.5 iPSC	28,71	23,15
	MJDC3.4 iMSC	28,16	24,47
	CT1.5 iMSC	28,24	23,88
	MJD5.3 iMSC	25,26	23,86
CD14			
	MJDC3.4 iPSC	33,29	24,76
	MJD5.3 iPSC	33,04	25,23
	MJD8.5 iPSC	32,15	25,85
	MJDC3.4 iMSC	31,85	28,22
	MJD5.3 iMSC	33,33	27,19

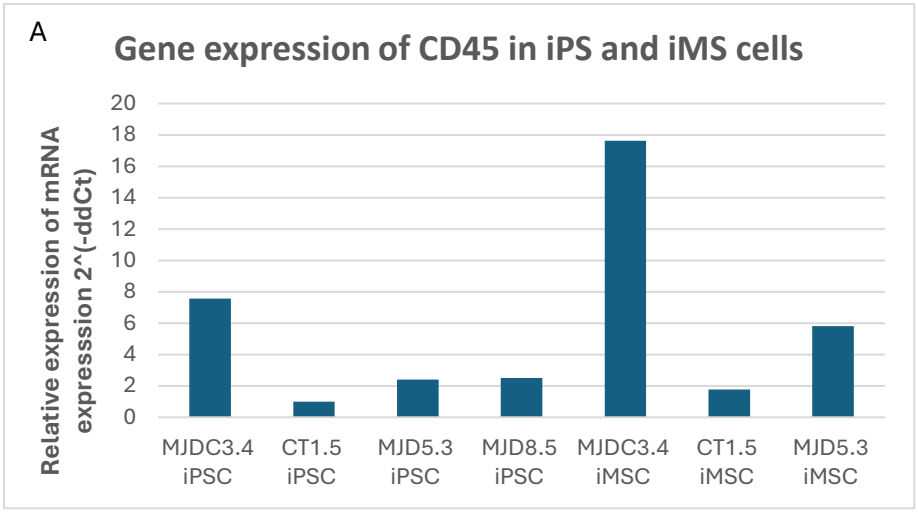

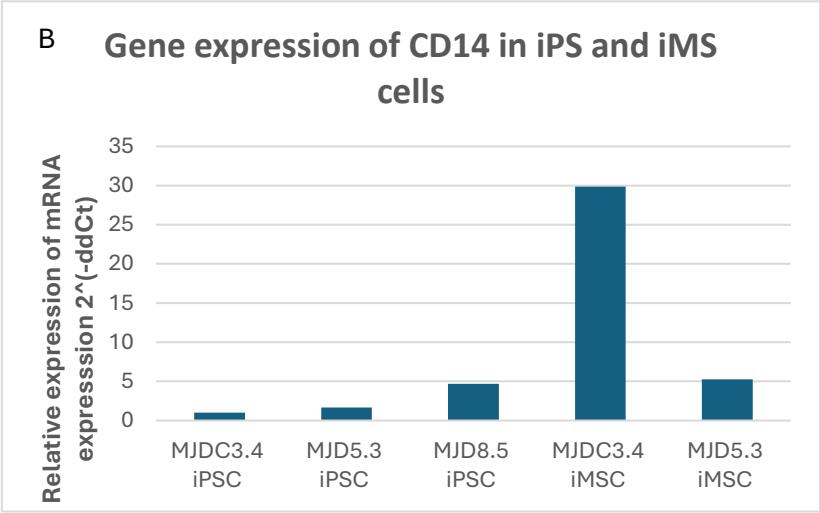

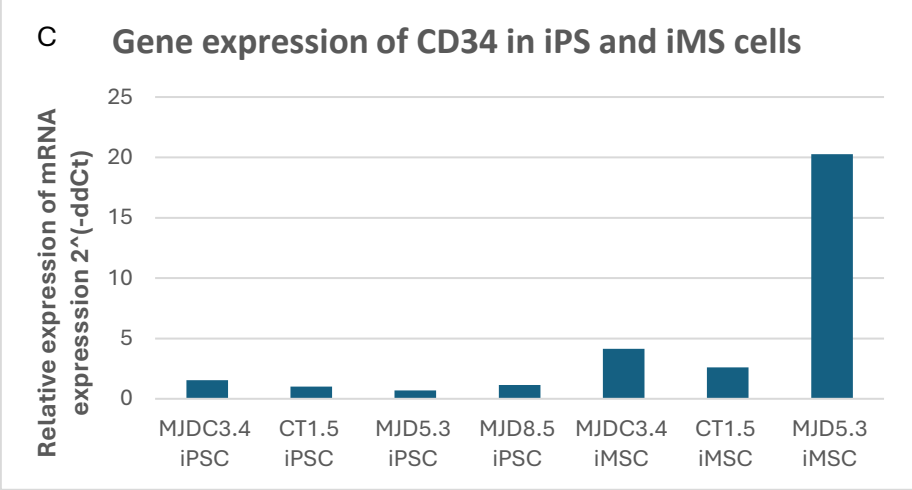

Figure 3.25. Expression levels of CD markers; CD45, CD34 and CD14, in iPSC and iMSC cells using qRT-PCR analysis. Similar expression levels of CD45 and CD14 were observed in both iPS and iMS cells, except in MJDC3.4 which seemed to have a higher expression in iMSCs. Elevated expression levels of CD34 were observed in iMSCs. Human GUSβ was used as a housekeeping gene, and qRT-PCR performed using the StepOne instrument, using SYBR green. The CT1.5 iPSC sample was used as a calibrator for CD45 and CD34, MJDC3.4 iPSC sample was used as a calibrator for CD14, n=1.

3.3.1.2 Trilineage differentiation of iPSC-derived MSCs

The ultimate test for the mesenchymal state is their ability to differentiate into various mesenchymal derivatives, including adipose tissue, bone and cartilage. To determine whether the derived iMSCs were multipotent, the induction of the trilineage differention was conducted and the cells analysed by histological staining and qRT-PCR. In the present study, only CT1.5 iMSCs were investigated.

To obtain the osteogenic lineage, iMSCs were cultured for 21 days in osteogenic differentiation medium made up as described in section 2.4.2.1 and included ascorbate, dexamethasone and glycerophosphate in DMEM basal medium. After 21 days, the non-induced (control) cells, cultured in low glucose iMSC medium, were typically spindle-shaped, and had a fibroblast-like morphology which was relatively uniform across the dish (Figure 3.26 A). In contrast, the osteogenically-induced cells lost their spindle-shape morphology (Figure 3.26 B). They formed cell clusters, indicated by the red box, and also produced fragments of bone matrix, which were absent in the non-induced samples (Figure 3.26 B – red arrows).

Alizarin Red S staining revealed that the non-induced control cells did not mineralize or produce calcium deposits, as no staining was observed (Figure 3.26 C). The osteogenically-induced cells displayed fragments that had a faint orange-red staining, indicating the presence of calcium in the extracellular matrix (deposit). This confirmed a successful differentiation into the osteogenic lineage (Figure 3.26 D – white arrows).

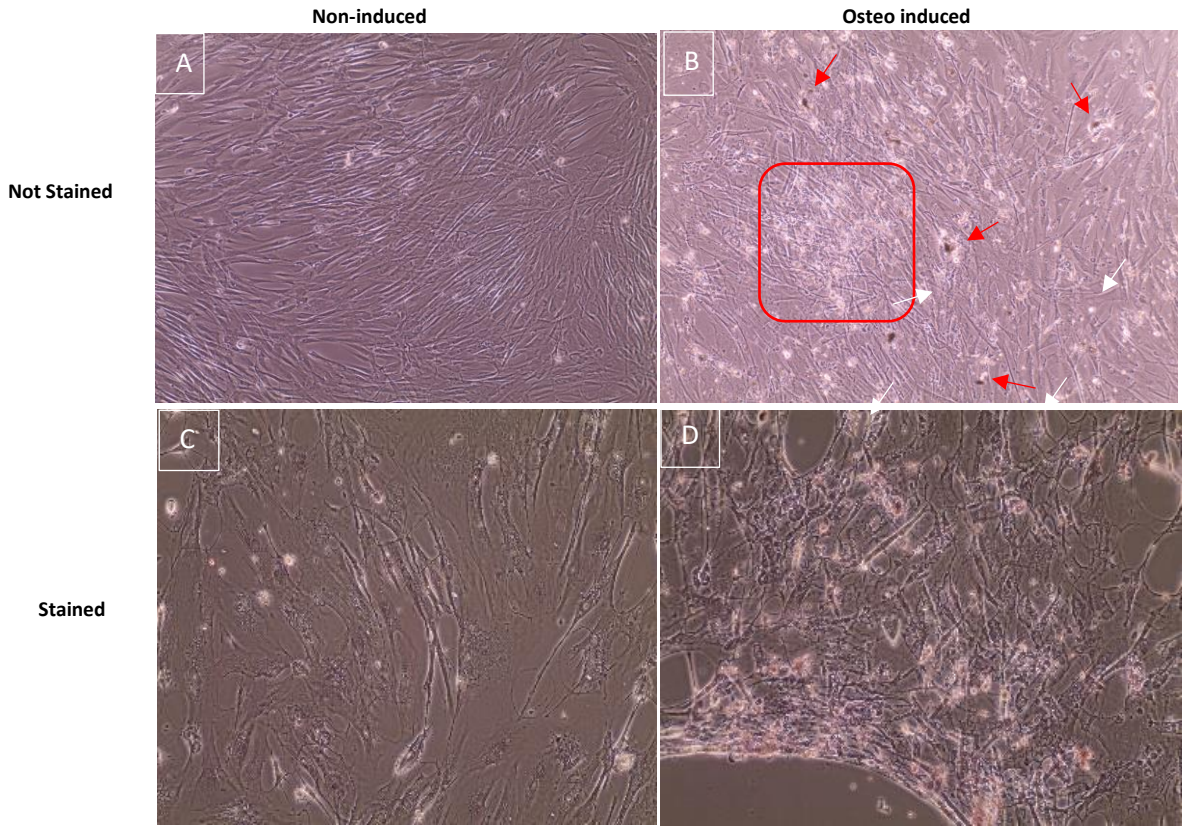

Figure 3.26. Morphology and Alizarin Red S staining of iMSCs after 21 days of differentiation towards the osteogenic lineage. Images show: A) day 21 of non-induced and B) induced cells before staining, while C) day 21 of non-induced and D) induced cells after staining. Images captured by an EVOS microscope at 10x objective magnification.

To obtain the adipogenic cells, iMSCs were cultured for 21 days in adipogenic differentiation medium containing IBMS, insulin, dexamethasone and indomethacin in DMEM basal medium. After day 21, while the control cells maintained their typically mesenchymal phenotype (Figure 3.27 A), when MSCs were induced to differentiate into adipogenic cells, the cells became larger and flatter (Figure 3.27 B - yellow arrows). Droplets or large vacuoles appeared in the cytoplasm, as seen by the green arrows, (Figure 3.27B).

On day 21, the Oil Red O staining confirmed the presence of lipid droplets in adipose-induced cells, with red lipid droplets visible inside the cells, clustering within the cytoplasm (Figure 3.27 D, white arrows). Staining was not visible in the control cells (Figure 3.27 C).

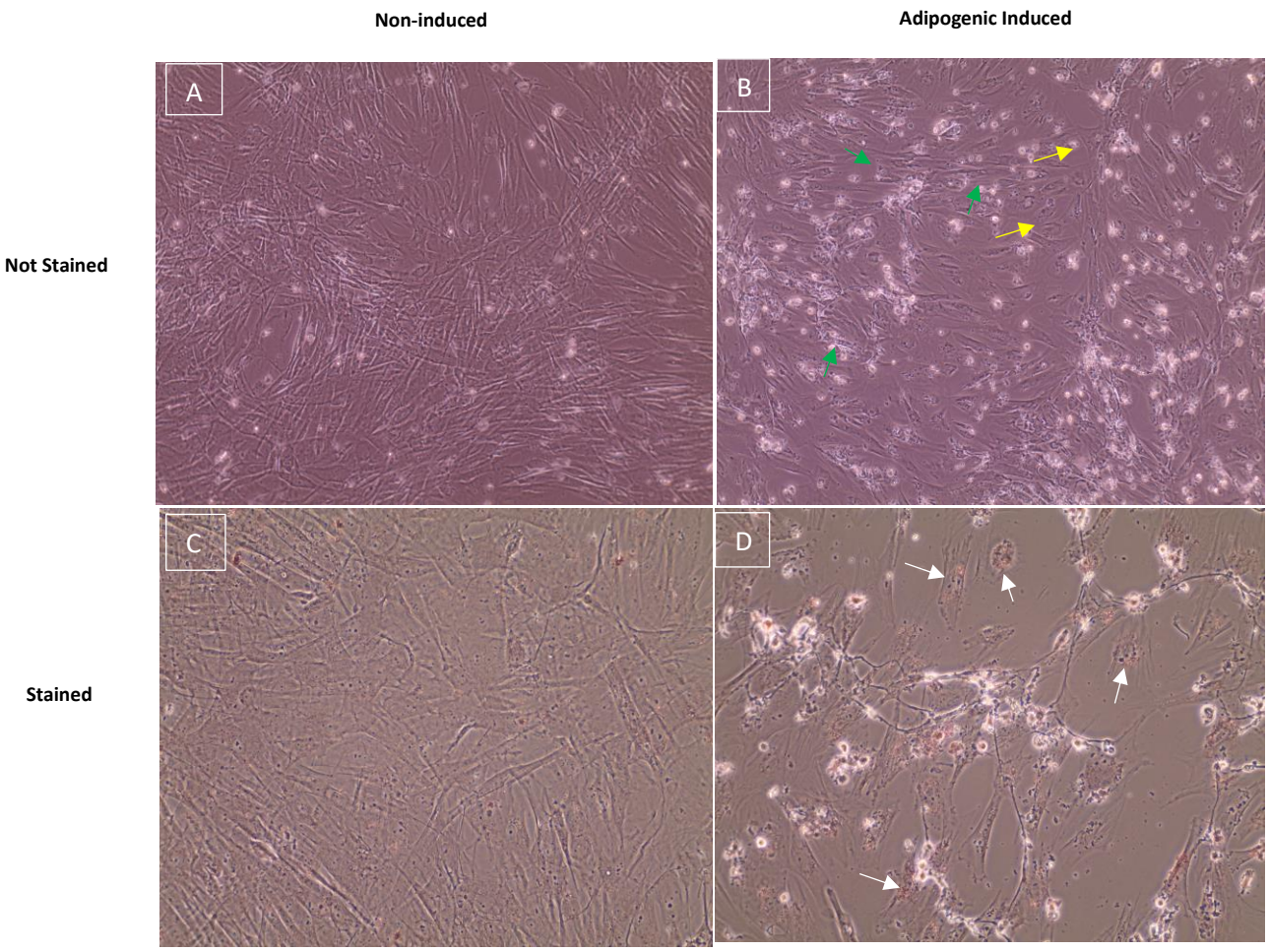

Figure 3.27. Morphology and Oil Red O staining of iMSCs after 21 days of differentiation towards the adipogenic lineage Images show: A) day 21 of non-induced and B) induced cells before staining, while C) day 21 of non-induced and D) induced cells after staining. Images captured by an EVOS microscope at 10x objective magnification.

Lastly, to obtain the chondrogenic cultures, micromasses were cultured in chondrogenic differentiation medium as described in section 2.4.2.2. Cells were grown in serum free medium containing TGFB3, BMP-2, dexamethasone, ascorbate-2-phosphate proline and pyruvate plus ITS in DMEM basal medium. In the control dish, cultured in low glucose iMSC medium, the cells adhered to the dish and created 'mounds' of cells. On day 21, staining with Alcian Blue O solution did not reveal significant observable differences in the presence of proteoglycans between the chondrogenically induced micromasses and the non-induced micromasses (Figure 3.28). The similar intensity of the blue stain in both cultures suggests that the duration of induction may have been insufficient for the cells to produce an extracellular matrix characteristic of cartilage.

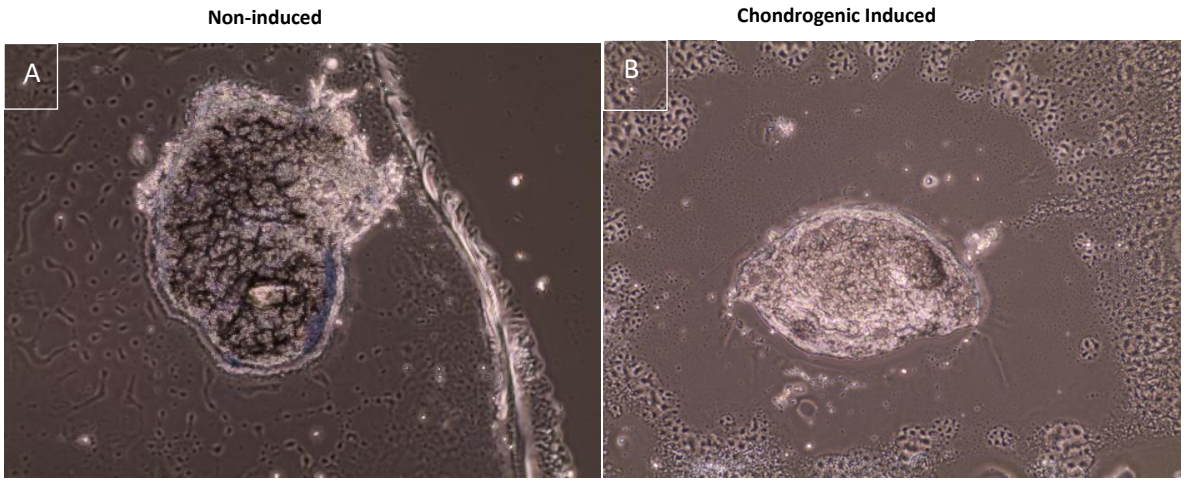

Figure 3.28. Alcian Blue staining of chondrogenically induced iMSCs at day 21. A) shows a non-induced mass of cells and B) shows an induced mass of cells after staining, with no significant observable difference. Images captured by an EVOS microscope at 10x objective magnification.

MJD8.5, MJD5.3, MJDC3.4 and CT1.5 displayed similar cellular and morphological transition patterns from iPSCs to iMSCs, eventually displaying a mesenchymal phenotype. As summarised in Table 3.4, the iMSCs observed, lacked the expression of pluripotency markers (NANOG, OCT3/4 and SOX2), had a positive expression of key mesenchymal CD markers (CD73, CD90 and CD105) and had low expression of the haematopoietic markers (CD34, CD45 and CD14). While using the trilineage differentiation trial process was carried out on CT1.5 iMSCs, they showed the potential to differentiate towards the osteogenic and adipogenic lineages and some potential towards the chondrogenic lineages. However, due to the weak Oil Red O staining and the weak Alizarin Red staining that was observed, an alternative approach was used in an attempt to improve the efficiency of the trilineage differentiation and hopefully increase the staining intensities with the special stains. In the subsequent experiments, StemPro Differentiation Media was used for the differentiation process.

Table 3.4 Summary of iMSCs characterization using the switch method by Zhou et al., (2018).

Sample ID	**iMSC characterization**			
	Morphological changes assessed as iPSCs differentiated towards iMSCs	**Gene expression Characterization - Positive expression of CD73, C90, and CD105 (qRT-PCR)**	**Gene expression Characterization - Low expression of CD45, CD34 and CD14. (qRT-PCR)**	**Trilineage differentiation: Osteogenic, Adipogenic, and Chondrogenic (Histology Staining)**
CT1.5	√	√	√ (except CD14)	√
MJD5.3	√	√	√	
MJD8.5	√		iPSCs only	
MJDC3.4	√	√	√	

3.3.2 Derivation of induced mesenchymal stem cells from induced pluripotent cells-Protocol II

The rationale behind the second protocol was as follows: On considering that both the iPSC lines growing on inactivated MEFs often started disaggregating within three days of plating (see section 3.2.2.1 above and Figure 3.29 below), the thought was that perhaps these colonies are starting to spontaneously undergo EMT to become mesenchyme cells. Since we wished to produced mesenchyme cells, maybe one could take advantage of this phenomenon and encourage it.

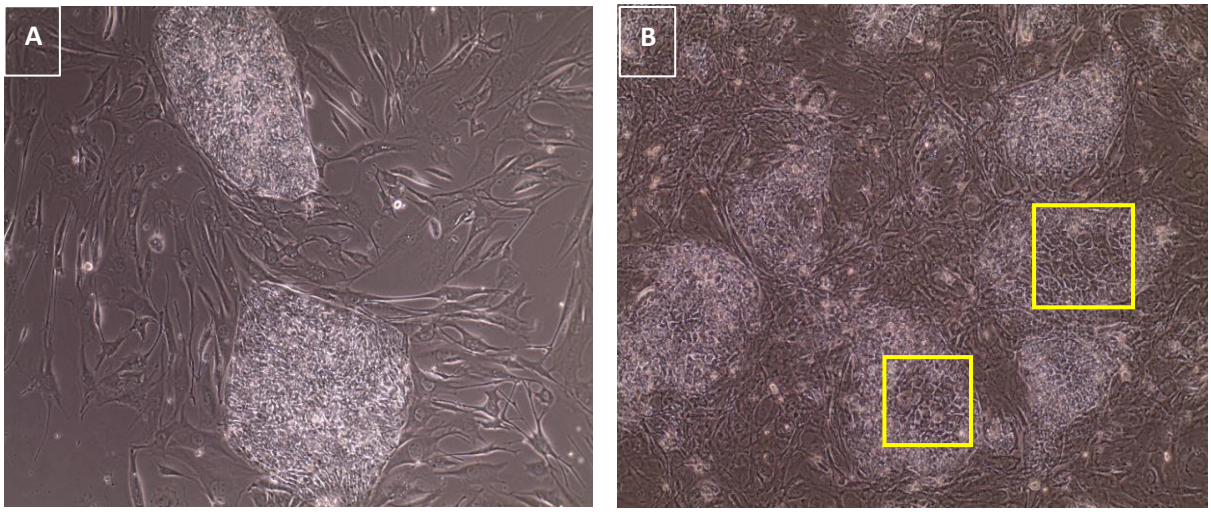

Figure 3.29. Morphology of CT1.5 iPSC colonies. A) shows a typical undifferentiated iPSC colonies on inactivated MEF layer at passage 23, while B) shows a differentiated iPSC colonies on inactivated MEF layer. Images taken by an EVOS microscope at 10x objective magnification.

Therefore, the next experiment proceeded as follows. A dish of differentiated iPSCs from both cell lines was treated with TrypLE and the cells were dissociated by trituration. They were seeded into two gelatine coated dishes each; one containing hESC medium and the other containing DMEM supplemented with 10% FBS and antibiotics ($DMEM^{++}$). The aim at this stage was to determine whether the cells could continue to grow in these two different media and to test whether they continued to develop into a mesenchymal phenotype.

The cells were cultured for 14 days with medium changes every other day, and each line passaged 1:3 into gelatine-coated dishes containing either hESC medium or $DMEM^{++}$ medium. Thereafter cells were passaged every seven days or when they were confluent. The changes in morphology were noted and recorded at various passages. The results for each of the media will be described separately.

3.3.2.1 Cells cultured in hESC medium

After 2 days of culture, there was a range of various cellular morphologies for both CT1.5 and MJD5.3 cell lines, including flat elongated cells (Figure 3.30 A, yellow arrow), spindle-shaped cells (Figure 3.30 A, green arrow), and spindle-spiked cells (Figure 3.30 A, red arrow). Many of these cells appeared to have granular clusters surrounding the nucleus and vacuoles within their cytoplasm (Figure 3.30A, black arrows). By day 3, these vacuoles became more prominent, and the peri-nuclear area appeared more granulated (Figure 3.20 B, black arrows).

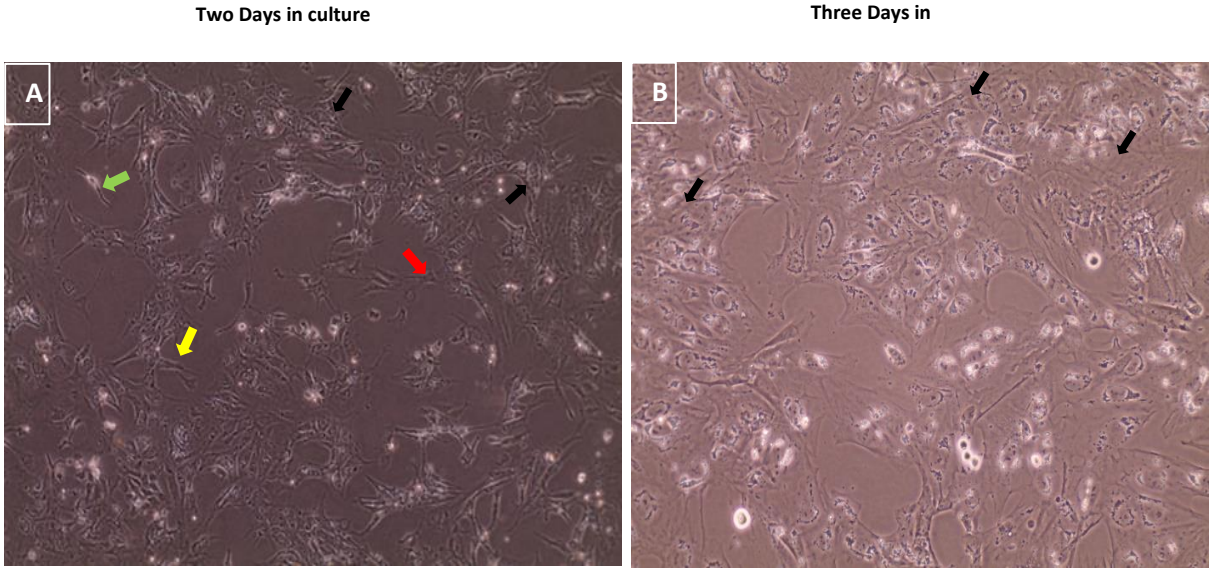

Figure 3.30: CT1.5 cells cultured on gelatine coated dishes at passage 23 (P0). Cells were cultured in hESC medium containing bFGF. Two - and three-days after enzymatic passage Images taken by an EVOS microscope at 10x objective (A) and at 20x objective (B).

At the first passage (P1), the cells were plated at a density of $1x10^4$ cells/cm^2 into fresh gelatine coated dishes. Good cell attachment was observed. Two days later, most of the cells were narrow and more spindle-shaped, and on occasion, formed cell clusters (Figure 3.31A insert). After three more days (Figure 3.31 B) 80-90% confluency was reached. The cells appeared slightly elongated, with a loss of their initial cell-clustering feature (Figure 3.31, green arrow).

Two Days in culture

Five Days in culture

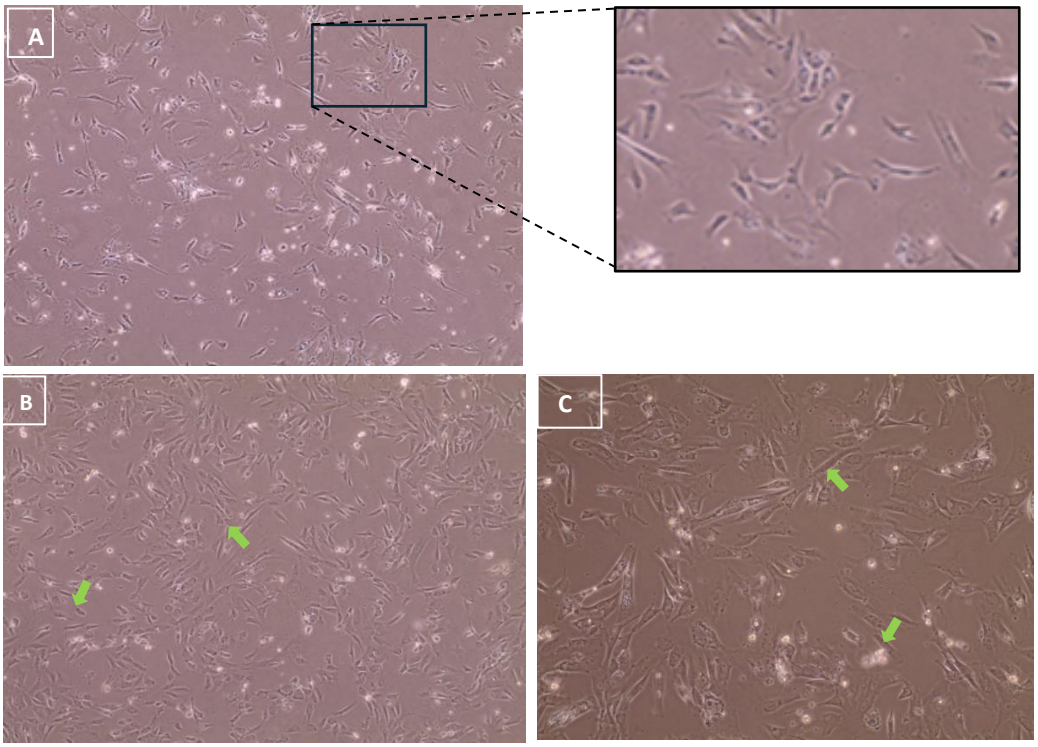

Figure 3.31. The general morphology of cells passaged to gelatine coated dishes and cultured in hESC medium with bFGF. A) - two and B&C) – five days after passaging onto gelatine coated dishes. Images taken using EVOS microscope at 10x objective (A&B) and at 20x objective (C).

Thereafter, cells maintained a consistent morphology. As they continued to proliferate (P3), and were left longer in culture, the cells favoured growing in compact clusters (Figure 3.32A), also creating empty spaces between the clusters. At this stage the cells were very elongated and mesenchymal/fibroblast-like. This suggests that once the cells are confluent, breaks in the cell sheet cause the cells to retract towards each other, resulting in more empty spaces (Figure 3.32A, extended image). This behaviour was particularly evident as the cultures progressed further and is typical of fibroblast cultures that become very confluent.

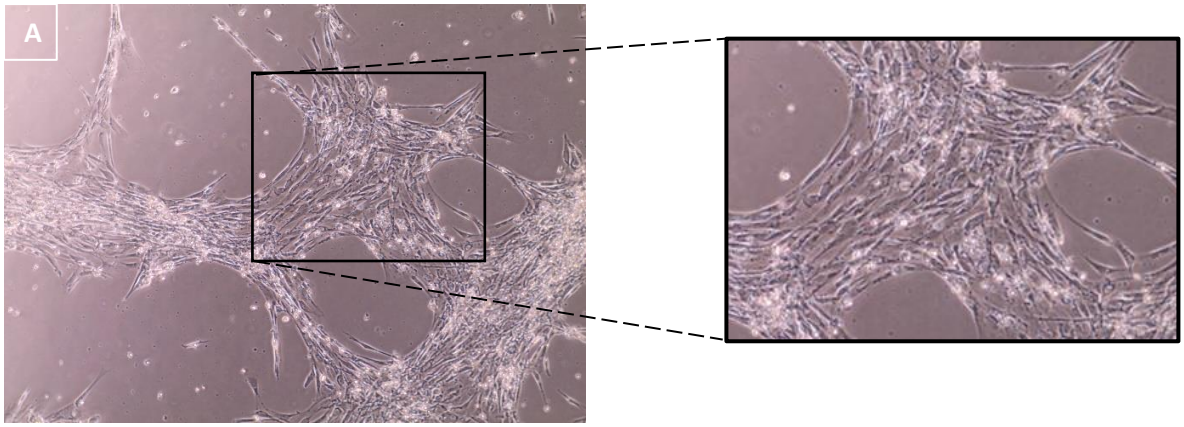

Figure 3.32. The morphology of cells cultured in hESC medium passaged to gelatine coated dishes, now at P3. The morphology of cells cultured in hESC medium is similar to those at previous passages (P1-2). Images captured at 10x objective using the EVOS microscope.

3.3.2.2 Cells cultured in DMEM^{++} medium and comparison with cultures in hESC medium

At day 2, the CT1.5 and MJD5.3 cells appeared strikingly different in morphology to those that were cultured in hESC medium. They were larger and flatter in size (Figure 3.33) and more densely packed and by day 2, the dishes were sub-confluent. They were seen as sheets of cells and there were very few spindle-shaped cells (Figure 3.33 A, green arrow). The flattened shape of the cells made it difficult to determine whether the rate of proliferation was higher than that of the cells cultured in hESC medium. By day 3, the cells continued to proliferate, and the cultures became almost completely confluent. The cells contained vacuole-like structures with peri-nuclear granules (Figure 3.33B, black arrows).

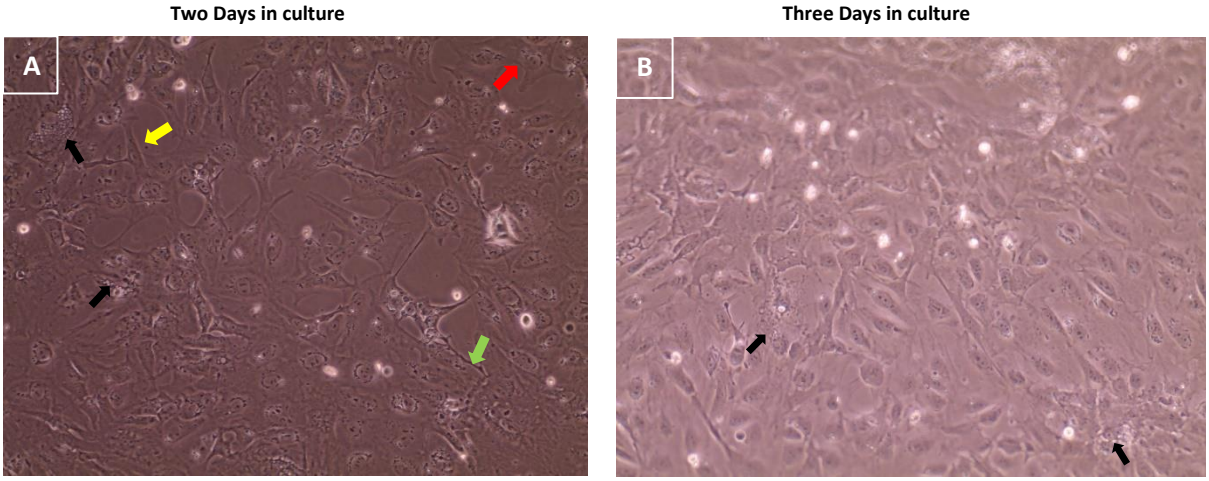

Figure 3.33: The morphology of cells cultured in DMEM^{++} passaged to gelatine coated dishes, now P0. The morphology of cells cultured in DMEM medium containing serum. Two - and three-days after enzymatic passage. Images taken by an EVOS microscope at 10x objective (A) and at 20x objective (B).

After the first passage, the flattened round structures were no longer seen, and cells were starting to become more spindle shaped. This can clearly be seen by day 5. They reached around 80–90% confluency and adopted a very typical mesenchymal/fibroblast-like morphology, with a mix of spindle-shaped cells alongside larger, round, flat cells (Figure 3.34B -coloured boxes).

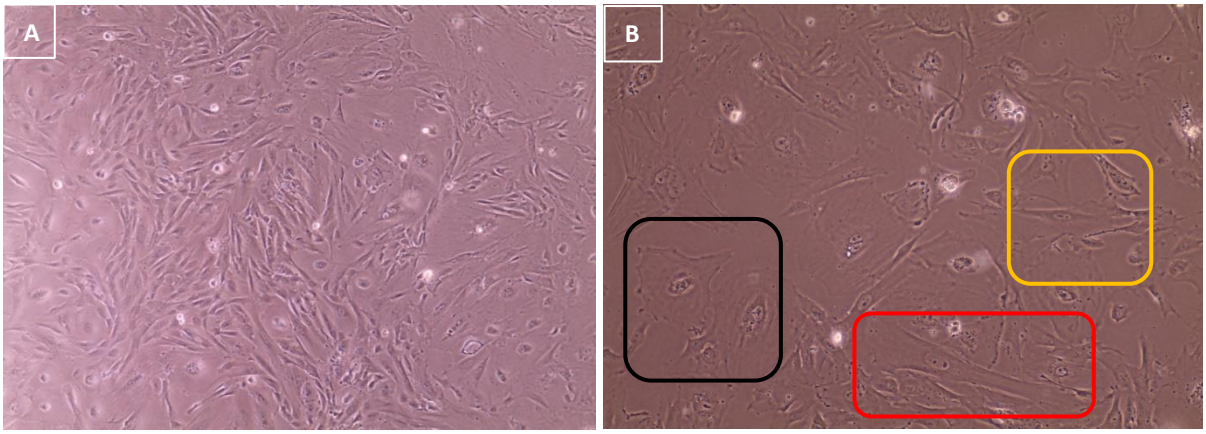

Figure 3.34. The morphology of cells cultured in DMEM^{++} passaged to gelatine coated dishes, now P1. Cells are five days in culture in DMEM^{++} and are fibroblast like in morphology. The different colour boxes were used to highlight the different cell morphologies. Images captured at 10x objective (A) and at 20x objective (B) using the EVOS microscope.

At passage 4, the cells grown in DMEM^{++} were tested for the expression of the mesenchymal markers CD73 and CD105 (Figure 3.35). As can be seen, there was a relatively high expression of CD73 in both CT1.5 and MJD5.3 samples compared to very low expression in iPSCs. The cells grown in hESC medium had a slightly higher expression of CD73 compared to those cultured in DMEM^{++} .

Similar analysis was carried out for CD105 for the MJD5.3 cell line (There was insufficient RNA to analyse CT1.5). As can be seen in Figure 3.35, a similar pattern of much higher expression in hESC cultured cells compared to DMEM cultures cells was obtained. There was also insufficient RNA to analyse the negative CD markers for the iMSCs derived with Protocol II.

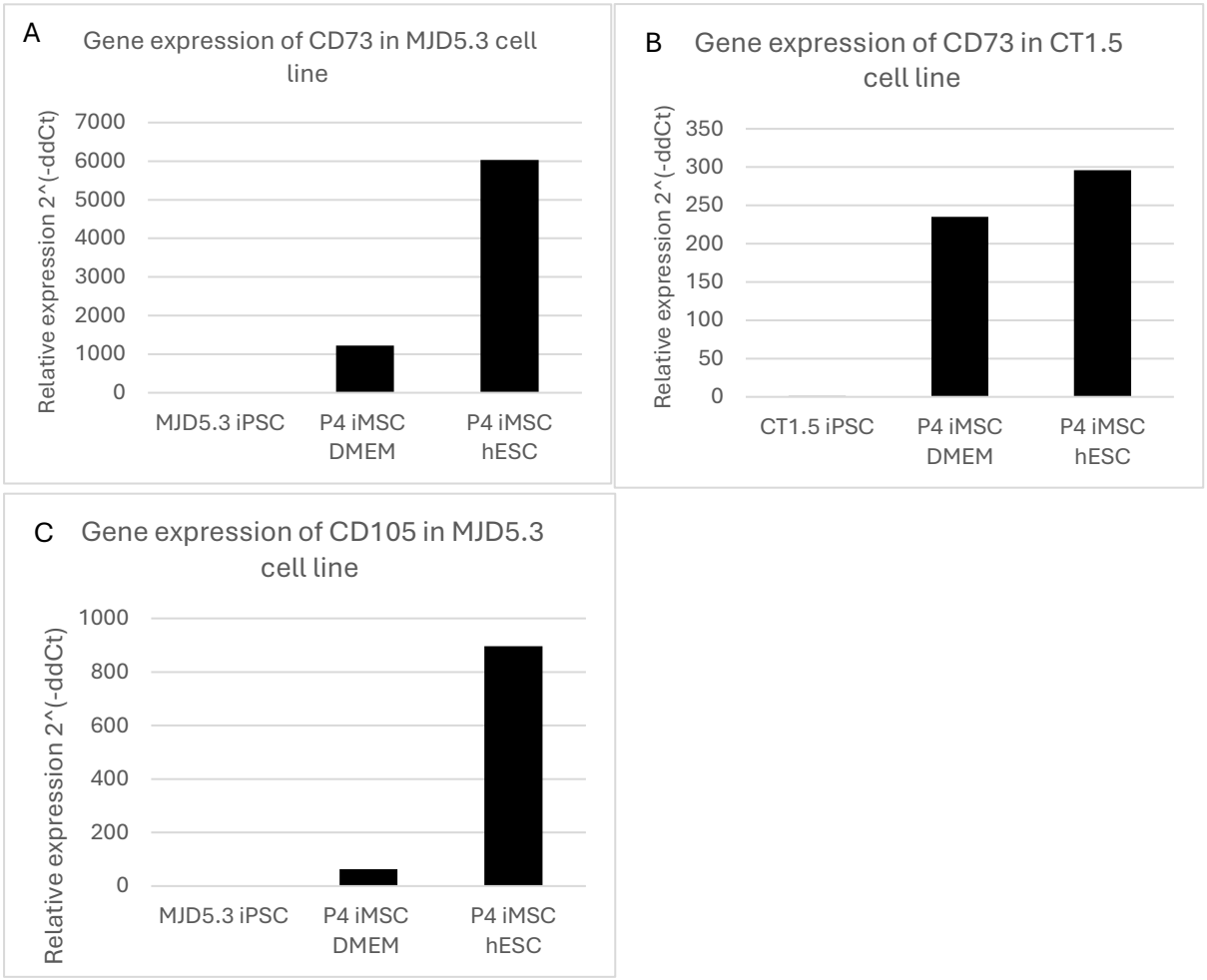

Figure 3.35. Expression levels of CD markers using qRT-PCR analysis. A) CD73 in MJD5.3 iPSCs and iMSCs derived using protocol II, B) CD73 in CT1.5 iPSCs and iMSCs derived using protocol II, and C) CD105 in MJD5.3 iPSCs and iMSCs derived using protocol II. Low levels of CD73 and CD105 were observed in all the iPSC lines, while iMSCs exhibited relatively higher expression levels of CD73 and CD105. Human GAPDH was used as a housekeeping gene, and qRT-PCR performed using the StepOne instrument, using SYBR green. The iPSC sample used as a calibrator, n=1.

Most interestingly, it was found that both cell lines cultured in hESC medium expressed very high levels of NANOG at the same time as the cells were expressing CD73 and CD105 (Figure 3.36). This has been reported previously that NANOG has a role*, inter alia* in cell cycle and DNA repair in several cell types (Zhang et al. 2016)

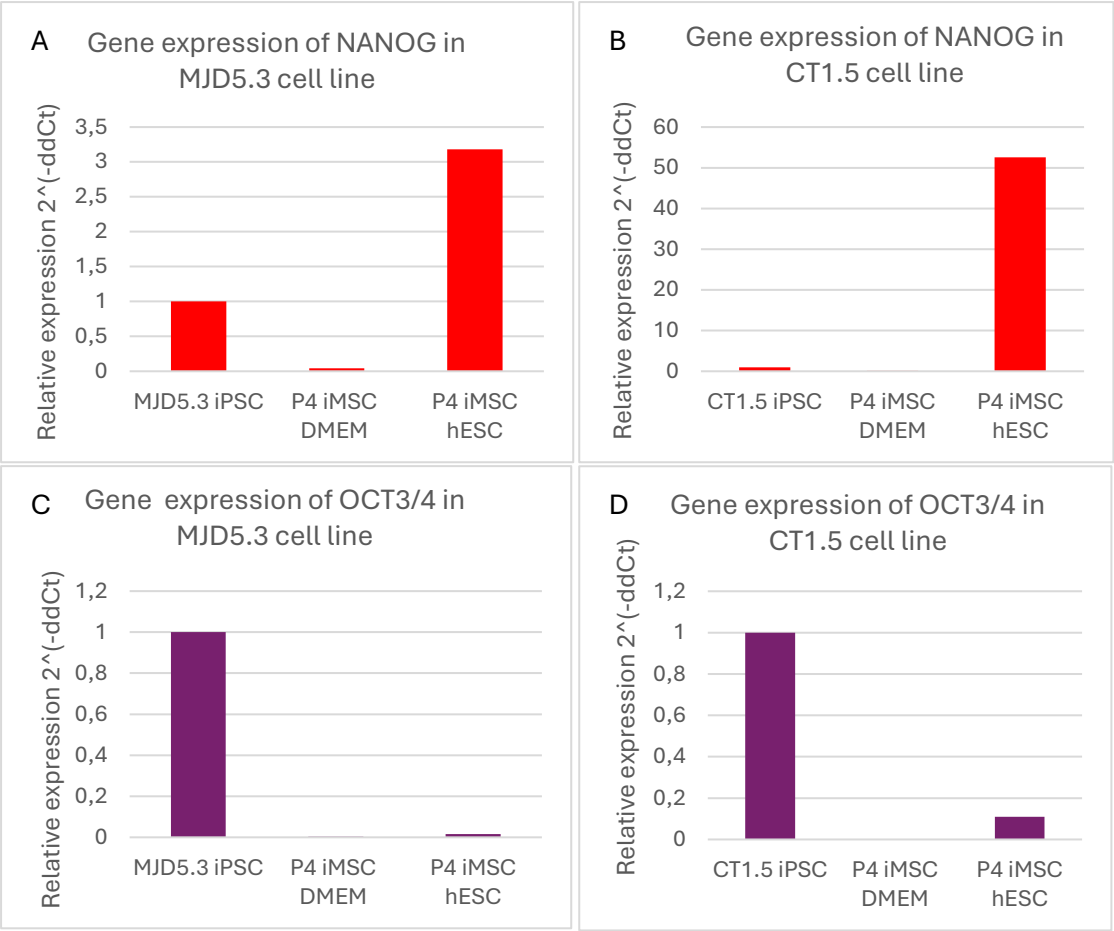

Figure 3.36. Expression levels of pluripotency markers, NANOG and OCT3/4, using qRT-PCR analysis. NANOG levels in A) MJD5.3 and B) CT1.5 iPSCs and iMSCs derived using DMEM^{++} and hESC. OCT3/4 levels in C) MJD5.3 and D) CT1.5 iPSCs and iMSCs derived using DMEM^{++} and hESC. iMSCs derived from hESC exhibited relatively higher expression levels of NANOG compared to iPSCs and iMSCs derived from DMEM^{++}. All iPSCs showed relatively high expression of OCT3/4 compared to all iMSC samples. Human GAPDH was used as a housekeeping gene, and qRT-PCR performed using the StepOne instrument, using SYBR green. The iPSC sample used as a calibrator, n=1 .

3.3.2.3 The ability of iPSC- derived mesenchymal stem cells had trilineage potential.

The aim of the next step was to determine whether the iMSCs were able to differentiate into bone, cartilage and adipose precursors.

Adipogenesis differentiation

The CT1.5 and MJD5.3 iMSCs cells derived in either hESC or DMEM^{++} media were tested for their adipogenic potential using the StemPro® Adipogenesis Differentiation Kit. Cells were grown for 14 days, and histological staining was then carried out.

By day 14, CT1.5 cells treated in adipogenic differentiation medium had changed from the mesenchymal-like shape to a large and flat shape (Figure 3.37 B, D). Oil Red O staining indicated positive lipid droplets deposited around the nucleus within the cytoplasm (Figure 3.37 B, D). This showed a successful adipogenic differentiation. For the untreated cells grown in either the hESC or DMEM^{++} medium, it could be seen that cells continued to proliferate. In the hESC medium, cells lifted off in patches leaving a sparse population of clusters (Figure 3.37 A). In the DMEM^{++} cultures the confluent cells remained adherent (Figure 3.37 C). Oil Red O staining for these untreated cells showed no staining for the DMEM^{++} cultures, but in the hESC cultures, there did appear to be some stain that looked mostly none-specific or "trapped". However, there did seem to be some cells with specific staining, suggesting that they might have spontaneously differentiated. This apparent willingness of the untreated hESC derived MSCs to differentiate towards the adipogenic lineage could be related to the increase concentration of FGF-2 (supplemented to the hESC medium). Literature has indicated that when mesenchymal stem cells are stressed, they tend to release FGF-2 which then facilitates proliferation and the promotion of osteoblast differentiation via the ERK pathway (Ogura et al. 2023). Something similar could be happing with the adipogenesis (see Discussion).

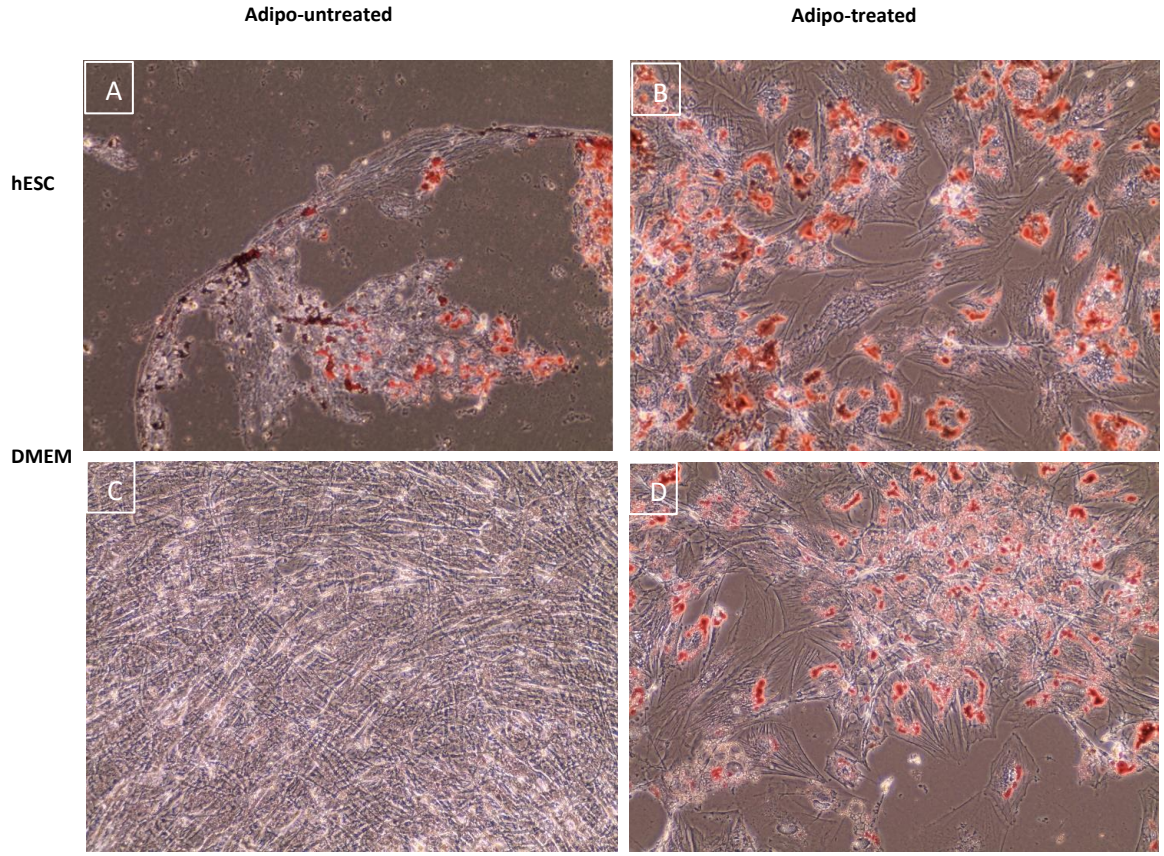

Figure 3.37. Oil Red O staining of day 14 CT1.5 cells either in treated or untreated adipogenic differentiation medium. hESC cultured (A, B) and DMEM cultured cells (C, D). A, C- untreated, B, D- treated. Images captured at 20x objectives using the EVOS microscope

Similarly to CT1.5, adipogenesis was determined in MJD5.3 cells derived from either hESC or DMEM^{++} media for 14 days. The MJD5.3 pattern of staining was the same as for the CT1.5 cells. That is, strong positive staining in treated hESC derived cells with a small amount of staining in the hESC untreated cells. The treated cells derived from the DMEM^{++} medium displayed some staining, but it was much less than what is displayed by the hESC derived cells. In contrast to the CT1.5 cells, the untreated MJD5.3 cells survived better in hESC medium compared to DMEM^{++} medium (Figure 3.38).

Some adipose-derived human mesenchymal cells (hMSC) (gift from Prof Pepper, University of Pretoria) cultured in DMEM^{++}, exhibited typical mesenchymal morphology before the differentiation process (Figure 3.39 A). They were grown in Adipogenic Differentiation Medium for 14 days and stained for adipogenesis. In Figure 3.39 A, these typical human mesenchymal cells can be seen. On day 14, the Oil Red O positive staining was seen in the cells cultured in Adipose Differentiation Medium with lipid droplets visible within the cytoplasm of some of the cells, but many of them remained fibroblast-like (Figure 3.39 C). The control cells were completely negative for Oil Red O.

In Summary, the overall results confirmed that the iPSC-derived iMSCs were able to differentiate into adipose cells.

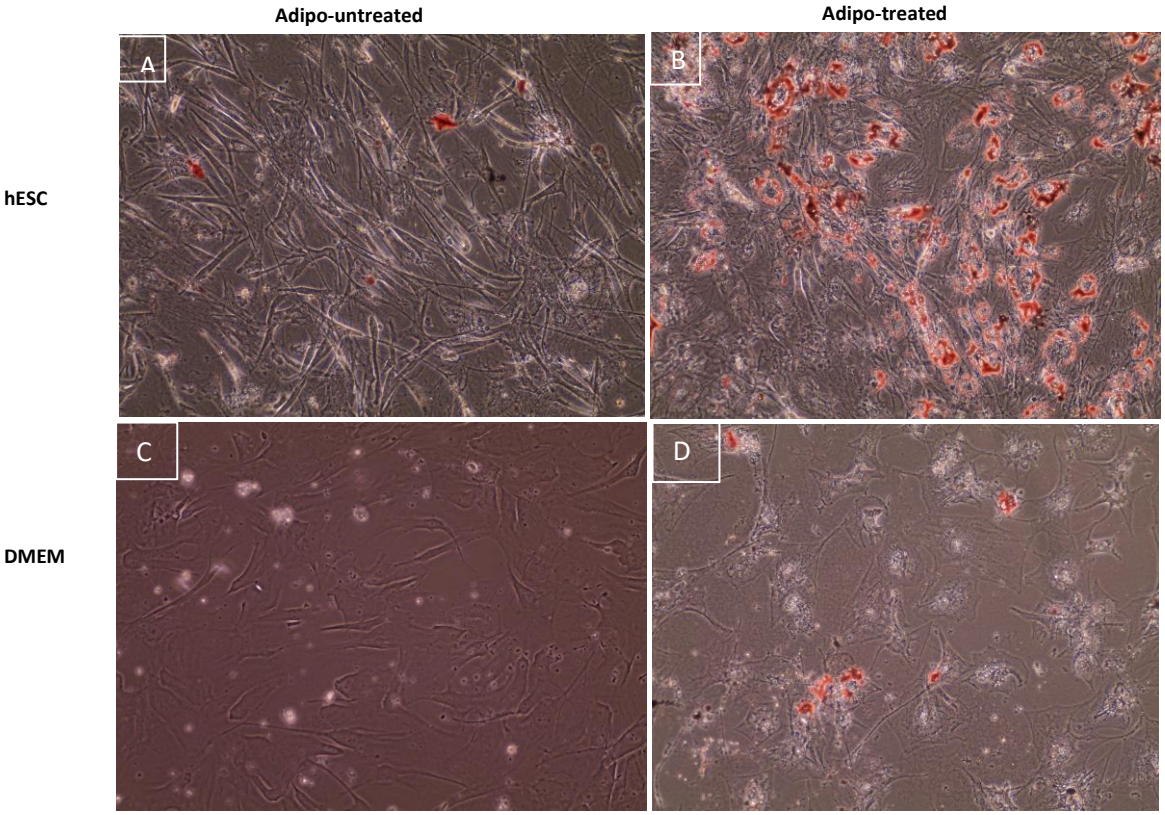

Figure 3.38. Oil Red O staining of day 14 MJD5.3 cells either in treated or untreated adipogenic differentiation medium. hESC cultured (A, B) and DMEM cultured cells (C, D). A, C- untreated, B, D- treated. Images captured at 20x objectives using the EVOS microscope

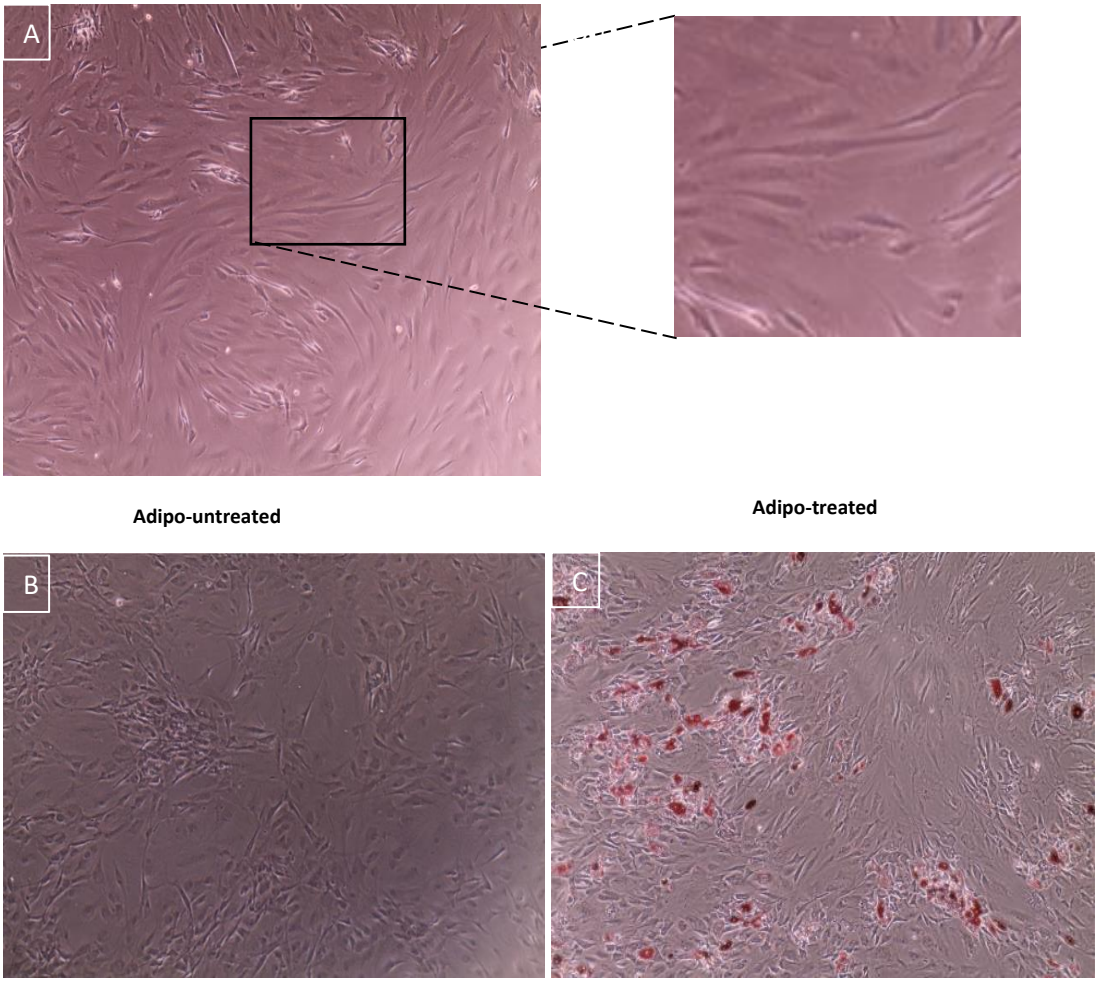

Figure 3.39. Morphology of Human mesenchymal stem cells (hMSC) cultured in DMEM^{++} at passage 4. (Untreated - A and B, Treated - C). C) Oil Red O staining confirming adipogenic differentiation of day 14 hMSC cells compared to undifferentiated samples (B). Images captured at 10x objective using the EVOS microscope

Osteogenesis Differentiation

To determine whether the CT1.5 and MJD5.3 iPSC-derived MS cells can become bone cells, they were cultured in StemPro® Osteogenesis Differentiation medium for a period of 21 days, then stained with Alizarin Red. Control cells were cultured in either hESC medium or DMEM^{++}.

As can be seen on day 21, the Alizarin Red staining was observed in the treated (differentiated) samples for both hESC and DMEM^{++} CT1.5 cells (Figure 3.40 B, D) whereas the controls were all negative (Figure 3.40 A, C). This confirmed a positive calcium deposition indicative of osteogenesis only in treated cells. The undifferentiated hESC culture formed clusters and those in DMEM^{++} became overconfluent but there was no Alizarin Red staining observed.

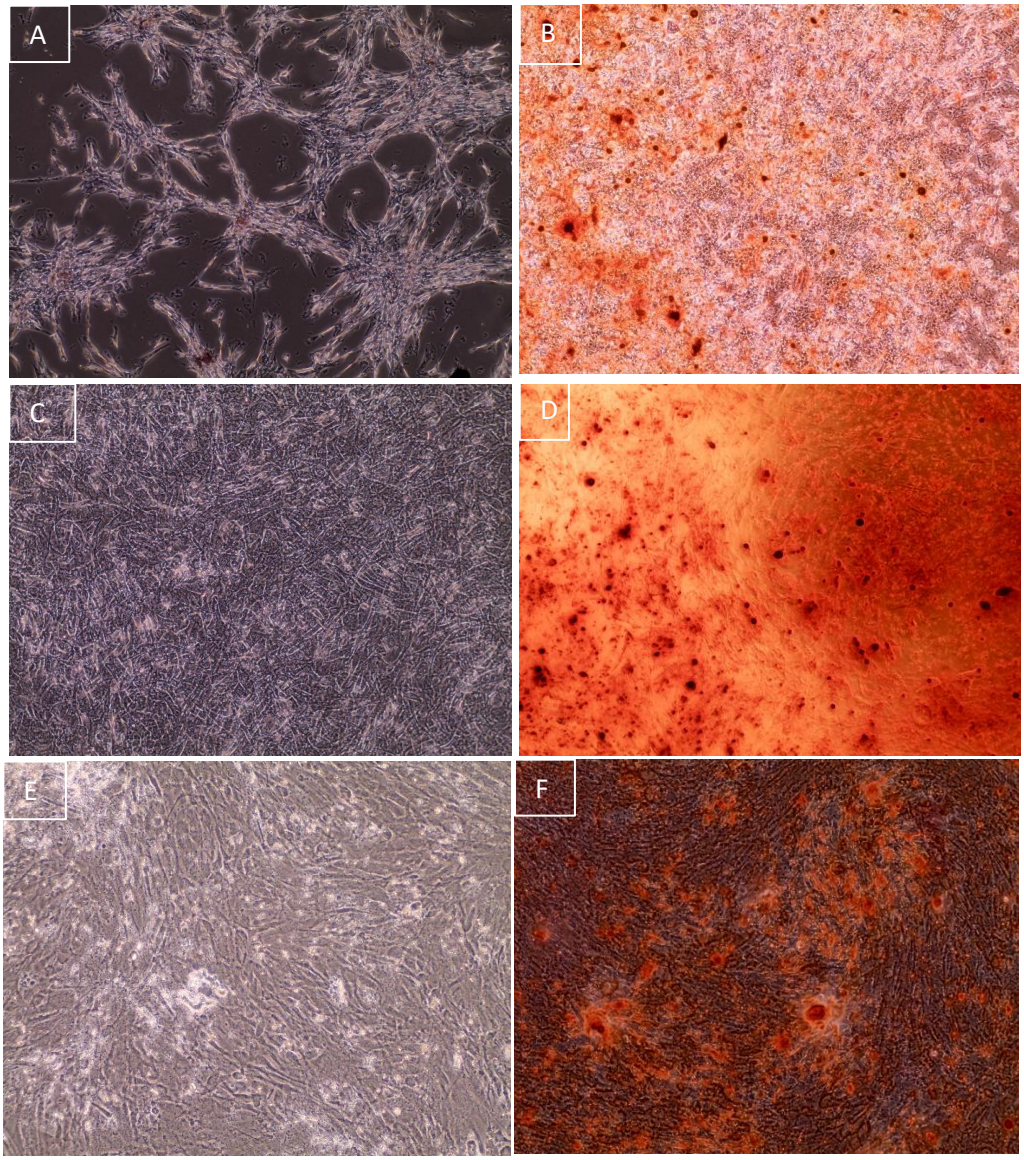

Figure 3.40. Alizarin Red staining of CT1.5 cells either in treated or untreated osteogenic differentiation medium on hESC cultured (A,B) and DMEM^{++} cultured medium (C,D) at Day 21. Day 21 of MJD5.3 cells either in treated or untreated osteogenic differentiation medium DMEM cultured medium (E,F). A,C, E- untreated, B,D, F - treated. Images captured at 10x objectives using the EVOS microscope

It is known that osteogenic cells express alkaline phosphatase (reviewed by Vimalraj, 2020) as do iPSCs. To investigate whether any changes might have occurred as the cells transitioned from stem cell state to differentiated state, qRT-PCR analysis of alkaline phosphatase (ALP) was carried out. The results from the real time data are presented graphically. Agarose gel analysis of the qRT-PCR product size was carried out to check PCR product size and determine rough expression levels. As expected, the iPSC cells expressed the ALP gene. On days 0, 7, 14 and 21, CT1.5 cells expressed various levels of ALP; the highest being at day 14 (Figure 3.41 A). Overall, both the iPSCs and the differentiated samples showed positive ALP expression. These are similar results seen by (P. Zhou et al. 2021).

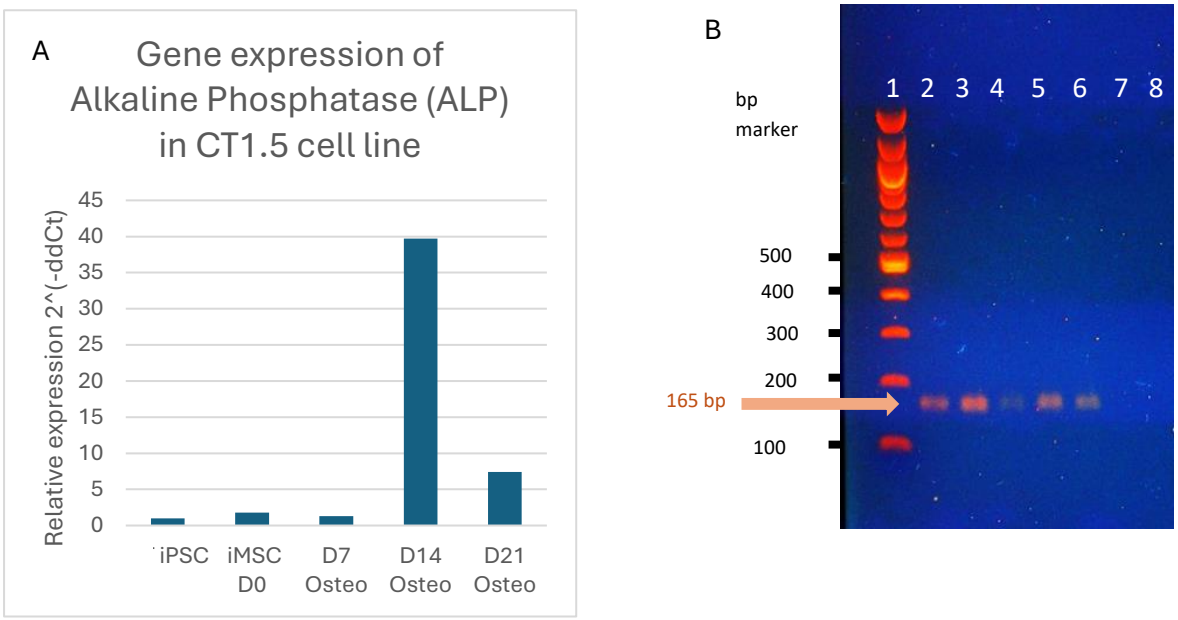

Figure 3.41. A) Relative gene expression of Alkaline phosphatase during the 21-day differentiation towards osteogenesis for CT1.5 DMEM^{++} cultured cells. B) 2 % agarose gel loaded with Lane 1 = Quick-Load 100 bp DNA ladder, Lane 2= iPSCs, Lane 3= Day 0/ iMSC (untreated), Lane 4 = Day 7, Lane 5 = Day 14, Lane 6 = Day 21, Lane 7 = Day 21 -RT control and Lane 8 = NTC.

A similar analysis was carried out with the patient MJD5.3 cells; qRT-PCR data was plotted and the PCR products run on an agarose gel (Figure 3.42 A, B). Both the iPSC cells and the differentiated cells showed the expected ALP expression, but in this experiment the D0 sample did not express ALP. In contrast to the results obtained in CT1.5 cells, in MJD5.3 the iPSC cells expressed higher levels of ALP than iMSC cells and the osteo differentiated cells. However, it should be noted that although these samples were run in duplicate, the qRT-PCR analysis was not repeated, and the pattern of expression could not therefore be verified. But it is evident that both iPSCs and differentiated cells do express ALP in both CT1.5 and MJD5.3.

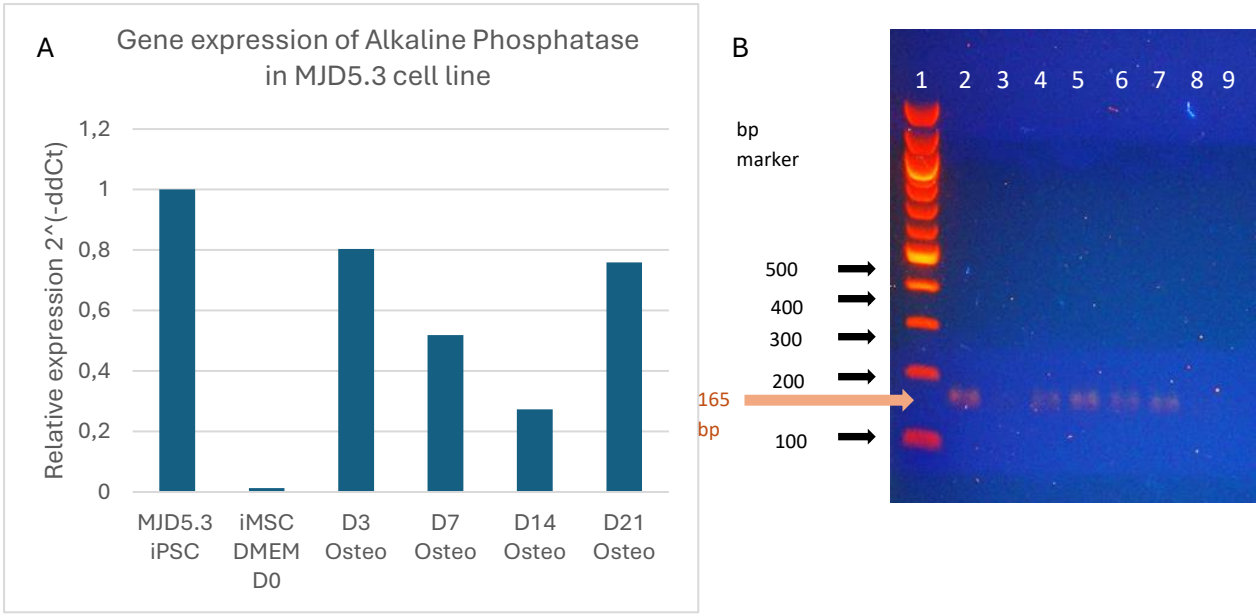

Figure 3.42. A) Relative genetic expression of Alkaline phosphatase during the 21-day differentiation towards osteogenesis for MJD5.3 DMEM^{++} cultured cells. B) Agarose gel loaded with Lane 1 = Quick-Load 100 bp DNA ladder, Lane 2= iPSCs, Lane 3= Day 0 iMSC (untreated), Lane 4 = Day 3, Lane 5 = Day 7, Lane 6 = Day 14, Lane 7 = Day 21, Lane 8 = Day 21 -RT control and Lane 9 = D14 -RT control.

Osteocalcin, known to be synthesized by osteoblasts, was also investigated as a key bone development marker. The temporal expression of osteocalcin was measured over a 21-day culture period by qRT-PCR analysis. Results were presented graphically and the qRT-PCR product checked on agarose gels (Figure 3.43 A, B). For each of the osteo-induced iMSC samples, two bands were seen. A weak band of 158 bp and a much stronger band of about 50bp A similar result was obtained with the CT1.5 samples. Two bands were obtained for each of the samples, of 158 bp and 50 bp. The graphical analysis reveals a slight decrease from day 7 to 21 (Most likely the results of poor-quality RNA). These results show that osteocalcin is expressed in iMSCs subjected to osteogenic differentiation reagents. The two bands seen of 158bp and 50bp suggest that they arise from alternative splicing of the transcripts (see Discussion).

Analysis of the qPCR product sizes as seen on the agarose gels, revealed an interesting result. The RNA from the iPSC MJD5.3 cells gave a product of 158 bp. This was surprising because it was expected that pluripotent stem cells would not express the differentiation specific gene osteocalcin. This will be considered in the Discussion

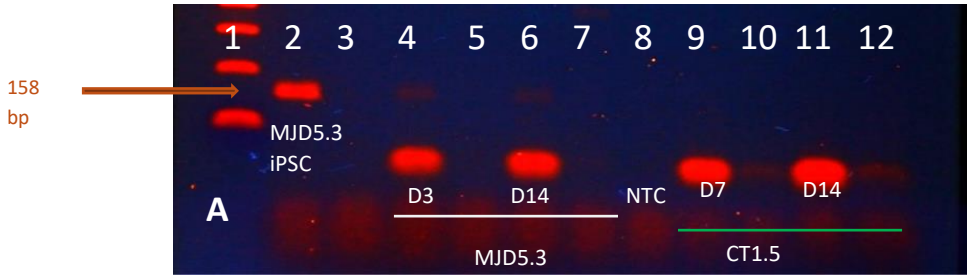

Osteogenic differentiation

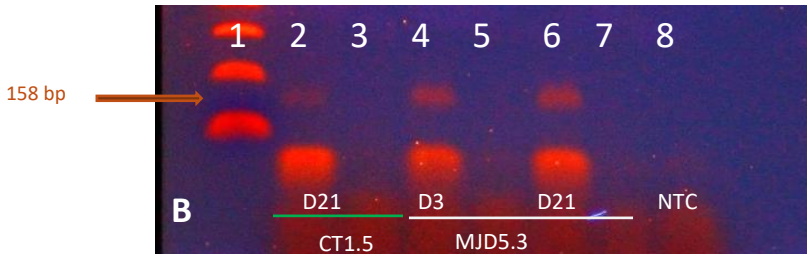

Osteogenic differentiation

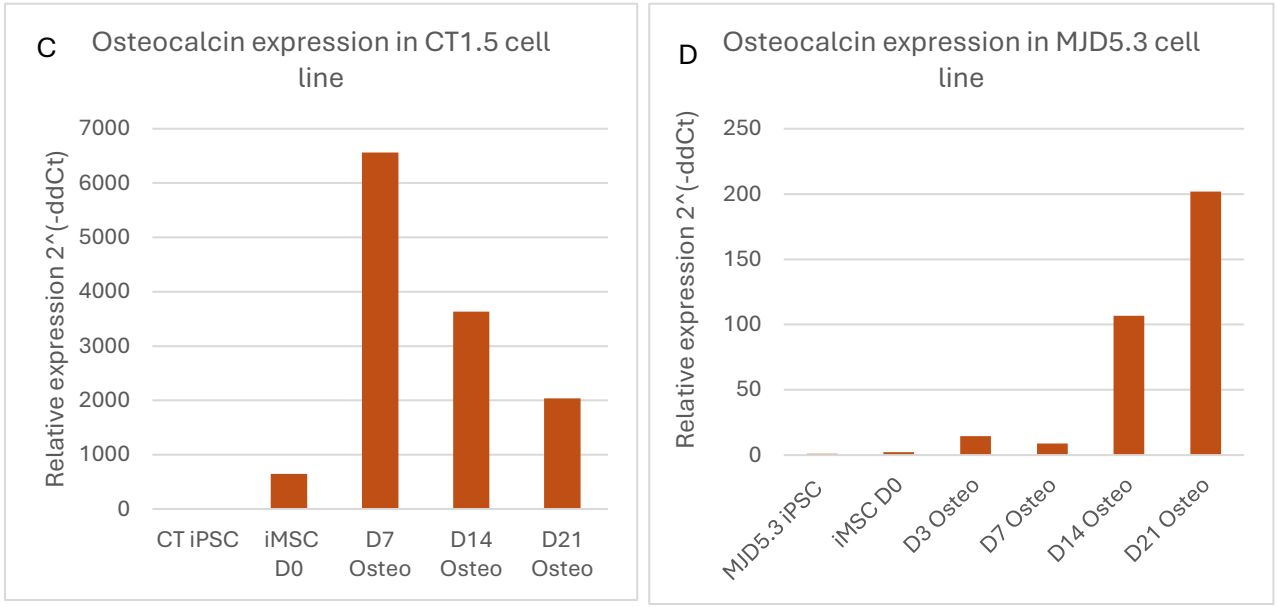

Figure 3.43. A) Agarose gel loaded with Lane 1 = Quick-Load 100 bp DNA ladder, Lane 2= MJD5.3 iPSC cells, Lane 3= MJD5.3 iPSC cells -RT control, Lane 4 = MJD5.3 Day 3, Lane 5 = MJD5.3 Day 3 -RT control, Lane 6 = MJD5.3 Day 14, Lane 7 = MJD5.3 Day 14 -RT control, Lane 8= NTC, Lane 9 = CT1.5 Day 7, Lane 10 = CT1.5 Day 7 -RT control, Lane 11 = CT1.5 Day 14, Lane 12 = CT1.5 Day 14 -RT. B) agarose gel loaded with Lane 1 = Quick-Load 100 bp DNA ladder, Lane 2 = CT1.5 Day 21, Lane 3 = CT1.5 Day 21 -RT control, Lane 4= MJD 5.3 Day 3, Lane 5 = MJD 5.3 Day 3 -RT control, Lane 6 = MJD 5.3 D21, Lane 7 = MJD 5.3 D21 -RT control, Lane 8 = NTC. C, D) Relative genetic expression of Osteocalcin during the 21-day osteogenic differentiation for CT1.5 (C) and MJD5.3 (D) DMEM^{++} cultured cells.

Chondrogenic differentiation:

The final step in the trilineage differentiation was to investigate both CT1.5 and MJD5.3 cell lines for their potential for chondrogenic differentiation. In a trial experiment, the DMEM^{++} derived CT1.5 iMSCs were cultured as micromasses in 5 wells of a 12 well plate in either StemPro® Chondrocyte Differentiation medium for 21 days., then stained with toluidine blue. The untreated control cells were cultured in DMEM^{++} medium.

The micromasses treated with chondrogenic medium developed a dense composition and became compact with increasing time in culture (Figure 3.44). I t is worth noting that in one or two wells the micromasses disintegrated leaving very few micromasses for staining and qRT-PCR analysis. After 21 days, the treated micromasses stained dark blue with toluidine blue. In contrast, the untreated micromass grown in DMEM^{++}, grew as a monolayer of cells in the middle of the well and displayed a light blue background with toluidine blue (Figure 3.44 A). This could have been either non-specific trapping of the blue dye, or it could have been that the collections of adhering cells synthesized some sort of extra cellular matrix that picked up the toluidine blue stain.

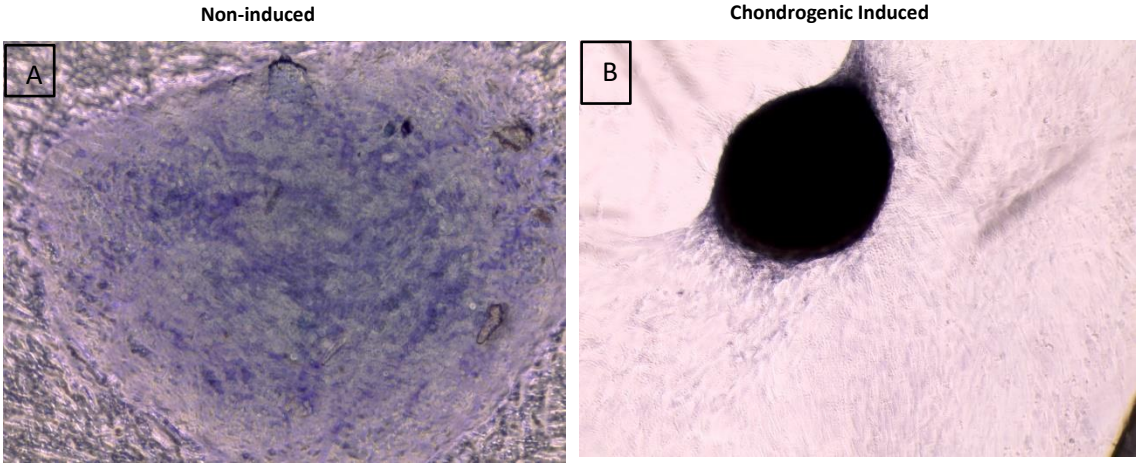

Figure 3.44. Toluidine blue staining of CT1.5 chondro-differentiated micromasess. A) Control sampled on day 21 displaying a pale blue background, B) differentiated sample on day 21 showing a very compact mass with an intensely dark blue staining. Images taken by an EVOS microscope with phase contrast.

Having demonstrated that control and MJD iMSC cells differentiate into cartilage *in vitro* in both low glucose and DMEM^{++} medium, the final step was to determine the temporal sequence of this process to compare the control and the patient samples. In addition, the second aim was to determine whether the cartilage produced was of the hypertrophic type or of the articular type of cartilage. The approach was to first check for the temporal expression pattern of COL2A1, a pan cartilage marker.

The next step was to determine the expression of COL10A1, which is expressed exclusively in hypertrophic cartilage.

Briefly, CT1.5 and MJD5.3 iMSCs derived from low glucose DMEM^{++} medium (protocol I) were cultured, and RNA extracted from samples on days 0, 3, 5, 7, 14 and 21. qRT-PCR was carried out and the 122bp PCR product checked on a 2% agarose gel. As seen in Figure 3.45A (lanes 2-7), the final product was seen in all samples. A very faint band was observed for the day 14, untreated control (lane 8). The iPSC samples were run at the same time (gel not shown). Using the iMSC values as a calibrator for the 2^{-ddCt} analysis, the results seen in Figure 3.45B shows that COL2A1 increased expression from day 3 to day 21. (C_T values are in the appendix) C). CT1.5 iMSC samples derived from DMEM^{++} (lane 9) showed a positive band expression and hESC (lane 10) showed a low positive expression of COL2A1.

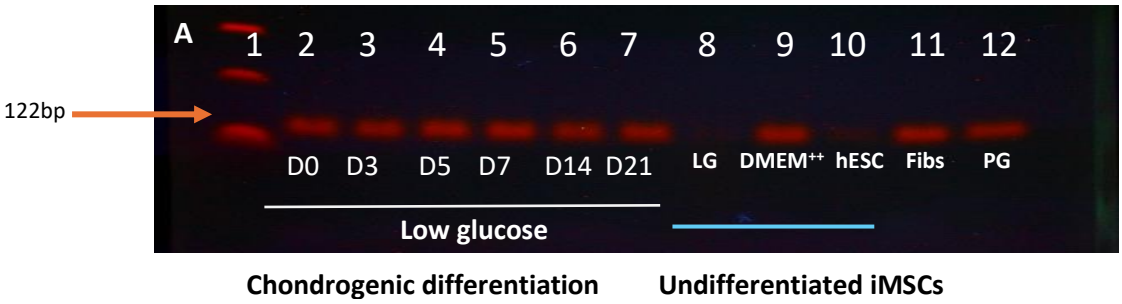

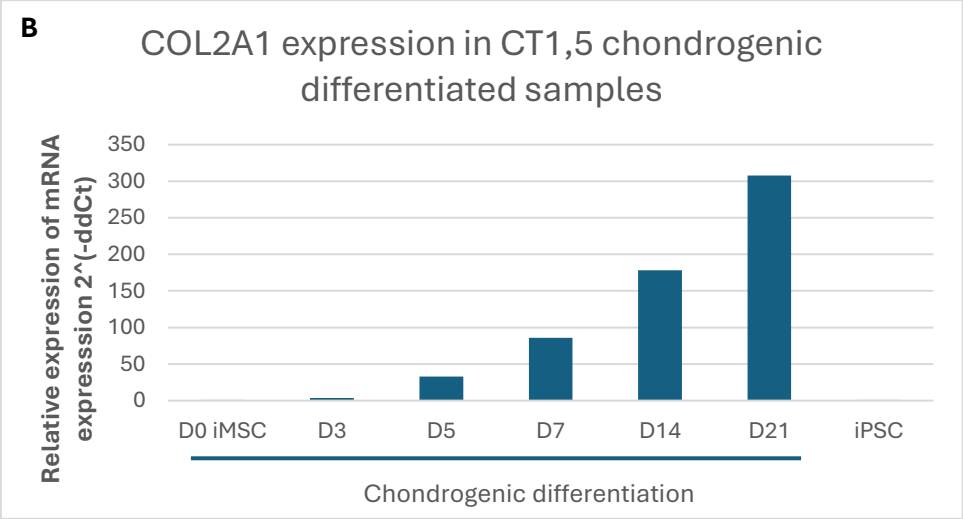

Figure 3.45. COL2A1 expression in chondrogenically induced CT1.5 iMSC samples derived from low glucose DMEM. A) Agarose gel loaded with Lane 1= 100bp Marker, Lane 2= Day 0; Lane 3= Day 3, Lane 4= Day 5, Lane 5= Day 7, Lane 6 = Day 14, Lane 7= Day 21, Lane 8= iMSCs- Day 14 untreated control condensed, Lane 9= iMSC derived using DMEM^{++}, Lane 10= iMSC derived using hESC, Lane 11= MJDC2 Fibroblast, Lane 12= Chondro nodule Day 20 (PG sample); B) Relative genetic expression of COL2A1 during the 21-day chondrogenic differentiation for CT1.5.

Similarly, qRT-PCR analysis was performed for MJD5.3 chondro-differentiated cultures originating from iMSCs derived in low glucose DMEM (Protocol I). The correct 122bp PCR product size was seen for all samples (Lanes 3-8). As can be seen from Figure 3.46A and B, COL2A1 increased expression to day 3, whereafter expression decreased to day 21. When cells were cultured in DMEM^{++} medium (protocol II), an increase was also seen from day 0 to day 5 (lanes 9 and 10); unfortunately, there were insufficient samples for the later timeline (Figure 3.46 C).

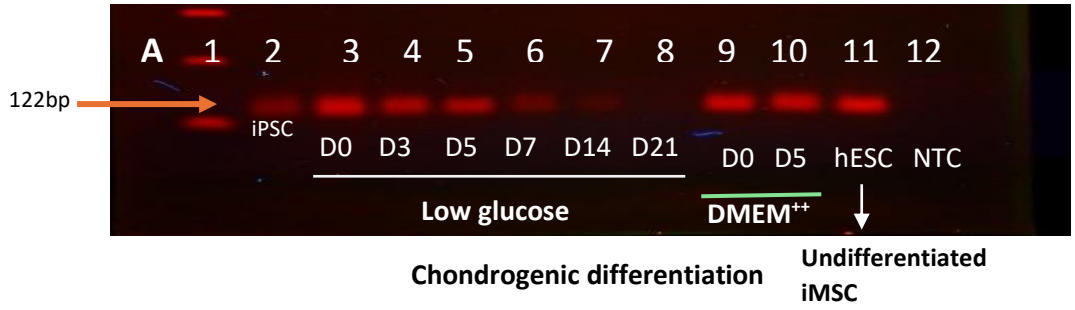

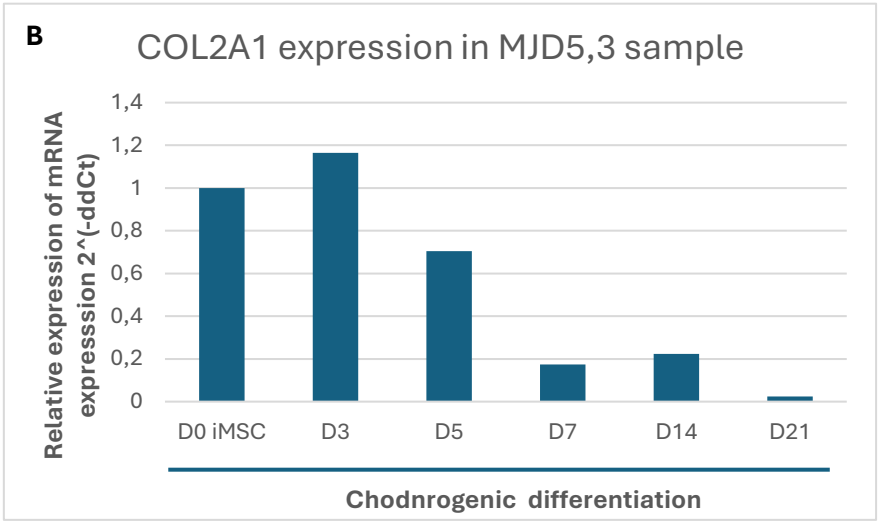

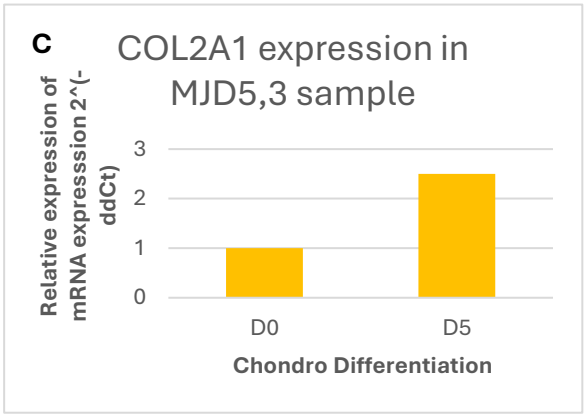

Figure 3.46. COL2A1 expression in chondrogenically induced MJ5.3 iMSC samples derived from low glucose DMEM and DMEM^{++}. A) Agarose gel loaded with; Lane 1= 100bp Marker, Lane 2= iPSC, Lane 3 = Day 0, Lane 4= Day 3, Lane 5 = Day 5, Lane 6 = Day 7, Lane 7 = Day 14, Lane8 = Day 21, Lane 9 = Day 0 DMEM^{++} derived; Lane 10 = Day 5 DMEM^{++} derived, Lane 11 = iMSC hESC derived. B) Relative genetic expression of COL2A1 during the 21-day chondrogenic differentiation for MJD5.3 from iMSCs derived from DMEM^{++} (B) and hESC (C).

In summary, COL2A1 expression is seen in control and MJD cultured iMSC cells from day 3 onwards. It is not clear whether the decrease in expression seen in MJD cultures after day 5 is real or whether there was a problem with RNA quality.

One additional concern with these results was that the primers, routinely used by many investigators, fall within a single exon, exon 54. Therefore, a second set of primers was designed to cross from exons 53 to 54. These primers were then used to do qRT PCR analysis on the RNA used in the previous analysis.

Using the second set of primers, COL2A1 expression was observed in CT1.5, chondro-differentiated samples from days 0 to 21 (Figure 3.47 B). At day 14 there was a slight decrease before a further increase. [*Note with apologies: lane 2 sample started to run before the other samples were loaded*. It is therefore not a lower molecular weight band]. The untreated day 14 mass did not express COL2A1 (Lane 8) (Figure 3.47 A).

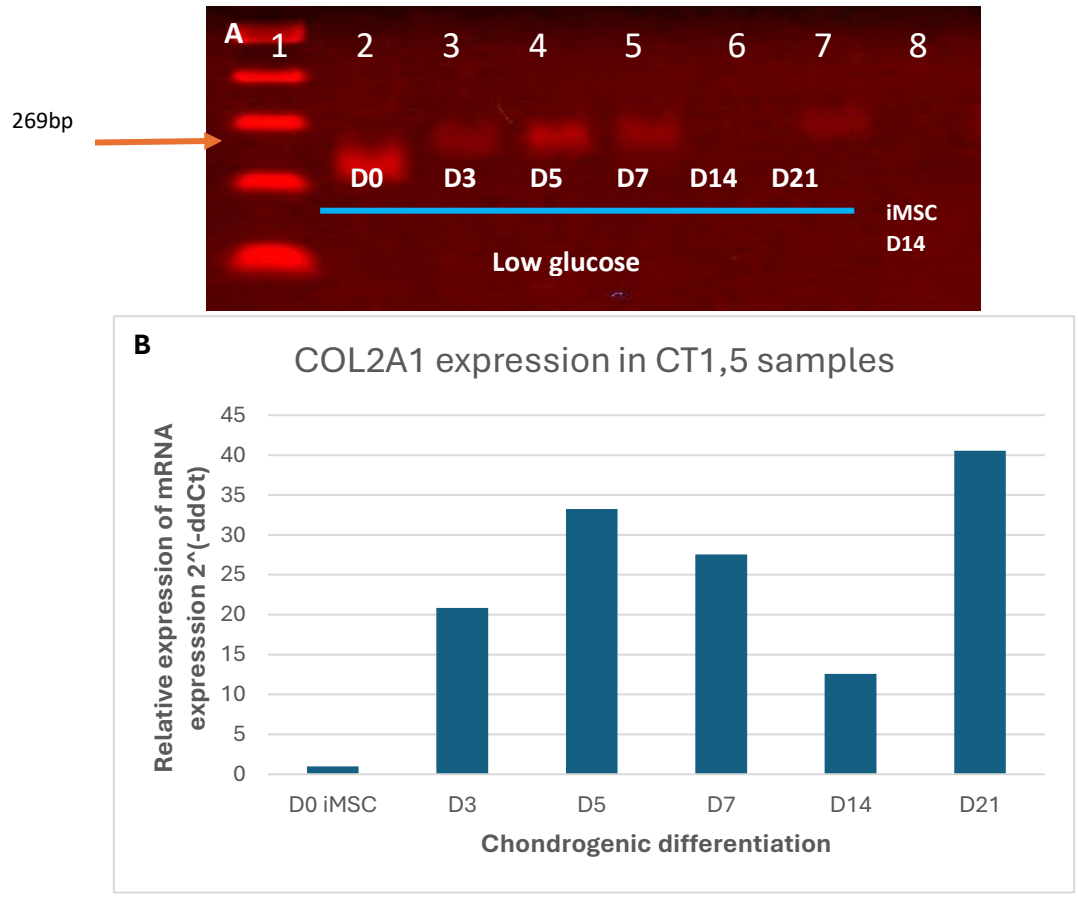

Figure 3.47. COL2A1 expression in chondrogenically induced CT1.5 samples, using primer set 2. A) Agarose gel loaded with; Lane 1= 100bp Marker, Lane 2= Day 0, Lane 3= Day 3, Lane 4 = Day 5, Lane 5 = Day 7, Lane 6 = Day 14, Lane 7 = Day 21, Lane 8 = iMSC- D14 untreated control. B) relative expression of COL2A1 during the chondrogenic differentiation CT1.5 samples. The induced samples all express COL2A1, at varying levels. Human GAPDH was used as a housekeeping gene, and qRT-PCR performed using the StepOne instrument, using SYBR green. The iMSC sample used as a calibrator.

As with the CT1.5 analyses, the MJD5.3 iMSCs grown in either low glucose DMEM (Lane 3), DMEM^{++} (lanes 9) or hESC medium lane 11) expressed COL2A1 (Figure 3.48). However, no expression was seen in the chondro-differentiated samples, from days 3-21 (lanes 4-8). In contrast, there was COL2A1 expression in chondro-differentiation from MJD5.3 cells derived from DMEM^{++} at day 5 (Lanes 10) (Figure 3.48).

These results demonstrate 1) that primer set 2 gave rise to appropriate size qRT PCR product of 269bp, 2) that iMSCs derived from either hESC or DMEM express COL2A1. 3). In CT1.5 control cells, COL2A1 expression increased from day 3 to 21 while expression in MJD5.3 cells was not detected in cells derived from low glucose, but expression was detected in cells derived from DMEM^{++}.

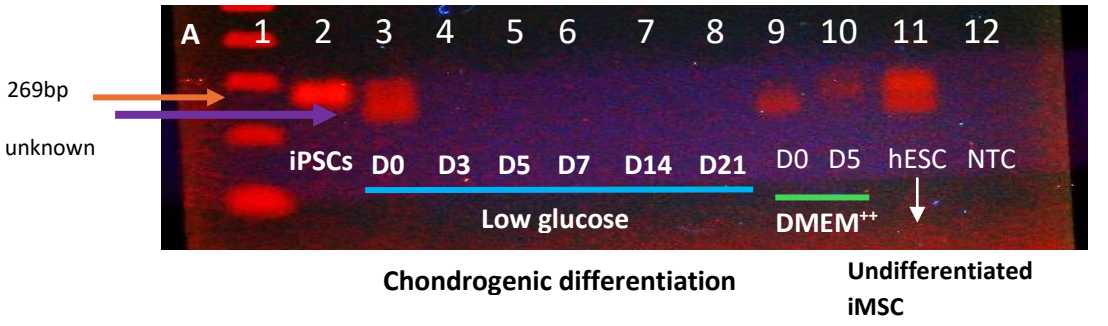

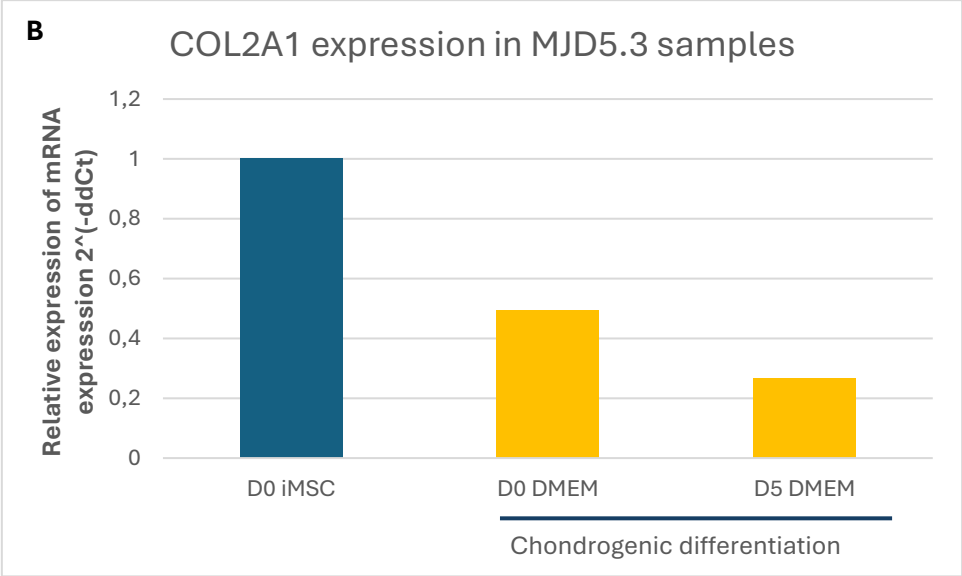

Figure 3.48. COL2A1 expression in chondrogenically induced MJD5.3 samples, using primer set 2. A) Agarose gel loaded with; Lane 1= 100bp Marker, Lane 2= iPSCs, Lane 3= Day 0, Lane 4= Day 3, Lane 5 = Day 5, Lane 6 = Day 7, Lane 7 = Day 14, Lane 8 = Day 21, Lane 9 = Day 0 iMSC - DMEM^{++} derived, Lane 10 = Day 5, DMEM^{++} derived, Lane 11 = iMSC - hESC derived, Lane 12 = NTC. B) relative expression of COL2A1 during the chondrogenic differentiation MJD5.3 samples. The low glucose derived iMSCs induced samples did not express COL2A1, while all the iMSC samples expressed COL2A1 at varying levels, including the D5 DMEM^{++} derived sample. Human GAPDH was used as a housekeeping gene, and qRT-PCR performed using the StepOne instrument, using SYBR green. The iMSC sample used as a calibrator.

The final step in this investigation was to determine whether the cartilage produced in this experiment was the articular type or endochondral type of cartilage. The endochondral cartilage lineage can be identified by the expression of the COL10A1 gene (Zheng et al. 2003).

RNA from CT1.5 and MJD5.3 cells, cultured over a period of 21 days was used for a qRT PCR analysis of COL10A1.

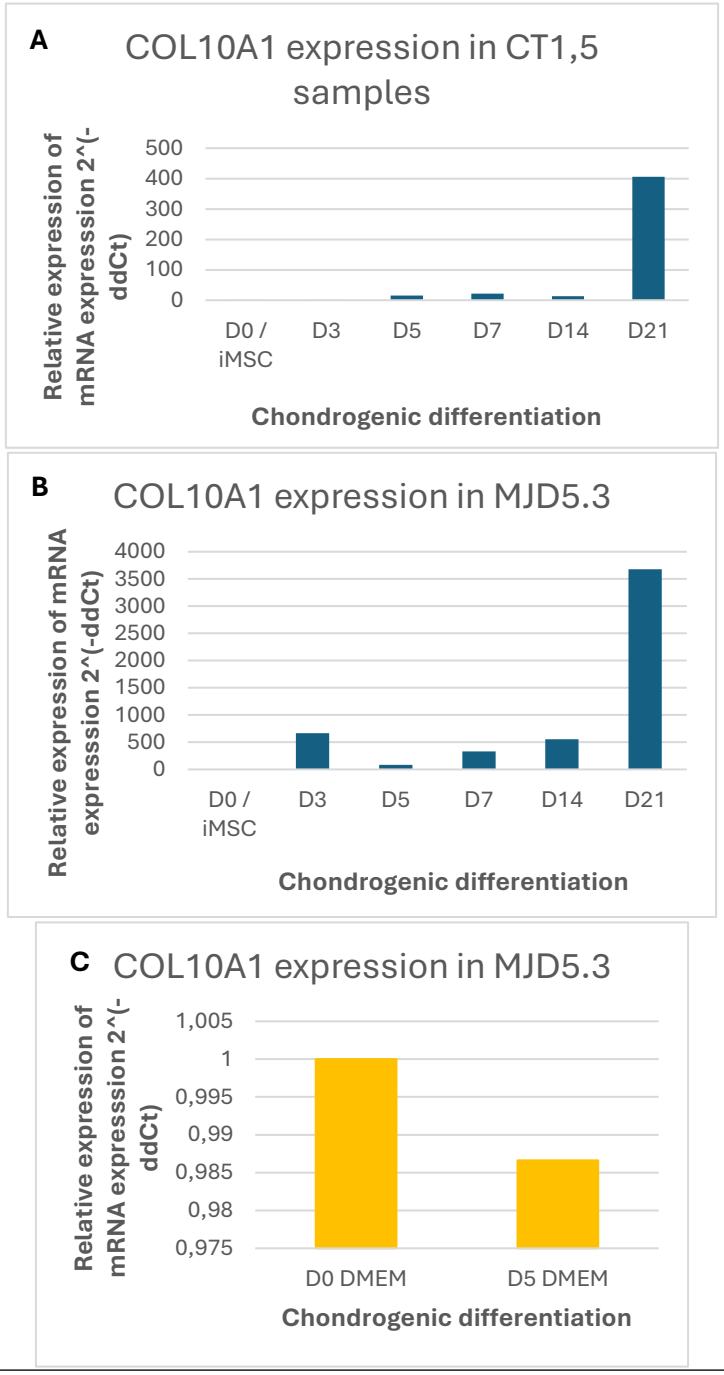

Figure 3.49. COL10A1 expression in chondrogenically induced CT1.5 and MJD5.3 samples. A) Gene expression CT1.5 samples. B) Gene expression in MJD5.3 samples. C) Gene expression in MJD5.3 DMEM^{++} derived. The differentiated samples expressed COL10A1. Human GAPDH was used as a housekeeping gene, and qRT-PCR performed using the StepOne instrument, using SYBR green. The iMSC sample used as a calibrator.

Figures 3.49 A and B showed that both CT1.5 and MJD5.3 cells expressed COL10A1 and showed an increase over the time period studied. This result demonstrate that the cartilage produced in these studies was of the endochondral type and not articular type.

COL2A1 is expressed in undifferentiated iPSCs and multipotent MSCs

In the above experiments, RNA from pluripotent iPSCs was used in all the qRT PCR analyses because it was expected that they would not express the cartilage COL2A1 gene. It was therefore a surprise when this transcript of 122bp was detected in the gels and in the 2^{-DDCt} calculations (Figure 3.46 – lane 2 and Figure 3.50 - lane 2).

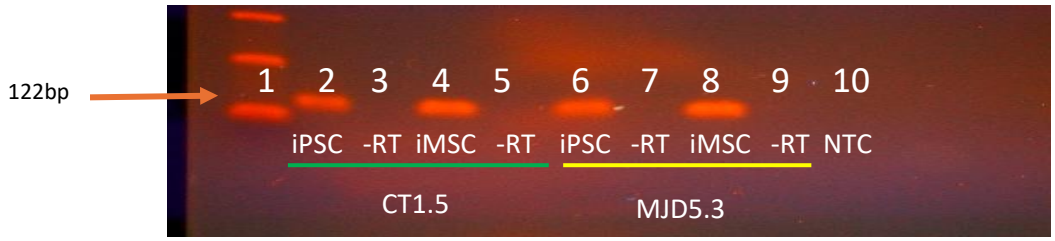

Figure 3.50. COL2A1 expression in undifferentiated iPSCs and iMSC samples. The agarose gel is loaded with; Lane 1= 100bp marker; Lane 2= CT1.5 iPSC sample, Lane 3= CT1.5 iPSC -RT control, Lane 4= CT1.5 iMSC, Lane 5 =CT1.5 iMSC -RT control, Lane 6= MJD5.3 iPSC, Lane 7= MJD5.3 iPSC -RT control, Lane 8= MJD5.3 iMSC, Lane 9 = MJD5.3 iMSC -RT control, Lane 10 = NTC.

After performing many optimisations to exclude the possibility of contaminants, none were found, and the same results were repeatedly obtained. All the control cDNAs without reverse transcriptase resulted in no PCR products, which eliminated the possibility of genomic DNA or any other contamination. Therefore, a new set of primers for the 122bp transcript was purchased, but this gave the same result. Lastly, a third set of primers (primer set 2 mentioned above) designed to cross exons was obtained and tested. In these experiments, the iPSCs also showed expression of COL2A1 (Figure 3.48 lane 2).

To further investigate whether this was an anomaly due to some unknown factor in this study, additional samples were tested using the 122 bp primer set included the following cell lines: CT1.5 and MJD5.3 iMSCs, cDNA from CT1.5 iMSC cells obtained independently by a colleague who had derived them using the embryoid body technique (Dimakatso Gumede, PhD thesis, 2019); two different lines of normal human fibroblasts; 1.2 iMSC from Dimakatso Gumede, (PhD thesis, 2019). In all cases, expression of the correct size product, 122bp, was seen (gel in Appendix C). This interesting result requires further investigation-see discussion.

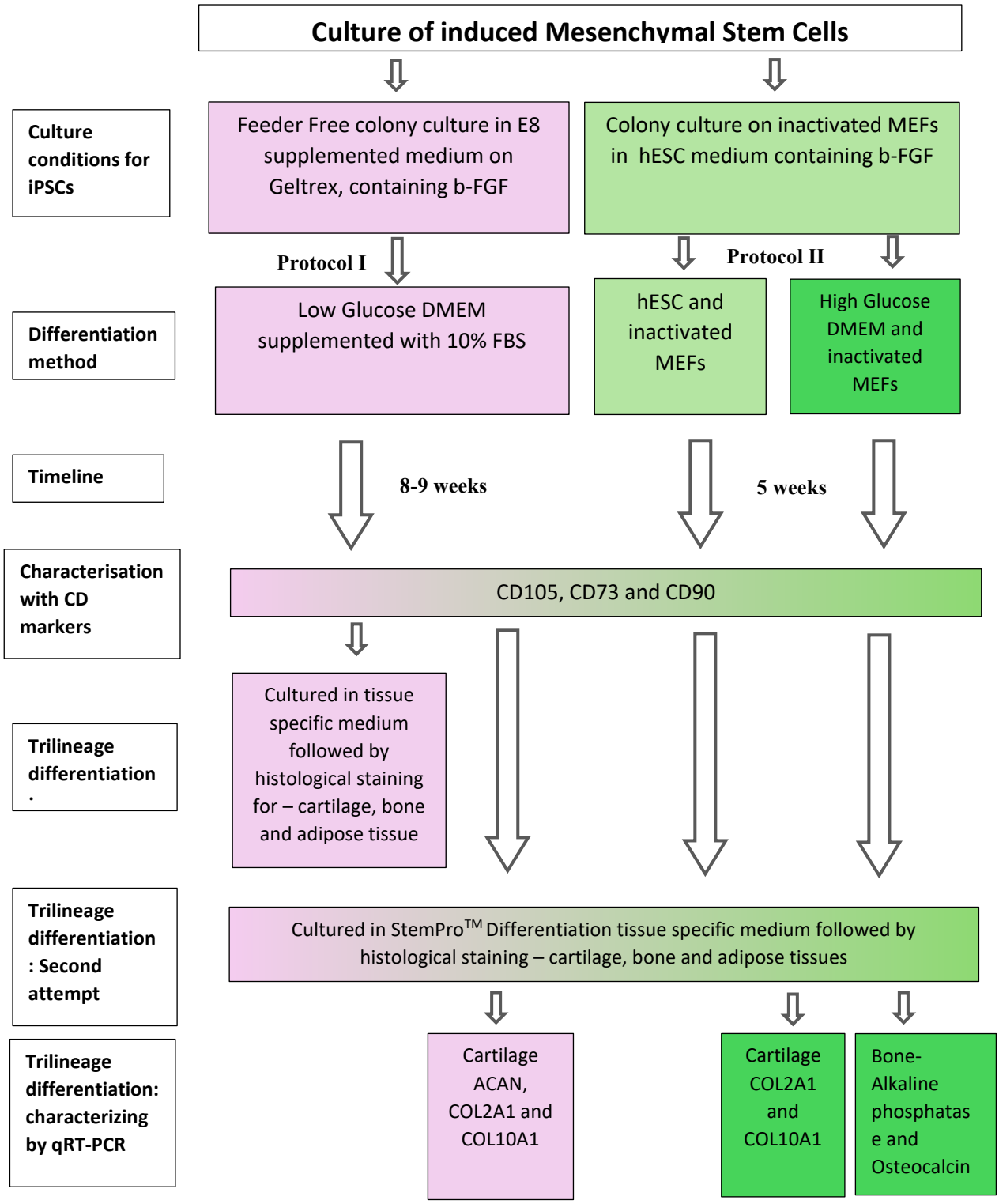

Figure 3.51. A schematic representation depicting the experiments performed on iPSC derived MSCs and highlighting the findings of this study.

Chapter 4 Discussion

The first step of this study was to derive, expand, maintain and characterise the iPSCs from Mseleni patient and control fibroblasts. The first steps in this process, the iPS cell derivation from patient fibroblasts, were carried out by a colleague prior to the start of the present project. In brief, a trip to the Mseleni region of Kwa-Zulu Natal led by anthropologist Professor Vicky Gibbon, enabled the collection of skin punch biopsies from Mseleni patients and control samples. They were transported back to Cape Town on ice. Two patient biopsies and one control biopsy were selected for this study. Fibroblasts were grown and cultured from these biopsies by Mrs Desiree Bowers at the University of Cape Town. After an unsuccessful attempt by Elizabeth Dinkele, a PhD student at the UCT laboratory, to derive iPS cells from these fibroblasts, samples were sent to the CSIR in Pretoria where they were successfully reprogrammed by Dr Janine Scholefield using the CytoTune^{TM} iPS 2.0 Sendai reprogramming kit (Invitrogen). After characterization at P3 by her, the iPSCs were cryopreserved at P3, and sent to the Cape Town laboratory on dry ice.

At the outset of this project, several technical problems were faced in culturing and expanding the iPSCs on inactivated MEFs, and these are discussed below. The first problem I encountered was that the colonies looked normal at first, but they all started to spontaneously differentiate either after the first passage or one or two passages later. To solve this problem, a range of possible causes were considered and tested.

The first concern was the quality of the mouse feeder cells (MEFs). These cells play two important roles in stem cell culture. They secrete two important growth factors, b-FGF and TGF-β into the medium which helps maintains pluripotency, and they provide an extracellular matrix for iPSCs to attach (Amit et al. 2000). One consideration was that the working batch of inactivated MEFs might not have been functioning optimally, possibly because of a prolonged storage time. Therefore, a new batch of MEFs was inactivated with Mitomycin C and tested for their ability to maintain pluripotency. However, this didn't help resolve the problem and the cells continued to differentiate spontaneously. A different matter pointed out by Heng, Liu and Gao, (2004), is that the density of the inactivated MEFs might have an influence on their effectiveness as feeder cells. Working with embryonic stem cells (ES), they showed that an inactivated MEF cell density of 60 000 cells/cm^2 was more efficient at maintaining ES pluripotency than a cell density of 32 000 cells/cm^2. In the present study, two different densities were tested: the recommended density of 17 000 cells/cm^2 and a density of 34 000 cells/cm^2. However, neither density allowed for successful propagation without spontaneous differentiation,

suggesting that feeder density was not the primary problem. Alternatively, an even higher density might have been needed, but this was not tested.

Another possible cause of the spontaneous differentiation has been explained by Uhrig, Ezquer and Ezquer, (2022), who reported that iPSCs are highly sensitive during the first three passages after reprogramming and often undergo spontaneous differentiation or cell death after freezing then thawing. They advised that iPSCs should therefore not be frozen at P3 but rather be cultured to later passages before being frozen. Unfortunately, in the present study, we were unaware of this possible problem. The cells were cultured in a laboratory in Pretoria and had to be frozen to be sent to Cape Town as soon as possible to allow this study to be initiated. (Had we known at the time that problems might arise, we might have suggested that the cultures be passaged one or two more times before being sent to us.).

The next problem-solving step was to focus on the role of growth factors in iPSC cultures. Fibroblast growth factor 2 (FGF-2), plays a key role in regulating pluripotency by directly controlling the expression of pluripotency genes. As can be seen in Figure 4.1, FGF-2 functions in a complex pathway to trigger phosphorylation and post-translational modifications of target proteins through the PI3K/Akt and ERK pathways. This results in self-renewal and maintenance of pluripotency in stem cells (Oke and Manohar 2024). In addition, FGF-2 achieves this critical role through the activation of the inactivated MEFS, which leads to the release of factors such as TGF-β and more FGF to help maintain pluripotency (Bendall et al. 2007). The FGF-2 works together with factors such as TGF-β synergistically to support pluripotency (Greber, Lehrach, and Adjaye 2007).

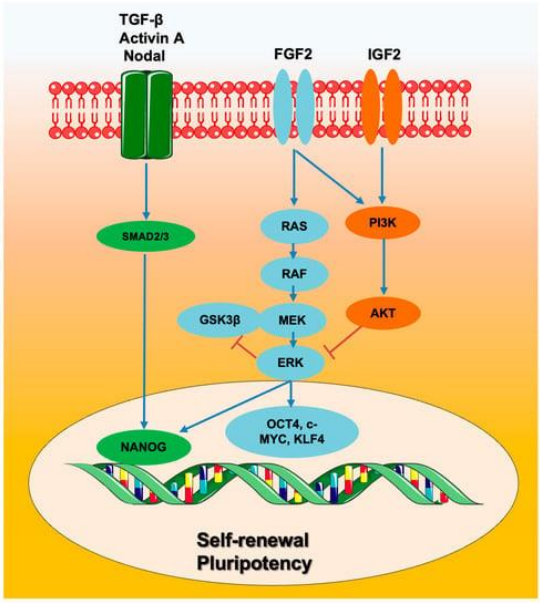

Figure 4.1. Key signaling pathways regulating pluripotency in hES and iPS cells. FGF-2 binds to its receptor FGFR which activates several downstream pathways such as Ras/Raf/MEK/ERK and PI3K/Akt and thereby maintains pluripotency of hESCs. (Varzideh et al. 2023)

There have been many studies to clearly understand the mechanism in which FGF-2 can maintain pluripotency of stem cells. It has also been found to play a role in maintaining pluripotency while inhibiting cell death (Mossahebi-Mohammadi et al. 2020). In addition, the seemingly conflicting response of cells to FGF might be explained by differences in culture conditions, cell lines or even pathway dose-dependency (Haghighi et al. 2018).

Taking the above information of b-FGF into account, in the present study, various b-FGF concentrations were tested, starting from 10 ng/ml increasing to 20 ng/ml, with medium that was changed every day. The increase in b-FGF to 20 ng/ml resulted in improved iPSC cultures and prevented spontaneous differentiation. (It is possible that the new batch of inactivated MEFs contributed to this, however the increase concentration of b-FGF with the old inactivated MEFS was not tested).

After the iPSC culture problems were resolved with the increased b-FGF concentration, it was possible to routinely passage and characterise all three cell lines MJD5.3, MJD8.5 (Mseleni patients) and MJDC3.4 (Mseleni control). iPSC colonies between P8- P10 were grown on coverslips, processed with immunocytochemistry and were all shown to express the pluripotency proteins NANOG, TRA-160 and OCT3/4. Subsequently, cells were cultured in specialised medium and all effectively expressed

mesoderm, endoderm and ectoderm markers. This strongly suggested that the iPSCs were pluripotent.

As noted in the Results, an additional control cell line (CT1.5), independently derived in Cape Town, did not undergo spontaneous differentiation as observed in the Mseleni derived cells. Unlike the Mseleni cell lines which were derived from skin biopsies from adult donors, the CT1.5 cell line was derived from a juvenile foreskin tissue in 2014 by Dr Robea Ballo. Several factors might have benefited this line: it was derived by a researcher in Cape Town, who had time to culture the cells to a higher passage number before freezing. Furthermore, the CT1.5 iPSCs were derived using reagents from different batches and lot numbers which could have also contributed to its stability. Additionally, for this MSc project, the cells used were from passage 18-20, stable enough to be propagated for further research and did not require further optimisation. Lastly, the young age of the donor may have influenced the cell line's robust pluripotency.

Following the successful culture of iPSCs, several ideas were considered as to how to further improve the culture conditions of iPSCs and to reduce spontaneous differentiation in order to have successful downstream applications. The main factors considered were the processes of thawing, passaging, and freezing of the cells.

Thawing new vials of iPSC cells from liquid nitrogen stocks: whether to culture on inactivated mouse feeder cells or to culture in a feeder free environment requires carefully controlled freezing and thawing conditions to avoid the problems associated with spontaneous differentiation (Uhrig, Ezquer, and Ezquer 2022). The freezing down step is especially critical. In the present study, all freezing down occurred in 40 % FBS and 10 % DMSO in KODMEM. One possible cause for the spontaneous differentiation observed in this study is that stem cell specific FBS was required in the freeze down medium. However, HIPSC-qualified FBS proved to be prohibitively costly. It was therefore recommended to increase the concentration of normal FBS from 40 to 60% with 10% DMSO in KODMEM for freezing down of iPS cells, the rationale being that higher concentrations of FBS would deliver higher concentrations of growth factors and the serum proteins provide greater protection from ice crystal formation. However, it is known that medium containing FBS promotes differentiation of iPSCs towards the mesenchymal (mesodermal) lineages because of the multiple growth factors it contains (Uhrig, Ezquer, and Ezquer 2022). Intriguingly, and it has been shown, it also encourages differentiation even during a typical cryopreservation process that involves a controlled freezing rate (approximately 1 ^{O}C per minute) that occurs when vials are placed at -80 ^{O}C, and the fast-thawing

process that occurs at 37 ^{O}C. Although these processes are considered as quick processes, it has been claimed that they allow for the 60% FBS to influence some differentiation in the iPS cells (Liu and Chen 2014). They, together with others, recommend replacing FBS with alternatives such as 90% supplemented Essential 8™ (E8) medium with 10% DMSO or replacing the FBS with lower KOSR concentration (25%) and 10 % DMSO in KODMEM, if 90 % supplemented Essential 8™ (E8) medium is too expensive. In future, replacing the FBS with E8 supplemented medium should be considered to decrease the chances of differentiation.

Passaging of iPSCs is important for propagating and expanding them. However, the timing of passaging is important. As with all other cells, the iPSCs have a logarithmic cell growth phase, which is 2-4 days after seeding. This means that iPSCs must be lifted from the culture vessel during the growth phase for enhanced survival after plating. In the present study, iPSC culture growth periods were 5-8 days in order to obtain colonies of sufficient size for manual passaging; however, in the review by Uhrig, Ezquer and Ezquer, (2022), it was noted that culturing iPS cells for longer than the suggested period of 2-4 days takes them into a stationary phase. This would cause the cells to struggle to recover after a passage or a thaw, as was observed in the present study. Freezing down during the logarithmic phase is especially important as it has been shown that the iPSCs recover better after thawing by Liu and Chen, (2014).

For future studies, should the problem of iPSC differentiation persist, another consideration would be to use multiple clones from one iPSC line to overcome clone-clone variability and to make sure that the observations seen in my iPSC cultures are due to technical problems and not cell line specific problems. In this study, due to the time delay resulting from the many problems faced, it was not possible to investigate additional clones for each cell line.

Culture in feeder free (FF) conditions

In the present study, having established the conditions for culture on feeder layers, the next challenge was to establish cultures in feeder-free conditions. This was necessary in order to measure the level of expression of pluripotency genes in the iPSCs and to eliminate the influence of the RNAs coming from the inactivated MEFs. iPSCs grown on feeder layers were transferred to Geltrex-coated dishes as described in culture medium containing b-FGF. However, unexpected problems arose; cells settled on the Geltrex matrix for a day or so but started to lift 48 hours after they were seeded. Many different attempts proved unsuccessful. This was a consistent observation that occurred with all the iPSC including the CT1.5 line. Several factors could be causing the lifting of the cells, leading to premature

cell death, but this discussion will focus on one key possibility, the effect of Geltrex as a substrate in feeder-free conditions.

Geltrex is a simplified extracellular matrix, extracted from Engelbreth-Holm-Swarm (EHS) tumour cells. It is one of the most widely used growth-factor enriched basement matrices (hiPSC-Qualified) used as a substrate for maintaining iPSCs. It contains components such as laminin, heparin sulfate proteoglycan, entactin and collagen IV that are all required for the growth and attachment of iPS cells. Another commonly used iPSC substrate is Corning® Matrigel® Matrix (Matrigel, USA). The origin and composition of Geltrex and Matrigel are similar. However, Geltrex was less expensive compared to Matrigel and was therefore chosen for this project (Kawase and Nakatsuji 2023)[1]. It is possible that Matrigel could have been a better matrix, however, this was not affordable. Another possible cause for iPS cells not seeding well onto Geltrex could be due to the freezing conditions prior to seeding onto the matrix as discussed in the previous section.

A "breakthrough" in the culture of cells in feeder free conditions occurred as follows. During the various attempts to optimize feeder free cultures it was noted that although most cells lifted and died, a few cells remained attached after 2-3 days. With the idea that these cells might survive given a few more days, medium was replaced to remove the dead floating cells, and the plates were then left for 4-8 days in the incubator without a medium change. Fortuitously, these cells survived and divided, and this resulted in 1-3 colonies per dish that started to grow in a typical iPSC fashion. E8 medium containing b-FGF was then changed regularly. The colonies were passaged as normal, enabling the next steps of the project to continue. It is not easy to explain how the cells seen at days 2-3 retained pluripotency despite the lack of a medium change. Pluripotency was confirmed by positive gene expression for NANOG, OCT3/4 and SOX2 using qRT-PCR. It is possible that the problems seen later (see discussion below) might have been the consequence of the unusual start of these colonies. Maybe the cells were not fully pluripotent which might explain why problems were seen in later experiments for example, spontaneous differentiation. Overall, although the colonies were obtained, the challenges faced under feeder free conditions led to insufficient cells and in the end experiments could not be repeated.

[1] https://www.researchgate.net/post/What_is_the_difference_between_Geltrex_and_Matrigel_used_in_primed_hiPSCs_culture/64ded799e9c4cf7796024147/citation/download?_tp=eyJjb250ZXh0Ijp7ImZpcnN0UGFnZSI6InF1ZXN0aW9uIiwicGFnZSI6InF1ZXN0aW9uIn19

Deriving MSCs from iPSCs

The main focus of this study was to derive osteogenic and cartilage precursors to investigate whether there were any differences in these processes between the Mseleni patients and the controls. To achieve this, the next step was to derive mesenchymal stem cells from iPSCs by inducing epithelial-to-mesenchymal transition (EMT) (Høffding and Hyttel 2015). The mesenchyme cells thus produced have been called “induced mesenchymal stem cells” or iMSCs.

EMT is a well-defined process; *in vivo*, EMT is involved in many processes during embryogenesis, where epithelial cells delaminate and migrate to form distant organs, and as well as in wound healing. EMT also produces cancer cells that invade and metastasize (Kalluri and Weinberg 2010). EMT is regulated at multiple levels by various factors, including cell signalling, transcriptional control, epigenetic modification, and post-translational modification (reviewed by (Serrano-Gomez, Maziveyi, and Alahari 2016)). EMT induces changes in cell morphology and the cells transition from a cobble stone like morphology (epithelial) to a spindle shaped mesenchymal phenotype. During this process, the tight cell-cell junctions and cytokeratin intermediate filaments are lost, while cytoskeletal remodelling occurs with the development of vimentin and fibronectin intermediate filaments. In addition to this, cells gain the ability to produce and migrate through the ECM (reviewed by Kim *et al.*, (2018)). In Figure 4.2, these changes have been clearly sketched by Høffding and Hyttel, (2015) in the description of the reverse process of MET (Figure 4.2).

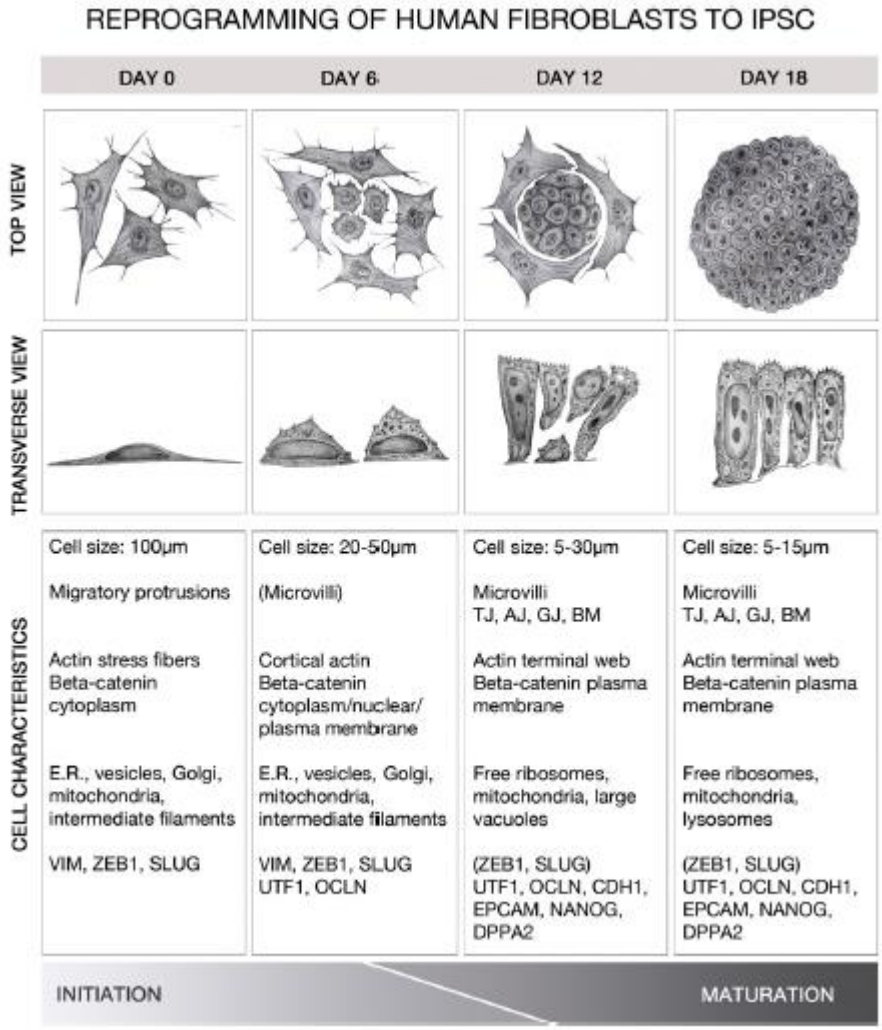

Figure 4.2. Overview of morphological changes and gene expression dynamics during episomal reprogramming of human fibroblasts to iPSC. Abbreviations: TJ: tight junctions, AJ: adherens junctions, GJ: gap junctions, BM: basement membrane, E.R: endoplasmatic reticulum. [image taken from Høffding and Hyttel, (2015)]

To induce the transition of iPSCs to MSCs, two protocols were followed as summarised in Figure 4.3. In Protocol I, following Zhou *et al.*, (2018), feeder free iPSCs were cultured on Geltrex in E8 stem cell culture medium, followed by replacing the E8 medium with low glucose supplemented DMEM. In Protocol II, iPSCs were passaged from the feeder layer, transferred into gelatine coated dishes and were either treated with DMEM containing FBS or with hESC medium containing b-FGF. Both protocols showed iPSCs undergoing a transition towards the mesenchymal phenotype through the EMT process. The edges of the iPS colonies in the first 24-hour period of medium change **(see Figures 3.16-3.20 under section 3.3.1 and Figures 3.30, 3.31 and 3.33 under section 3.3.2)** immediately displayed the loss of the tight iPS colony organization. The cells at this region became flat and lost their tight cell-to-

cell contacts as they transitioned towards the mesenchymal phenotype. The cells cultured in low glucose medium were noticeably smaller in size compared to the DMEM^{++} and hESC cultured cells at the earlier passage numbers (P0-P2). However, they eventually took up the same mesenchymal morphology and cell size at later passages (P3-P4). Even though the CT1.5 and MJD5.3 cells in this project were not stained for vimentin and fibronectin proteins, prominent migratory protrusions and vesicles were observed as seen in in Figures 3.16-3.20 and Figures 3.30 – 3.34. Overall, the cellular changes were consistent with EMT transitions. These changes have been clearly sketched by Høffding and Hyttel, (2015) in the description of the reverse process of MET (Figure 4.2). In the diagram figure 4.2, Høffding and Hyttel, (2015) outline the process of MET.

The next step was to examine gene expression profiles as the cells underwent EMT, using some key CD markers characteristic of mesenchymal stem cells. The definitive characterisation of mesenchymal stem cells from a range of somatic sources has been under much investigation over many years (Choudhery et al. 2022). In general, the guideline commonly used is that MSCs express markers such as CD105, CD90, CD73 and do not express typical haemopoietic markers such as CD34, CD45 and CD35 (Dominici et al. 2006). This guideline is often used in flow cytometry and cell sorting experiments to purify or enrich for the particular cell line in which they are interested. There have also been some studies on the derivation of MSCs from iPSCs, where investigators have sorted cells by flow cytometry (Rajasingh et al. 2021). They have also used trilineage differentiation and transcriptome analysis to characterise MSCs or the differentiated cells (Spitzhorn et al. 2019). Similar to Rajasingh *et al.*, (2021), in the present study, gene expression analysis by qRT-PCR was conducted to determine whether the cells expressed the markers typical of mesenchymal cells. In general, all three markers, CD105, CD90, CD73, were expressed in cells cultured in low glucose (Protocol I) while CD105 and CD73 were expressed in those cultured in DMEM^{++} and hESC (Protocol II). However, in interpreting this, three factors needed to be taken into account; firstly, the results were from single experimental runs which were not repeated; secondly the cells analysed would have been a mixed population (i.e. not all mesenchymal) which could have given rise to many variations and, thirdly, it was found that CD90 was expressed in the iMSCs and in the iPSCs as reported by Wang, Sweeney and Malech, (2011). Interestingly, the overall expression of the CD positive MSC markers revealed that the hESC-derived MSCs, especially the MJD5.3 patient line, had high expression levels of CD105 and CD73 compared to CT1.5. In addition, DMEM^{++} derived MSCs expressed these CD markers better than those derived from low glucose DMEM (Protocol I). Without repeating these experiments, it is not possible to give a good explanation for the differences in gene expression observed in the MJD5.3 and CT1.5 cell lines when using the three different media.

When reviewing the expression of CD105, the trend with the high expression of CD105 expression in hESC-derived iMSCs seemed to correlate with the spike in NANOG expression in the hESC-derived iMSCs we observed. These cells were cultured with medium supplemented with FGF-2, which could suggest a link between the two (FGF-2 and NANOG expression). However, it could also possibly suggest that the culture contains two distinct populations of cells: NANOG positive cells may not be the same cells that express the iMSC positive CD markers, as suggested by Pierantozzi *et al.*, (2011). If it is the former case, the iMSCs derived using FGF-2 supplemented hESC medium, expressing NANOG, could be similar to those isolated from bone marrow and adipose tissue (Heo et al. 2016). However, a full gene profiling would be necessary to confirm and clarify these observations.

iPSCs are able to differentiate into bone cartilage and adipose:

The final stage of this project was to assess the differentiation potential of the iPS cells into adipogenic, osteogenic and chondrogenic lineages. This trilineage differentiation was first carried out using the media prepared in the UCT laboratory (section 2.4.2). However, the results obtained were poor and could not be repeated. Therefore, commercially available StemPro® Differentiation medium was purchased and used as described in the Materials and Methods and successful trilineage differentiation using samples from Protocol II was achieved (as summarised in Figure 3.51). In summary, adipogenic lineage was confirmed by Oil red O staining. The osteogenic lineage was confirmed by Alizarin Red staining and the positive expression of the bone- specific genes, alkaline phosphatase and osteocalcin. The chondrogenic lineage was confirmed by Toluidine Blue staining for the extracellular matrix and the expression of COL2A1 and COL10A1 genes.

The two main tissues of interest in the present study are bone and cartilage because these are the tissues involved in the formation and physiology of joints. Specifically, it is hypothesized that the joint abnormalities in MJD arise from a disturbance of either cellular proliferation and /or differentiation during articular cartilage development. Such abnormalities in cartilage formation may influence the shape of the joint, the joint surface and the growth of the long bones. This would explain the pathology of early joint arthritis in MJD patients and would also provide a clue to the understanding of dwarfism associated with MJD. For this reason, the results from the osteogenic differentiation and the chondrogenic differentiation will be discussed in more detail here.

For the osteogenic differentiation, CT1.5 and MJD5.3 were used to assess the expression of alkaline phosphatase and osteocalcin, both markers of bone formation. Alkaline phosphatase (ALP) is a critical enzyme involved in bone and cartilage development and is widely distributed across tissues, with significant expression in bones and mineralizing structures. It is regulated by complex pathways that

are governed by signalling molecules, hormonal influences, and epigenetic factors (Golub and Boesze-Battaglia 2007). During early bone differentiation, ALP is produced and located on the cell surface of bones and calcifying cartilage (Siller and Whyte 2018). As the bone matures, the ALP expression reduces while bone specific genes like osteocalcin are upregulated (P. Zhou et al. 2021). In this study, both CT1.5 and MJD5.3 cell lines cultured in DMEM medium resulted in positive ALP expression with CT1.5 showing a relatively high expression compared to MJD5.3. In order to determine whether the ALP expression decreases as the cells differentiate towards bone, longer culture periods may be needed.

Osteocalcin (OC), as mentioned above, plays a critical role during osteogenesis and it was analysed in this project. As with the results for ALP, the CT1.5 control cell line displayed an overall higher expression of osteocalcin compared to MJD5.3. Interestingly, when the qRT-PCR product was checked on an agarose gel, two qRT-PCR product bands were observed in both CT1.5 and MJD5.3 samples from days 0 to 21, with band sizes of 158bp and a lower band of 50bp. It is known that the osteocalcin gene product undergoes alternative splicing, which produces multiple transcript variants encoding different isoforms (Jung et al. 2001). These isoforms have been shown to result from frame shifts in the downstream coding sequence, leading to distinct C-termini ([2]). In summary, the results show that there is no difference in osteocalcin expression between the MJD patients and control samples. Interestingly, the results also revealed that osteocalcin is expressed in the iPSC cells, but at much lower expression levels compared to the differentiated samples. However, in the iPSCs, only the 158bp band was seen. The function of osteocalcin in iPSCs is not known: it seems unlikely that it would play the same role as it does in bone. One important follow up experiment would be to determine whether the osteocalcin transcript is functional in iPSCs, by determining whether the protein is present.

One of the key aims of this study was to generate iPSCs derived cartilage precursors from MJD and control samples. This would enable us to study and understand whether there are any molecular differences or abnormalities occurring during chondrogenic differentiation in individuals with MJD. In addition, the development of articular cartilage *in vitro* is of widespread interest to stem cell biologists because of the pressing need to find ways to repair articular cartilage in patients suffering from severe osteoarthritis (Sandell and Aigner 2001; Sandell 2012). One of the biggest difficulties has been the development of a type of cartilage, like articular cartilage, that does not undergo hypertrophy either *in vitro* or when transplanted *in vivo*.

[2] https://www.ncbi.nlm.nih.gov/gtr/genes/100527963/

In this study, iPSCs derived MSCs were differentiated using the StemPro® Chondrocyte Differentiation medium for 21 days. Overall, there was a temporal increase in COL2A1 gene expression in the control sample compared to the patient line, which seemed to have a decrease in expression from day 5. The results, however, reveal that the cartilage produced was of the endochondral type as evidenced by the expression of the hypertrophic marker COL10A1. Although it is not known what is in the StemPro® Chondrocyte Differentiation medium (as their policy is not to reveal the composition), it is highly likely that it contains the ingredients that direct cells towards the endochondral type of cartilage.

[As a side issue: I wish to consider some thoughts regarding the repeated observations that the cell lines from Mseleni (i.e the control and MJD cell lines that were derived by a colleague at CSIR) differentiated more readily compared to the control cell line that was derived independently much earlier at UCT. In addition, these cell lines gave more trouble than the control cell line and in addition it was difficult for cartilage nodules to form. One possibility is that in the earlier experiments, to overcome the spontaneous differentiation a higher concentration of bFGF was used (20 ng/ml instead of 10 ng/ml); it is possible that this set the cells into a state that it made them more resistant to chondrogenesis.]

In designing future experiments, it would be necessary to create conditions that drive iPSCs toward the articular cartilage lineage and prevent hypertrophic cartilage formation. There have been a number of investigators who have pursued this difficult problem. For example, Pothiawala *et al.*, (2022), found that by selecting out the cells expressing SOX9 and including those expressing GDF5, they succeeded in producing articular cartilage. Their approach, in brief, was to use transgenic mice expressing SOX9 and GDF5 fluorescent transgenes. This enabled them to separate the fast-growing SOX9 cells from the slow growing GDF5 cells. They found that the SOX9 expressing cells developed into hypertrophic cartilage whereas the GDF5 expressing chondrospheroids were of the articular cartilage type. They went on to show that these nodules did not ossify when transplanted into immunodeficient mice.

In contrast, Gadomski *et al.*, (2024), have reported that SOX9 positive chondrospheroids express high levels of COL2A1 but minimal expression of COL10A1 and ALP. On transplantation into the joints of immunodeficient rodents they found that the cartilage did not heal but the spheroids persisted for over 5 months *in vivo*. These differences in findings, between Pothiawala *et al.*, (2022) and Gadomski *et al.*, (2024), could be explained because different cell lines, different protocols and different reagents

were used. There have been few other studies of this nature which highlights the difficulty in developing articular cartilage invitro.

In the present study to determine expression of COL2A1 in chondrogenic micromass, it was expected that the undifferentiated iPSCs would not express the COL2A1 since COL2A1 encodes a collagen protein that is associated with differentiation. Therefore, it was a surprise to repeatedly find that iPSCs seemed to express a version of COL2A1. On a recent intensive literature research, I came upon a paper Oganesian, Zhu and Sandell, (1997) that showed that COL2A1 is expressed in developing human embryos at day 50 and day 53. Their results demonstrated that Type II procollagen is synthesized by alternative splicing of COL2A1 mRNA of exon 2 (Oganesian, Zhu, and Sandell 1997). Specifically, the chondro-progenitor cells as well as a number of non-cartilaginous cells and tissues synthesize Type IIA procollagen, while Type IIB procollagen is synthesized by mature chondrocytes. In the present study, it was found that the relative expression of COL2A1 revealed that iPSCs expressed much lower levels of the transcript compared to the differentiated samples. The present study made use of different primers compared to Oganesian, Zhu and Sandell, (1997). Nevertheless, they gave similar results. Lastly, Lui *et al.*, (1995) also found COL2A1 in human foetuses using *in situ* hybridisation. Their very high quality *in situ* results showed expression in a number of non-chondrogenic tissues including tooth bud, liver, and the meninges of the brain. They theorised that this widespread expression of COL2A1 suggests that "…in addition to contributing to the structural integrity of the cartilage extracellular matrix, type II procollagen may serve a morphogenetic role in embryonic development."

Lastly, a paper by Zimmermann *et al.*, (2008) provided useful information on the methylation patterns in the promoter region of COL2A1 and COL10A1. Their study included human articular chondrocytes, MSCs and MSC-derived-chondrocytes. They found that "the transcription site of COL2A1 was unmethylated in all cell groups and this was independent of COL2A1 expression. In contrast, the promoter of COL10A1 gene was consistently methylated in human articular chondrocytes." They concluded that methylation based COL10A1 gene silencing is established in cartilage tissue and in human articular chondrocytes. However, the altered methylation of CpG sites in the COL10A1 promoter during *in vitro* chondrogenesis, would induce COL10A1 expression (Zimmermann et al. 2008).

Concluding remarks

In summary, in the present study, despite having faced a number of technical challenges, iPS cells were successfully cultured, expanded and characterised. Using two different protocols, iMSCs were derived from the iPSCs that showed strong multipotency potential through their expression of CD positive markers, CD73 and CD105 and as well as their ability to form adipose, bone and cartilage tissues.

Chondrogenic cultures were achieved using both control and MJD patient cell lines, which then showed that they could generate cartilage precursors to study differences and any abnormalities that may be present between the patient and control lines. It was encouraging to see that there might be potential differences between the control and patient line, in the COL2A1 expression. This, of course, could very well result from the technical issues faced throughout this study.

It is very important to note that these experiments are preliminary and were influenced by several technical problems that had to be addressed along the way. Moving forward, in order to study variations in key genes that play important roles in structural and functional properties of articular cartilage, future experiments should include:

1. Multiple clones for each cell lines, to support and confirm trends in gene expression and morphological features observed.
2. The use of a chondrogenic differentiation protocol that encourages iMSCs to express GDF5, as they have been shown to produce stable articular like cartilage type (Pothiawala et al. 2022).
3. The culture periods should be longer and be reproducible.

One of the limitations of the study was the large number of iMSCs required for the chondrogenic differentiation experiments. Cells had to be cultured in big, T175, flask, while also facing challenges such as cellular senescence before reaching the required number of cells. Therefore, doing a growth curve experiment of the control and patient iMSCs would be beneficial in understanding their proliferation rates and capabilities.

Lastly, obtaining sufficient RNA of good quality to study qRT-PCR analyses was one the biggest limitations. The micromasses solidified as early as day 5 and not having enough iMSC cells to plate enough wells for later time points of the study was challenging.

Despite these challenges, this research shows great promise of using iPS cells to make a disease model that will lead to the understanding of how the MJD develops and how it potentially differs from the other osteoarthritis.

List of References

Agarwal, S., Phadke, S., Fredlund, V., Viljoen, D. & Beighton, P. 1997. Mseleni and Handigodu familial osteoarthropathies: syndromic identity? *American Journal of Medical Genetics.* 72(4):435-439. https://doi.org/10.1002/(SICI)1096-8628(19971112)72:4%3C435::AID-AJMG12%3E3.0.CO;2-S

Alexander, Colin. 1965. "The Aetiology of Primary Protrusio Acetabuli." *The British Journal of Radiology* 38: 567–80. https://doi.org/10.1259/0007-1285-38-452-567.

Aliborzi, Ghaem, Akbar Vahdati, Davood Mehrabani, Seyed Ebrahim Hosseini, and Amin Tamadon. 2016. "Isolation, Characterization and Growth Kinetic Comparison of Bone Marrow and Adipose Tissue Mesenchymal Stem Cells of Guinea Pig." *International Journal of Stem Cells* 9 (1): 115–23. https://doi.org/10.15283/ijsc.2016.9.1.115.

Amin, A. K., J. S. Huntley, A. H.R.W. Simpson, and A. C. Hall. 2009. "Chondrocyte Survival in Articular Cartilage: The Influence of Subchondral Bone in a Bovine Model." *Journal of Bone and Joint Surgery - Series B* 91 (5): 691–99. https://doi.org/10.1302/0301-620X.91B5.21544.

Amit, Michal, Melissa K. Carpenter, Margaret S. Inokuma, Choy Pik Chiu, Charles P. Harris, Michelle A. Waknitz, Joseph Itskovitz-Eldor, and James A. Thomson. 2000. "Clonally Derived Human Embryonic Stem Cell Lines Maintain Pluripotency and Proliferative Potential for Prolonged Periods of Culture." *Developmental Biology* 227 (2): 271–78. https://doi.org/10.1006/dbio.2000.9912.

Anokye-Danso Frederick, Trivedi Chinmay M, Juhr Denise, Gupta Mudit, Cui Zheng, Tian Ying, Zhang Yuzhen, Yang Wenli, Gruber Peter J, Epstein Jonathan A, Morrisey Edward E. 2011. "Highly Efficient MiRNA-Mediated Reprogramming of Mouse and Human Somatic Cells to Pluripotency." *Cell Stem Cell* 8 (4): 376–88. https://doi.org/10.1016/j.stem.2011.03.001.

Arnold, Michael A., Yuri Kim, Michael P. Czubryt, Dillon Phan, John McAnally, Xiaoxia Qi, John M. Shelton, James A. Richardson, Rhonda Bassel-Duby, and Eric N. Olson. 2007. "MEF2C Transcription Factor Controls Chondrocyte Hypertrophy and Bone Development." *Developmental Cell* 12 (3): 377–89. https://doi.org/10.1016/j.devcel.2007.02.004.

Ballo, Robea, D. Viljoen, M. Machado, D Keene, W Horton, V. Fredlund, M Jacobs, R Martell, P. Beighton, and R Ramesar. 1996. "Mseleni Joint Disease - a Molecular Genetic Approach to Defining the Aetiology."

Barrera, Christian A., Sara A. Cohen, Wudbhav N. Sankar, Victor M. Ho-Fung, Raymond W. Sze, and Jie C. Nguyen. 2019. "Imaging of Developmental Dysplasia of the Hip: Ultrasound, Radiography and Magnetic Resonance Imaging." *Pediatric Radiology* 49 (12): 1652–68. https://doi.org/10.1007/s00247-019-04504-3.

Beers, Jeanette, Daniel R. Gulbranson, Nicole George, Lauren I. Siniscalchi, Jeffrey Jones, James A. Thomson, and Guokai Chen. 2012. “Passaging and Colony Expansion of Human Pluripotent Stem Cells by Enzyme-Free Dissociation in Chemically Defined Culture Conditions.” *Nature Protocols* 7 (11): 2029–40. https://doi.org/10.1038/nprot.2012.130.

Bendall Sean C, Stewart Morag H, Menendez Pablo, George Dustin, Vijayaragavan Kausalia, Werbowetski-Ogilvie Tamra, Ramos-Mejia Veronica, Rouleau Anne, Yang Jiabi, Bossé Marc, Lajoie Gilles, Bhatia Mickie. 2007. “IGF and FGF Cooperatively Establish the Regulatory Stem Cell Niche of Pluripotent Human Cells in Vitro.” *Nature* 448 (7157): 1015–21. https://doi.org/10.1038/nature06027.

Bonafe Luisa, Cormier-Daire Valerie, Hall Christine, Lachman Ralph, Mortier Geert, Mundlos Stefan, Nishimura Gen, Sangiorgi Luca, Savarirayan Ravi, Sillence David, Spranger Jürgen, Superti-Furga Andrea, Warman Matthew, Unger Sheila. 2015. “Nosology and Classification of Genetic Skeletal Disorders: 2015 Revision.” *American Journal of Medical Genetics, Part A* 167 (12): 2869–92. https://doi.org/10.1002/ajmg.a.37365.

Brew, C. J., P. D. Clegg, R. P. Boot-Handford, J. G. Andrew, and T. Hardingham. 2010. “Gene Expression in Human Chondrocytes in Late Osteoarthritis Is Changed in Both Fibrillated and Intact Cartilage without Evidence of Generalised Chondrocyte Hypertrophy.” *Annals of the Rheumatic Diseases* 69 (1): 234–40. https://doi.org/10.1136/ard.2008.097139.

Briggs, Michael D, Michael J Wright, and R Geert. 2019. “Multiple Epiphyseal Dysplasia , Autosomal Dominant Summary Genetic Counseling Suggestive Findings,” 1–23.

Briggs MD, Wright MJ, Mortier GR. Multiple Epiphyseal Dysplasia, Autosomal Dominant. 2003 Jan 8 [Updated 2024 Jul 4]. In: Adam MP, Feldman J, Mirzaa GM, et al., editors. GeneReviews® [Internet]. Seattle (WA): University of Washington, Seattle; 1993-2025. https://www.ncbi.nlm.nih.gov/books/

Burger, F. J., C. D. Elphinstone, S. A. Fellingham, P. C. Grey, and Z. A. Hogewind. 1973. “Mseleni Joint Disease: Biochemical Survey.” *South African Medical Journal* 47 (48): 2331–38.

Camp J. Gray, Badsha Farhath, Florio Marta, Kanton Sabina, Gerber Tobias, Wilsch-Bräuninger Michaela, Lewitus Eric, Sykes Alex, Hevers Wulf, Lancaster Madeline, Knoblich Juergen A, Lachmann Robert, Pääbo Svante, Huttner Wieland B, Treutlein Barbara. 2015. “Human Cerebral Organoids Recapitulate Gene Expression Programs of Fetal Neocortex Development.” *Proceedings of the National Academy of Sciences of the United States of America* 112 (51): 15672–77. https://doi.org/10.1073/pnas.1520760112.

Castro-Viñuelas, R., C. Sanjurjo-Rodríguez, M. Piñeiro-Ramil, T. Hermida-Gómez, I. M. Fuentes-Boquete, F. J. de Toro-Santos, F. J. Blanco-García, and Silvia María Díaz-Prado. 2018. “Induced

Pluripotent Stem Cells for Cartilage Repair: Current Status and Future Perspectives." *European Cells and Materials* 36 (2006): 96–109. https://doi.org/10.22203/eCM.v036a08.

Cerneckis, Jonas, Hongxia Cai, and Yanhong Shi. 2024. "Induced Pluripotent Stem Cells (IPSCs): Molecular Mechanisms of Induction and Applications." *Signal Transduction and Targeted Therapy* 9 (1): 1–26. https://doi.org/10.1038/s41392-024-01809-0.

Ceruti, P.O., Fey, M. & Pooley, J. 2003. Soil nutrient deficiencies in an area of endemic OA (Mseleni Joint Disease) and dwarfism in Maputaland, South Africa. In *Geology and Health: Closing the Gap.* H. Skinner and A. Berger, Eds. New York: Oxford University Press. 151-154.

Chijimatsu, Ryota, and Taku Saito. 2019. "Mechanisms of Synovial Joint and Articular Cartilage Development." *Cellular and Molecular Life Sciences* 76 (20): 3939–52. https://doi.org/10.1007/s00018-019-03191-5.

Chomczynski, Piotr, and Nicoletta Sacchi. 2006. "The Single-Step Method of RNA Isolation by Acid Guanidinium Thiocyanate-Phenol-Chloroform Extraction: Twenty-Something Years On." *Nature Protocols* 1 (2): 581–85. https://doi.org/10.1038/nprot.2006.83.

Choudhery, Mahmood S., Ruhma Mahmood, David T. Harris, and Fridoon J. Ahmad. 2022. "Minimum Criteria for Defining Induced Mesenchymal Stem Cells." *Cell Biology International* 46 (6): 986–89. https://doi.org/10.1002/cbin.11790.

Craft, April M., Jason S. Rockel, Yulia Nartiss, Rita A. Kandel, Benjamin A. Alman, and Gordon M. Keller. 2015. "Generation of Articular Chondrocytes from Human Pluripotent Stem Cells." *Nature Biotechnology* 33 (6): 638–45. https://doi.org/10.1038/nbt.3210.

Czarny-Ratajczak Malwina, Lohiniva Jaana, Rogala Piotr, Kozlowski Kazimierz, Perälä Merja, Carter Liisa, Spector Tim D, Kolodziej Lukasz, Seppänen Ulpu, Glazar Renata, Królewski Jan, Latos-Bielenska Anna, Ala-Kokko Leena. 2001. "A Mutation in COL9A1 Causes Multiple Epiphyseal Dysplasia: Further Evidence for Locus Heterogeneity." *American Journal of Human Genetics* 69 (5): 969–80. https://doi.org/10.1086/324023.

Decker, Rebekah S., Hyo Bin Um, Nathaniel A. Dyment, Naiga Cottingham, Yu Usami, Motomi Enomoto-Iwamoto, Mark S. Kronenberg, et al. 2017. *Cell Origin, Volume and Arrangement Are Drivers of Articular Cartilage Formation, Morphogenesis and Response to Injury in Mouse Limbs*. *Developmental Biology*. Vol. 426. https://doi.org/10.1016/j.ydbio.2017.04.006.

Doetschman, T. C., H. Eistetter, and M. Katz. 1985. "The in Vitro Development of Blastocyst-Derived Embryonic Stem Cell Lines: Formation of Visceral Yolk Sac, Blood Islands and Myocardium." *Journal of Embryology and Experimental Morphology* VOL. 87: 27–45. https://doi.org/10.1242/dev.87.1.27.

Dominici, M., K. Le Blanc, I. Mueller, I. Slaper-Cortenbach, F. C. Marini, D. S. Krause, R. J. Deans, A.

Keating, D. J. Prockop, and E. M. Horwitz. 2006. “Minimal Criteria for Defining Multipotent Mesenchymal Stromal Cells. The International Society for Cellular Therapy Position Statement.” *Cytotherapy* 8 (4): 315–17. https://doi.org/10.1080/14653240600855905.

Drissi, M. Hicham, Xufeng Li, Tzong J. Sheu, Michael J. Zuscik, Edward M. Schwarz, J. Edward Puzas, Randy N. Rosier, and Regis J. O’Keefe. 2003. “Runx2/Cbfa1 Stimulation by Retinoic Acid Is Potentiated by BMP2 Signaling Through Interaction with Smad1 on the Collagen X Promoter in Chondrocytes.” *Journal of Cellular Biochemistry* 90 (6): 1287–98. https://doi.org/10.1002/jcb.10677.

Fellingham, S. A., C. D. Elphinstone, and W. Wittmann. 1973. “Mseleni Joint Disease: Background and Prevalence.” *South African Medical Journal* 47 (45): 2173–80.

Fincham, J. E. 1986. “Mseleni Joint Disease.” *The Lancet* 327 (8474): 206–7. https://doi.org/10.1016/S0140-6736(86)90671-9.

Fincham, J. E., F. S. Hough, J. J.F. Taljaard, A. Weidemann, and C. H. Schutte. 1986a. “Mseleni Joint Disease. Part II. Low Serum Calcium and Magnesium Levels in Women.” *South African Medical Journal* 70 (12): 740–42.

Fox, Alice J Sophia, Asheesh Bedi, and Scott A. Rodeo. 2009. “The Basic Science of Articular Cartilage: Structure, Composition, and Function.” *Sports Health* 1 (6): 461–68. https://doi.org/10.1177/1941738109350438.

Gadomski, Stephen J, Byron W H Mui, Daniel Martin, W McCaskie Andrew, G Pamela Robey, Stephen J Gadomski, Byron W H Mui, Raphael Gorodetsky, and Sriram S Paravastu. 2024. “Time- and Cell-Specific Activation of BMP Signaling Restrains Chondrocyte Hypertrophy Stephen.” https://doi.org/10.1016/j.isci.2024.110537.

Gibbon, Victoria E., John S. Harington, Clem B. Penny, and Victor Fredlund. 2010. “Mseleni Joint Disease: A Potential Model of Epigenetic Chondrodysplasia.” *Joint Bone Spine* 77 (5): 399–404. https://doi.org/10.1016/j.jbspin.2010.01.013.

Gilmour, John. 1936. “Adolescent Deformities of the Acetabulum,” 670–99.

Golub, Ellis E., and Kathleen Boesze-Battaglia. 2007. “The Role of Alkaline Phosphatase in Mineralization.” *Current Opinion in Orthopaedics* 18 (5): 444–48. https://doi.org/10.1097/BCO.0b013e3282630851.

Greber, Boris, Hans Lehrach, and James Adjaye. 2007. “Fibroblast Growth Factor 2 Modulates Transforming Growth Factor β Signaling in Mouse Embryonic Fibroblasts and Human ESCs (HESCs) to Support HESC Self-Renewal.” *Stem Cells* 25 (2): 455–64. https://doi.org/10.1634/stemcells.2006-0476.

Haghighi, Fereshteh, Julia Dahlmann, Saeideh Nakhaei-Rad, Alexander Lang, Ingo Kutschka, Martin

Zenker, George Kensah, Roland P. Piekorz, and Mohammad Reza Ahmadian. 2018. “BFGF-Mediated Pluripotency Maintenance in Human Induced Pluripotent Stem Cells Is Associated with NRAS-MAPK Signaling.” *Cell Communication and Signaling* 16 (1): 1–14. https://doi.org/10.1186/s12964-018-0307-1.

Harrison, T J. 1961. “The Influence of the Femoral Head on Pelvic Growth and Acetabular Form in the Rat.” *Journal of Anatomy* 95: 12–24. http://www.ncbi.nlm.nih.gov/pubmed/13711848%0Ahttp://www.pubmedcentral.nih.gov/articlerender.fcgi?artid=PMC1244430.

Heng, Boon Chin, Hua Liu, and Tong Gao. 2004. “FEEDER CELL DENSITY--A KEY PARAMETER IN HUMAN EMBRYONIC STEM CELL CULTURE” 16 (1): 1–23.

Heo, June Seok, Youjeong Choi, Han Soo Kim, and Hyun Ok Kim. 2016. “Comparison of Molecular Profiles of Human Mesenchymal Stem Cells Derived from Bone Marrow, Umbilical Cord Blood, Placenta and Adipose Tissue.” *International Journal of Molecular Medicine* 37 (1): 115–25. https://doi.org/10.3892/ijmm.2015.2413.

Høffding, M. K., and P. Hyttel. 2015. “Ultrastructural Visualization of the Mesenchymal-to-Epithelial Transition during Reprogramming of Human Fibroblasts to Induced Pluripotent Stem Cells.” *Stem Cell Research* 14 (1): 39–53. https://doi.org/10.1016/j.scr.2014.11.003.

Holder, N. 1977. “An Experimental Investigation into the Early Development of the Chick Elbow Joint.” *Journal of Embryology and Experimental Morphology* Vol. 39: 115–27. https://doi.org/10.1242/dev.39.1.115.

Humphreys, P. A. et al. (2022) ‘Developmental principles informing human pluripotent stem cell differentiation to cartilage and bone’, Seminars in Cell and Developmental Biology. Elsevier Ltd, 127(July 2021), pp. 17–36. doi: 10.1016/j.semcdb.2021.11.024.

Jacobsen Kaya Kvarme, Børte Sigrid, Laborie Lene Bjerke, Kristiansen Hege, Schäfer Annette, Martinsen, Amy E, Skogholt Anne Heidi, Brumpton Ben M, Willer Cristen J, Fors Egil A, Kristoffersen Espen S, Heuch Ingrid, Mundal Ingunn, Zwart John Anker, Nielsen Jonas B, Storheim Kjersti, Hagen Knut, Nilsen Kristian Bernhard, Hveem Kristian, Fritsche Lars G, Thomas Laurent F, Pedersen Linda M, Gabrielsen Maiken E, Lie Marie U, Stensland Synne, Zhou Wei, Gundersen Trude, Zayats Tetyana, Slagsvold Winsvold Bendik Kristoffer, Rosendahl Karen. 2024. COL11A1 Is Associated with Developmental Dysplasia of the Hip and Secondary Osteoarthritis in the HUNT Study.” *Osteoarthritis and Cartilage Open* 6 (1). https://doi.org/10.1016/j.ocarto.2023.100424.

Jung, Chaeyong, Yen Chuan Ou, Fan Yeung, Henry F. Frierson, and Chinghai Kao. 2001. “Osteocalcin Is Incompletely Spliced in Non-Osseous Tissues.” *Gene* 271 (2): 143–50.

https://doi.org/10.1016/S0378-1119(01)00513-3.

Kalluri, Raghu, and Robert A Weinberg. 2010. “The Basics of Epithelial-Mesenchymal Transition.” *Physics of Plasmas* To be subm (May): 1420–28. https://doi.org/10.1172/JCI39104.1420.

Kawase, Eihachiro, and Norio Nakatsuji. 2023. “Development of Substrates for the Culture of Human Pluripotent Stem Cells.” *Biomaterials Science* 11 (9): 2974–87. https://doi.org/10.1039/d2bm01473d.

Kim, Do Hyung, Tiaosi Xing, Zhibin Yang, Ronald Dudek, Qun Lu, and Yan Hua Chen. 2018. “Epithelial Mesenchymal Transition in Embryonic Development, Tissue Repair and Cancer: A Comprehensive Overview.” *Journal of Clinical Medicine* 7 (1): 1–25. https://doi.org/10.3390/jcm7010001.

Kim, Jihoon, Bon Kyoung Koo, and Juergen A. Knoblich. 2020. “Human Organoids: Model Systems for Human Biology and Medicine.” *Nature Reviews Molecular Cell Biology* 21 (10): 571–84. https://doi.org/10.1038/s41580-020-0259-3.

Kim, Yunhee, Inha Kim, and Kunyoo Shin. 2023. “A New Era of Stem Cell and Developmental Biology: From Blastoids to Synthetic Embryos and Beyond.” *Experimental and Molecular Medicine* 55 (10): 2127–37. https://doi.org/10.1038/s12276-023-01097-8.

Kimbrel, Erin A., and Robert Lanza. 2015. “Current Status of Pluripotent Stem Cells: Moving the First Therapies to the Clinic.” *Nature Reviews Drug Discovery* 14 (10): 681–92. https://doi.org/10.1038/nrd4738.

Kuivaniemi, Helena, Gerard Tromp, and Darwin J. Prockop. 1997. “Mutations in Fibrillar Collagens (Types I, II, III, and XI), Fibril- Associated Collagen (Type IX), and Network-Forming Collagen (Type X) Cause a Spectrum of Disease of Bone, Cartilage, and Blood Vessels.” *Human Mutation* 9 (4): 300–315. https://doi.org/10.1002/(SICI)1098-1004(1997)9:4<300::AID-HUMU2>3.0.CO;2-9.

Lefebvre, Veronique, and Mona Dvir-Ginzberg. 2017. “SOX9 and the Many Facets of Its Regulation in the Chondrocyte Lineage” 58 (1): 2–14. https://doi.org/10.1002/cncr.27633.Percutaneous.

Li, Jianmei, and Shiwu Dong. 2016. “The Signaling Pathways Involved in Chondrocyte Differentiation and Hypertrophic Differentiation.” *Stem Cells International* 2016: 1–12. https://doi.org/10.1155/2016/2470351.

Limraksasin, Phoonsuk, Takeru Kondo, Maolin Zhang, Hiroko Okawa, Thanaphum Osathanon, Prasit Pavasant, and Hiroshi Egusa. 2020. “In Vitro Fabrication of Hybrid Bone/Cartilage Complex Using Mouse Induced Pluripotent Stem Cells.” *International Journal of Molecular Sciences* 21 (2). https://doi.org/10.3390/ijms21020581.

Liu, Weiwei, and Guokai Chen. 2014. “Cryopreservation of Human Pluripotent Stem Cells in Defined

Medium." *Current Protocols in Stem Cell Biology* 2014: 1c.17.1-1c.17.13. https://doi.org/10.1002/9780470151808.sc01c17s31.

Lockitch, G., S. A. Fellingham, and C. D. Elphinstone. 1973. "Mseleni Joint Disease: A Radiological Study of Two Affected Families." *South African Medical Journal* 47 (49): 2366–76.

Lockitch, G., S. A. Fellingham, W. Wittmann, P. D. de Villiers, I. S. de Wet, and G. T. du Toit. 1973. "Mseleni Joint Disease: The Pilot Clinical Survey." *South African Medical Journal* 47 (47): 2283–93.

Lubbe, A. M., C. D. Elphinstone, and S. A. Fellingham. 1973. "Mseleni Joint Disease. Food and Water Supplies." *South African Medical Journal* 47 (46): 2225–33.

Lui, Vincent C H, Ling Jim Ng, John Nicholls, Patrick P L Tam, and Kathryn S.E. Cheah. 1995. "Developmental Dynamics - June 1995 - Lui - Tissue-Specific and Differential Expression .Pdf."

Marín-Llera, Jessica Cristina, David Garciadiego-Cázares, and Jesús Chimal-Monroy. 2019. "Understanding the Cellular and Molecular Mechanisms That Control Early Cell Fate Decisions During Appendicular Skeletogenesis." *Frontiers in Genetics* 10 (October): 1–17. https://doi.org/10.3389/fgene.2019.00977.

Mayne, Richard. 1989. "Cartilage Collagens. What Is Their Function, and Are They Involved in Articular Disease?" *Arthritis & Rheumatism* 32 (3): 241–46. https://doi.org/10.1002/anr.1780320302.

Mitalipov, Shoukhrat, and Don Wolf. 2015. "Totipotency, Pluripotency and Nuclear Reprogramming Shoukhrat." *Advances in Biochemical Engineering/Biotechnology* 123 (July 2015): 127–41. https://doi.org/10.1007/10.

Miyoshi Norikatsu, Ishii Hideshi, Nagano Hiroaki, Haraguchi Naotsugu, Dewi Dyah Laksmi, Kano Yoshihiro, Nishikawa Shinpei, Tanemura Masahiro, Mimori Koshi, Tanaka Fumiaki, Saito Toshiyuki, Nishimura Junichi, Takemasa Ichiro, Mizushima Tsunekazu, Ikeda Masataka, Yamamoto Hirofumi, Sekimoto Mitsugu, Doki Yuichiro, Mori Masaki. 2011. "Reprogramming of Mouse and Human Cells to Pluripotency Using Mature MicroRNAs." *Cell Stem Cell* 8 (6): 633–38. https://doi.org/10.1016/j.stem.2011.05.001.

Mossahebi-Mohammadi, Majid, Meiyu Quan, Jin San Zhang, and Xiaokun Li. 2020. "FGF Signaling Pathway: A Key Regulator of Stem Cell Pluripotency." *Frontiers in Cell and Developmental Biology* 8 (February): 1–10. https://doi.org/10.3389/fcell.2020.00079.

Normand, J., and M A Karasek. 1995. "A Method for the Isolation and Serial Propagation of Keratinocytes , Endothelial Cells , and Fibroblasts from a Single Punch Biopsy of Human Skin Author (s): J . Normand and M . A . Karasek Source : In Vitro Cellular & Developmental Biology . Animal , V" 31 (6): 447–55.

Nurse, G T, Trefor Jenkins, and C. D. Elphinstone. 1974. “Mseleni Joint Diseases: Population Genetic Studies.” *South African Journal of Science* 70.

Oganesian, Anush, Yong Zhu, and Linda J. Sandell. 1997. “Type IIA Procollagen Amino Propeptide Is Localized in Human Embryonic Tissues.” *Journal of Histochemistry and Cytochemistry* 45 (11): 1469–80. https://doi.org/10.1177/002215549704501104.

Ogura, Hiroyuki, Takashi Nakamura, Takenobu Ishii, Akiko Saito, Shoko Onodera, Akira Yamaguchi, Yasushi Nishii, and Toshifumi Azuma. 2023. “Mechanical Stress-Induced FGF-2 Promotes Proliferation and Consequently Induces Osteoblast Differentiation in Mesenchymal Stem Cells.” *Biochemical and Biophysical Research Communications* 684 (August): 149145. https://doi.org/10.1016/j.bbrc.2023.149145.

Oke, Anagha, and Sonal M. Manohar. 2024. “Dynamic Roles of Signaling Pathways in Maintaining Pluripotency of Mouse and Human Embryonic Stem Cells.” *Cellular Reprogramming* 26 (2): 46–56. https://doi.org/10.1089/cell.2024.0002.

Pacifici, Maurizio, Rebekah S. Decker, and Eiki Koyama. 2018. *Limb Synovial Joint Development from the Hips down: Implications for Articular Cartilage Repair and Regeneration*. *Developmental Biology and Musculoskeletal Tissue Engineering: Principles and Applications*. Elsevier Inc. https://doi.org/10.1016/B978-0-12-811467-4.00004-8.

Pacifici, Maurizio, Eiki Koyama, Yoshihiro Shibukawa, Changshan Wu, Yoshihiro Tamamura, Motomi Enomoto-Iwamoto, and Masahiro Iwamoto. 2006. “Cellular and Molecular Mechanisms of Synovial Joint and Articular Cartilage Formation.” *Annals of the New York Academy of Sciences* 1068 (1): 74–86. https://doi.org/10.1196/annals.1346.010.

Pasi C. E, Dereli-Öz A, Negrini S, Friedli M, Fragola G, Lombardo A, Van Houwe G, Naldini L, Casola S, Testa G, Trono D, Pelicci P. G, Halazonetis T. D. 2011. “Genomic Instability in Induced Stem Cells.” *Cell Death and Differentiation* 18 (5): 745–53. https://doi.org/10.1038/cdd.2011.9.

Patti, Aurora, Luigi Gennari, Daniela Merlotti, Francesco Dotta, and Ranuccio Nuti. 2013. “Endocrine Actions of Osteocalcin.” *International Journal of Endocrinology* 2013. https://doi.org/10.1155/2013/846480.

Pierantozzi, Enrico, Barbara Gava, Ivana Manini, Franco Roviello, Giuseppe Marotta, Mario Chiavarelli, and Vincenzo Sorrentino. 2011. “Pluripotency Regulators in Human Mesenchymal Stem Cells: Expression of NANOG but Not of OCT-4 and SOX-2.” *Stem Cells and Development* 20 (5): 915–23. https://doi.org/10.1089/scd.2010.0353.

Pomeranz, Maurice M. 2007. “Intrapelvic Protrusion of the Acetabulum (Otto Pelvis).” *Clinical Orthopaedics and Related Research* 465 (1922): 6–15. https://doi.org/10.1097/BLO.0b013e31815760f0.

Poole, C. Anthony. 1997. “Articular Cartilage Chondrons: Form, Function and Failure.” *Journal of Anatomy* 191 (1): 1–13. https://doi.org/10.1017/S0021878297002185.

Pothiawala, Azim, Berke E. Sahbazoglu, Bryan K. Ang, Nadine Matthias, Guangsheng Pei, Qing Yan, Brian R. Davis, Johnny Huard, Zhongming Zhao, and Naoki Nakayama. 2022. “GDF5+ Chondroprogenitors Derived from Human Pluripotent Stem Cells Preferentially Form Permanent Chondrocytes.” *Development (Cambridge)* 149 (11). https://doi.org/10.1242/dev.196220.

Qian Xuyu, Nguyen Ha Nam, Song Mingxi M, Hadiono Christopher, Ogden Sarah C, Hammack Christy, Yao Bing , Hamersky Greogory, Jacob Fadi, Zhong Chun, Yoon Ki-jun, Jeang William, Lin Li, Li Yujing, Thakor Jai, Berg Daniel, Zhang Ce, Kang Eunchai, Chickering Michael, Naeun David, Ho Cheng-Ying, Wen Zhexing, Christian Kimberly M, Shi Pei-Yong, Maher Brady J, Wy Hao, Jin Peng, Tang Hengli, Song Hongjun and Ming Guo. 2016. “Brain Region-Specific Organoids Using Mini-Bioreactors for Modeling ZIKV Exposure.” *Toxicology* 131 (3): 344–46. https://doi.org/10.1016/j.cell.2016.04.032.Brain.

Rajasingh, Sheeja, Vinoth Sigamani, Vijay Selvam, Narasimman Gurusamy, Shivaani Kirankumar, Jayavardini Vasanthan, and Johnson Rajasingh. 2021. “Comparative Analysis of Human Induced Pluripotent Stem Cell-Derived Mesenchymal Stem Cells and Umbilical Cord Mesenchymal Stem Cells.” *Journal of Cellular and Molecular Medicine* 25 (18): 8904–19. https://doi.org/10.1111/jcmm.16851.

Roughley, Peter J., and John S. Mort. 2014. “The Role of Aggrecan in Normal and Osteoarthritic Cartilage.” *Journal of Experimental Orthopaedics* 1 (1): 1–11. https://doi.org/10.1186/s40634-014-0008-7.

Salva, Joanna E., and Amy E. Merrill. 2017. “Signaling Networks in Joint Development.” *Developmental Dynamics* 246 (4): 262–74. https://doi.org/10.1002/dvdy.24472.

Sandell, Linda J. 2012. “Etiology of Osteoarthritis: Genetics and Synovial Joint Development.” *Nature Reviews Rheumatology* 8 (2): 77–89. https://doi.org/10.1038/nrrheum.2011.199.

Sandell, Linda J., and Thomas Aigner. 2001. “Articular Cartilage and Changes in Arthritis Matrix Degradation.” *Arthritis Research* 3 (6): 337–41. https://doi.org/10.1186/ar325.

Schmittgen, Thomas D., and Kenneth J. Livak. 2008. “Analyzing Real-Time PCR Data by the Comparative CT Method.” *Nature Protocols* 3 (6): 1101–8. https://doi.org/10.1038/nprot.2008.73.

Schnitzler, C. M., W. M. Pieczkowski, V. Fredlund, J. M. Mesquita, M. B.E. Sweet, and A. E. Smit. 1988. “Histomorphometric Analysis of Osteopenia Associated with Endemic Osteoarthritis (Mseleni Joint Disease).” *Bone* 9 (1): 21–27. https://doi.org/10.1016/8756-3282(88)90023-3.

Schutgens, Frans, and Hans Clevers. 2020. “Human Organoids: Tools for Understanding Biology and Treating Diseases.” *Annual Review of Pathology: Mechanisms of Disease* 15: 211–34. https://doi.org/10.1146/annurev-pathmechdis-012419-032611.

Selvamurugan, Nagarajan, Malini R. Pulumati, Darren R. Tyson, and Nicola C. Partridge. 2000. “Parathyroid Hormone Regulation of the Rat Collagenase-3 Promoter by Protein Kinase A-Dependent Transactivation of Core Binding Factor A1.” *Journal of Biological Chemistry* 275 (7): 5037–42. https://doi.org/10.1074/jbc.275.7.5037.

Seror, Jasmine, Linyi Zhu, Ronit Goldberg, Anthony J. Day, and Jacob Klein. 2015. “Supramolecular Synergy in the Boundary Lubrication of Synovial Joints.” *Nature Communications* 6. https://doi.org/10.1038/ncomms7497.

Serrano-Gomez, Silvia Juliana, Mazvita Maziveyi, and Suresh K. Alahari. 2016. “Regulation of Epithelial-Mesenchymal Transition through Epigenetic and Post-Translational Modifications.” *Molecular Cancer* 15 (1): 1–14. https://doi.org/10.1186/s12943-016-0502-x.

Siller, Alejandro F., and Michael P. Whyte. 2018. “Alkaline Phosphatase: Discovery and Naming of Our Favorite Enzyme.” *Journal of Bone and Mineral Research* 33 (2): 362–64. https://doi.org/10.1002/jbmr.3225.

Solomon, L., P. McLaren, L. Irwig, J. S. Gear, C. M. Schnitzler, A. Gear, and D. Mann. 1986. “Distinct Types of Hip Disorder in Mseleni Joint Disease.” *South African Medical Journal* 69 (1): 15–17.

Spitzhorn, Lucas Sebastian, Matthias Megges, Wasco Wruck, Md Shaifur Rahman, Jörg Otte, Özer Degistirici, Roland Meisel, Rüdiger Volker Sorg, Richard O.C. Oreffo, and James Adjaye. 2019. “Human IPSC-Derived MSCs (IMSCs) from Aged Individuals Acquire a Rejuvenation Signature.” *Stem Cell Research and Therapy* 10 (1): 1–18. https://doi.org/10.1186/s13287-019-1209-x.

Sweet, M. B.E., C. M. Schnitzler, and F. S. Hough. 1987. “Proteoglycans of Articular Cartilage in Mseleni Joint Disease.” *South African Medical Journal* 71 (5): 317–319.

Takahashi, Kazutoshi, Koji Tanabe, Mari Ohnuki, Megumi Narita, Tomoko Ichisaka, Kiichiro Tomoda, and Shinya Yamanaka. 2007. “Induction of Pluripotent Stem Cells from Adult Human Fibroblasts by Defined Factors.” *Cell* 131 (5): 861–72. https://doi.org/10.1016/j.cell.2007.11.019.

Takahashi, Kazutoshi, and Shinya Yamanaka. 2006. “Induction of Pluripotent Stem Cells from Mouse Embryonic and Adult Fibroblast Cultures by Defined Factors.” *Cell* 126 (4): 663–76. https://doi.org/10.1016/j.cell.2006.07.024.

Takeda, Shu, Jean Pierre Bonnamy, Michael J. Owen, Patricia Ducy, and Gerard Karsenty. 2001. “Continuous Expression of Cbfa1 in Nonhypertrophic Chondrocytes Uncovers Its Ability to Induce Hypertrophic Chondrocyte Differentiation and Partially Rescues Cbfa1-Deficient Mice.”

Genes and Development 15 (4): 467–81. https://doi.org/10.1101/gad.845101.

Thomson, James A. 1998. "Embryonic Stem Cell Lines Derived from Human Blastocysts." *Science* 282 (5391): 1145–47. https://doi.org/10.1126/science.282.5391.1145.

Toit, G. T. Du. 1979. "Hip Disease of Mseleni." *Clinical Orthopaedics and Related Research* NO 141: 223–36. https://doi.org/10.1097/00003086-197906000-00030.

Uhrig, Markus, Fernando Ezquer, and Marcelo Ezquer. 2022. "Improving Cell Recovery: Freezing and Thawing Optimization of Induced Pluripotent Stem Cells." *Cells* 11 (5). https://doi.org/10.3390/cells11050799.

Varzideh, Fahimeh, Jessica Gambardella, Urna Kansakar, Stanislovas S. Jankauskas, and Gaetano Santulli. 2023. "Molecular Mechanisms Underlying Pluripotency and Self-Renewal of Embryonic Stem Cells." *International Journal of Molecular Sciences* 24 (9). https://doi.org/10.3390/ijms24098386.

Viljoen, D., V. Fredlund, R. Ramesar, and P. Beighton. 1993. "Brachydactylous Dwarfs of Mseleni." *American Journal of Medical Genetics* 46 (6): 636–40. https://doi.org/10.1002/ajmg.1320460607.

Vimalraj, Selvaraj. 2020. "Alkaline Phosphatase: Structure, Expression and Its Function in Bone Mineralization." *Gene* 754 (April). https://doi.org/10.1016/j.gene.2020.144855.

Wang, Hongmei, Colin Sweeney, and Harry Malech. 2011. "Characterization of Surface Markers and DNA Regulatory Gene Expression during Neutrophil Differentiation from Human Induced Pluripotent Stem Cells." *Molecular Therapy* 19 (May): S219. https://doi.org/10.1016/s1525-0016(16)37144-1.

Wen, Wei, Jian Ping Zhang, Jing Xu, Ruijun Jeanna Su, Amanda Neises, Guang Zhen Ji, Weiping Yuan, Tao Cheng, and Xiao Bing Zhang. 2016. "Enhanced Generation of Integration-Free IPSCs from Human Adult Peripheral Blood Mononuclear Cells with an Optimal Combination of Episomal Vectors." *Stem Cell Reports* 6 (6): 873–84. https://doi.org/10.1016/j.stemcr.2016.04.005.

Wittman, W. & Fellingham, S. 1970. Unusual hip disease in remote part of Zululand. *The Lancet.* 295(7651):842-843.

Wright, Edwina, Murray R. Hargrave, Jeffrey Christiansen, Leanne Cooper, Jutta Kun, Timothy Evans, Uma Gangadharan, Andy Greenfield, and Peter Koopman. 1995. "The Sry-Related Gene Sox9 Is Expressed during Chondrogenesis in Mouse Embryos." *Nature Genetics* 9 (1): 15–20. https://doi.org/10.1038/ng0195-15.

Xu, Jinping, Wei Wang, Matt Ludeman, Kevin Cheng, Takayuki Hayami, Jeffrey C. Lotz, and Sunil Kapila. 2008. "Chondrogenic Differentiation of Human Mesenchymal Stem Cells in Three-Dimensional Alginate Gels." *Tissue Engineering - Part A.* 14 (5): 667–80.

https://doi.org/10.1089/tea.2007.0272.

Yoshida, Carolina A., Hiromitsu Yamamoto, Takashi Fujita, Tatsuya Furuichi, Kosei Ito, Ken Ichi Inoue, Kei Yamana, Akira Zanma, Kenji Takada, Yoshiaki Ito, Toshihisa Komori. 2004. "Runx2 and Runx3 Are Essential for Chondrocyte Maturation, and Runx2 Regulates Limb Growth through Induction of Indian Hedgehog." *Genes and Development* 18 (8): 952–63. https://doi.org/10.1101/gad.1174704.

Zelzer, Elazar, Donald J. Glotzer, Christine Hartmann, David Thomas, Naomi Fukai, Shay Soker, and Bjorn R. Olsen. 2001. "Tissue Specific Regulation of VEGF Expression during Bone Development Requires Cbfa1/Runx2." *Mechanisms of Development* 106 (1–2): 97–106. https://doi.org/10.1016/S0925-4773(01)00428-2.

Zhang, Wei, Yi Sui, Jun Ni, and Tao Yang. 2016. "Insights into the Nanog Gene: A Propeller for Stemness in Primitive Stem Cells." *International Journal of Biological Sciences* 12 (11): 1372–81. https://doi.org/10.7150/ijbs.16349.

Zheng, Qiping, Guang Zhou, Roy Morello, Yuqing Chen, Xavier Garcia-Rojas, and Brendan Lee. 2003. "Type X Collagen Gene Regulation by Runx2 Contributes Directly to Its Hypertrophic Chondrocyte-Specific Expression in Vivo." *Journal of Cell Biology* 162 (5): 833–42. https://doi.org/10.1083/jcb.200211089.

Zheng, Yue Liang. 2016. "Some Ethical Concerns About Human Induced Pluripotent Stem Cells." *Science and Engineering Ethics* 22 (5): 1277–84. https://doi.org/10.1007/s11948-015-9693-6.

Zhou, Guang, Qiping Zheng, Feyza Engin, Elda Munivez, Yuqing Chen, Eiman Sebald, Deborah Krakow, and Brendan Lee. 2006. "Dominance of SOX9 Function over RUNX2 during Skeletogenesis." *Proceedings of the National Academy of Sciences of the United States of America* 103 (50): 19004–9. https://doi.org/10.1073/pnas.0605170103.

Zhou, Ping, Jia Min Shi, Jing E. Song, Yu Han, Hong Jiao Li, Ya Meng Song, Fang Feng, Jian Lin Wang, Rui Zhang, and Feng Lan. 2021. "Establishing a Deeper Understanding of the Osteogenic Differentiation of Monolayer Cultured Human Pluripotent Stem Cells Using Novel and Detailed Analyses." *Stem Cell Research and Therapy* 12 (1): 1–16. https://doi.org/10.1186/s13287-020-02085-9.

Zhou, Yan, JinQi Liao, ChongZhou Fang, CuiPing Mo, GuangQian Zhou, and Yonglun Luo. 2018. "One-Step Derivation of Functional Mesenchymal Stem Cells from Human Pluripotent Stem Cells." *Bio-Protocol* 8 (22): 1–21. https://doi.org/10.21769/bioprotoc.3080.

Zimmermann, Peter, Stéphane Boeuf, Andrea Dickhut, Sandra Boehmer, Sven Olek, and Wiltrud Richter. 2008. "Correlation of COL10A1 Induction during Chondrogenesis of Mesenchymal Stem Cells with Demethylation of Two CpG Sites in the COL10A1 Promoter." *Arthritis and*

Rheumatism 58 (9): 2743–53. https://doi.org/10.1002/art.23736.

Appendix A – Preparation of reagents and molecular weight marker

1x PBS for general laboratory protocols

For 1 litre, dissolve the below in 800ml of double distilled water.

8g NaCl,

1.26g Na_2HPO_4,

0.2g KCl

0.2g KH_2PO_4

Mix thoroughly and adjust the pH to 7.4. Add double distilled water to a final volume of 1 litre using a measuring cylinder. Autoclave to sterilise and store at 4°C.

1x PBS for tissue culture use

10x DPBS (cat # 14200067, LTC) was diluted with double distilled water as below:

100ml of the 10x PBS in 900mls of double distilled water

1 x TE (0.05% trypsin/EDTA)

Dissolve 0.05g trypsin (Sigma-Aldrich, USA) in 100ml 1xPBS. Add 0.02g EDTA (Sigma-Aldrich, USA). Stir until fully dissolved. Filter sterilise the solution through a 0.22µm filter and aliquot into 50mL tubes. Store at -20°C.

0.5mM EDTA in DPBS

Working in the biosafety cabinet, mix 50 µL of 0.5M EDTA with 50 mL of 1x DPBS. Filter sterilize the solution through a 0.22 µm filter.

Making 4% Paraformaldehyde (PFA) in PBS

Mix 4g PFA (Merck, Germany) in 80ml of 1x PBS in the fume hood. Working in the fume hood, dissolve the solution by heating at 60 ^{O}C and pH to 7.4. Add 1x PBS to a final volume of 100 ml and store at 4°C.

Basic fibroblast growth factor (b-FGF) preparation

Reconstitute the lyophilized powder (Miltenyi Biotec, USA) in sterile SABAX water to a concentration of 100 µg/mL (10,000x). Store at -80°C in small aliquots.

For short-term storage, dilute aliquots to 1,000x with 0.1% bovine serum albumin (Miltenyi) (made in 1x PBS) and store at -20°C in 40 µl aliquots. Add 40 µl aliquots of the 100x b-FGF solution to 40 mL of hESC culture medium.

ROCK inhibitor, Y-27632, preparation

Make a 1mM stock solution by dissolving the 1mg vial of Y-27632 (Sigma Aldrich) with 2.96ml sterile SABAX water. Aliquot 100 µl in Eppendorf tubes and store at -20°C.

For use in culture (10µM): Use 10µl from the 100 µl aliquots for each 1ml of culture medium.

2x Freeze down medium for human fibroblasts and inactivated MEFs

Mix 40%60% DMEM, 20 % DMSO and 40% FBS.20%

1x Freeze down medium for human fibroblasts and inactivated MEFs

Mix 70%, DMEM , 10% DMSO and 20% FBS 20%

1x Freeze down medium for iPSCs

Mix 30 % KODMEM, 10 % DMSO and 60 % FBS

0.1% gelatine-coated dishes.

Add 0.5 g of gelatine powder (Sigma Aldrich) to 500 ml of double distilled water. Dissolve and sterilize by autoclaving. store at room temperature.

Preparation of Geltrex™

Geltrex™ LDEV-Free hESC-Qualified Reduced Growth Factor Basement Membrane Matrix (Cat. No. A1413301 (Protocol from the information sheet)

1. Dilute 1 mL of thawed Geltrex™ with 1 mL of cold DMEM/F-12. Freeze 100 µL aliquots at -20°C or use immediately.
2. To create working stocks, dilute a Geltrex™ aliquot 1:50 with cold DMEM on ice, achieving a total dilution of 1:100. Note: An optimal dilution of the Geltrex™ solution may need to be determined for each cell line. Try various dilutions ranging from 1:30 to 1:100.
3. Quickly cover the entire surface of each culture dish with the Geltrex™ solution. For example, add 1.5 mL for a 35-mm dish, or 3 mL for a 60-mm dish.
4. Incubate the dishes in a 37°C, 5% CO2 incubator for 1 hour. Note: Dishes can be used immediately or stored at 2–8°C for up to a week. Do not allow dishes to dry.

5. After the one incubation in a 37°C, 5% CO2 incubator for 1 hour, dishes are incubated for another hour at room temperature. Followed by the immediate use.
6. At the time of use, keep the plates at room temperature for one hour before aspirating. Carefully aspirate off the supernatant above the Geltrex™ Matrix coating, then immediately plate cells in the pre-equilibrated cell culture medium

1x Tris/Boric-acid/EDTA solution (TBE)

For 1 litre, dissolve 10.8g tris (Merck, Germany), 5.5g boric acid (Sigma-Aldrich, USA), and 0.75g EDTA (Sigma-Aldrich, USA) in 900ml distilled H20. Adjust the pH to 8.0. Adjust the final volume to 1 litre and store at room temperature. (Final concentration: 89mM Tris, 89mM Boric acid, 2mM EDTA)

Preparation of Agarose gel for gel electrophoresis

Add 3 g of Seakem LE agarose (Lonza) to 100ml of 1x TBE solution in a glass conical flask. Heat the solution in the microwave, remove it every time the bubbles formed, swirl it a few times and return it to the microwave until fully dissolved. Add a single drop or two of ethidium bromide solution (Sigma Aldrich) to the agarose gel solution. Once cooled to about 50oC, pour the agarose solution into a gel tray to set with the correct comb size.

100 bp Gene Marker

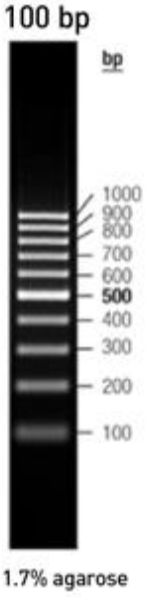

Preparation of Mitomycin C from Streptomyces caespitosus M4287

Add 2 ml of sterile SABAX water to 2 mg of M4287 Mit C and mix by gently pipetting up and down with a filter pipette until fully dissolve. Filter sterilize the solution through a 0.22 µm filter. Add 200 ul for each 20 ml culture medium to achieve a final concentration of 10µg/ml. From the remaining stock, aliquot the Mit C solution into 100 µl -500 µl to avoid multiple freeze thaw cycles.

Please note: Mitomycin C solution (Sigma Aldrich) is toxic and light-sensitive, so it should be handled with extra care. Always wear double gloves and use plastic pipette tips, which should be discarded immediately after use. The solution should be stored in tubes wrapped in aluminium foil to protect it from light.

Appendix B – General and standardized protocols

Endoderm *In vitro* differentiation medium

First: the PA6 cells were seeded at a density of 3 x 10^6 cells in T75 flask using Minimum Essential Medium alpha (MEM α (Gibco, ThermoFisher) supplemented with 10% FBS and 1% Pen-Strep. The cells were incubated overnight at 37°C. After the incubation, the cells were washed with 1x PBS, fresh ectodermal differentiation medium was added to the flask and the cultures incubated for an additional 24 hours at 37 ^{O}C. Following this incubation, the supernatant was transferred to a 50 ml tube and stored at 4 ^{O}C. Fresh ectodermal differentiation medium was added to the flask which was incubated another 24 hours. Following this, the supernatant was collected and added to the same 50 ml tube and stored at 4 ^{O}C. This process was repeated daily for 7 days and storing all the supernatant aliquots at 4 ^{O}C. After day 7, the collected supernatant was filtered with a 0.22 µm syringe membrane filter (Millipore, Billerica, MA, USA) to sterilise and remove any floating debris.

RNA extraction following the TriPure protocol. (Adapted form the Roche protocol)

At room temperature, remove the culture medium from the cells in the cell culture hood following by adding 1ml of TriPure Isolation Reagent (Roche, USA) per 10 cm^2 of cell culture area regardless of cell number. The lysate was thoroughly lysed by pipetting up and down a few times with a 1ml pipette, carefully not creating bubbles. The homogenized solution/sample was stored at -80^{O}C for at least one month before proceeding to the phase separation step. The homogenized sample was thawed at room temperature for 10 -15 minutes.

To separate the liquid-phase, 200 µl of 100% chloroform was added to the 1 ml sample homogenate. The Eppendorf tube was sealed securely with parafilm, followed by shaking vigorously by hand for 15 seconds. They were then centrifuged at 12 500 rpm(Labnet Prism R Refrigerated Microcentrifuge, Labnet International, Edison, NJ, USA) for 15 minutes at 4 ^{O}C. After the centrifugation, the top aqueous phase was removed and transferred to a clean labelled RNase and DNase free 1.5 ml Eppendorf tube and precipitated by adding 500µl isopropanol for every 1ml TriPure homogenate. Precipitation was not always visible after the addition of isopropanol, therefore an inert carrier, glycogen at 0.1 µg/µl, had to be added to facilitate precipitation and visualisation of the pellet. The tube was gently inverted a few times and stored at -80 ^{O}C overnight.

The following day, the tubes were thawed and spun at 12 000 rpm for 15 minutes at 4 ^{O}C. The supernatant was discarded, and the RNA pellet was washed twice with 75% ethanol prepared in SABAX/Nuclease-free water. After the second wash, the ethanol was removed, and the residual

ethanol was carefully removed using a 10 µl tip. The tubes were left to air dry for not more than 10 minutes. The RNA pellet was resuspended in 20 µl of RNase-free water by pipetting up and down a few times. To dissolve the RNA sample fully, the tubes were incubated at 60 ^{O}C for 10 to 15 minutes. The RNA samples were immediately transferred to ice to cool down. They were stored at 4 ^{O}C overnight. The following day, the total RNA concentration was measured using a nanodrop ND - 1000 spectrophotometer (ND-1000, ThermoFisher) before the samples were stored at -80 ^{O}C. The nanodrop ND - 1000 spectrophotometer also displayed the total RNA purity through the A260/A280 and A260/230 ratio readings.

Mycoplasma testing

Cells were cultured at a very low seeding density on sterile coverslips that were coated with 0.1% gelatine. The culture medium did not include the antibiotics (Pen-Strep). The cells were allowed to grow until they reached 50% confluency, usually day 4 or day 5. Medium was removed and cells were fixed with a fixing solution made up of 25% glacial acetic acid and 75% methanol, for 1 minute. After cells were fixed, the cells were washed twice with 1x PBS and air dried at room temperature. They were then stained with Hoechst 33258 (0.5 µg/ml) for 30 seconds. After the incubation, the Hoechst solution was discarded and cells rinsed twice with 1X PBS. The coverslip was mounted on a glass slide using Mowiol and viewed under the inverted Zeiss fluorescence microscope (Zeiss Axiovert 200M Fluorescence microscope, Axiocam HR camera, Axiovison 4.7 software) using the DAPI filter. The Hoechst 33258 binds to DNA, and mycoplasma positive cells would show blue staining in both the nucleus and in the cell membrane. The blue stain would also show up in the cell cytoplasm especially when infection is severe. Mycoplasma negative cells would only show blue stainning in the cell nucleus.

Converting objectives to scale bars from images captured using an EVOS XL Core microscope model

The EVOS microscope has pixel dimensions/standards that are correspond to different objective sizes, as shown in the table below:

Tabe B1: EVOS microscope pixel standards.

	X-axis Field (µm)	Y-axis Field (µm)	Image Size (pixels)
4x Objective	4506 µm	3379 µm	2080 x 1552
10x Objective	1802 µm	1352 µm	2080 x 1552
20x Objective	901 µm	676 µm	2080 x 1552

From these standards, the pixel size for each objective can be calculated using the x-axis field of view:

- 4x Objective:
  Pixel size ≈ 2.17 µm (4506 µm ÷ 2080 pixels)
  To draw a 100 µm scale bar: 100 µm ÷ 2.17 µm/pixel ≈ 46 pixels
- 10x Objective:
  Pixel size ≈ 0.87 µm (1802 µm ÷ 2080 pixels)
  To draw a 100 µm scale bar: 100 µm ÷ 0.87 µm/pixel ≈ 115 pixels
- 20x Objective:
  Pixel size ≈ 0.43 µm (901 µm ÷ 2080 pixels)
  To draw a 100 µm scale bar: 100 µm ÷ 0.43 µm/pixel ≈ 231 pixels

To add a scale bar using ImageJ:

1. Open the image in ImageJ.
2. Set the scale using Analyze > Set Scale, by entering the known distance (e.g., 4506 µm) and pixel length (e.g., 2080).
3. Use Analyze > Tools > Scale Bar to draw the bar of your desired length (e.g., 100 µm), adjusting the pixel width accordingly based on the calculations above.
4. Apply and save the image with the scale bar.

This process allows for scale bars to be accurately added to EVOS microscope images:

For an example: The image below is captured using the 10 Objective. Therefore:

A pixel is ≈ 0.866 µm (1802 µm / 2080 pixels)

Drawing a 100 µm scale bar would use about 114.9 pixels. (100 µm / 0.87 µm/pixel).

Following the instructions as above the image would be as below:

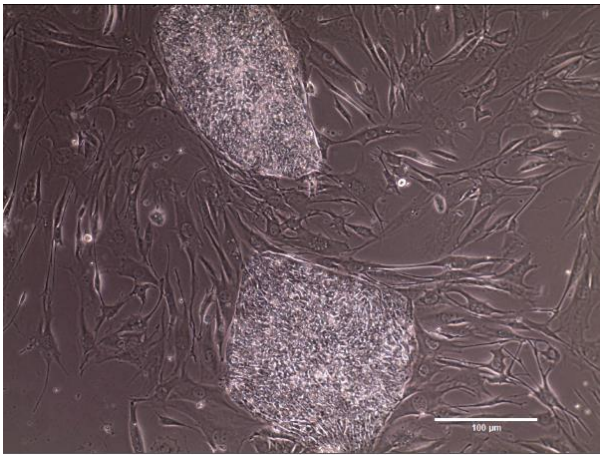

Figure B1. Morphology of iPSC colonies. CT1.5 iPSC colonies at passage 23, cultured on inactivated mouse embryonic fibroblasts. Images taken by an EVOS microscope.

Appendix C – Supplementary Results

Secondary only controls with DAPI.

CT1.5-OCT Merged, Cy3 and

Merged	CY3	Hoechst
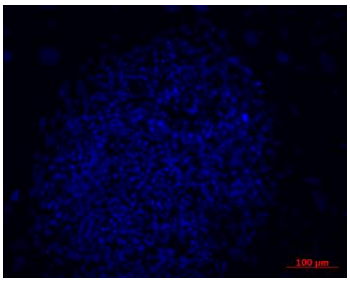	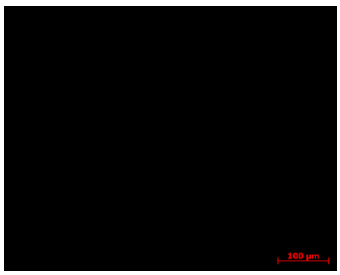	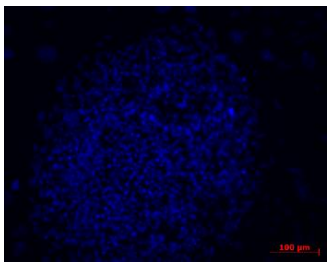

CT1.5 P25 **NANOG** Merged, Cy3 and DAPI (Nanog)

Merged	CY3	Hoechst
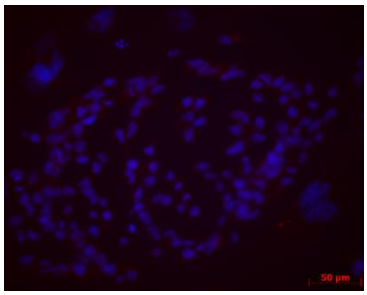	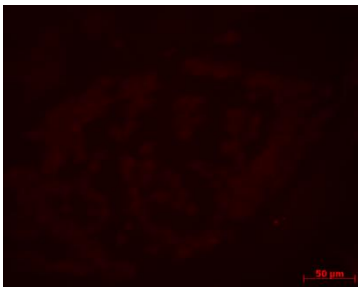	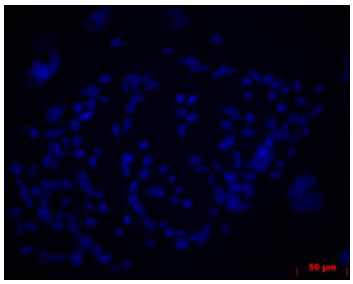

CT1.5 Tra-160 Alexa 488 Merged, cy3 and DAPI only

Merged	CY3	Hoechst

MJD5.3 - Nanog Merged, cy3 and DAPI only

Merged **CY3** **Hoechst**

MJD5.3 - OCT Merged, cy3 and DAPI only

Merged **CY3** **Hoechst**

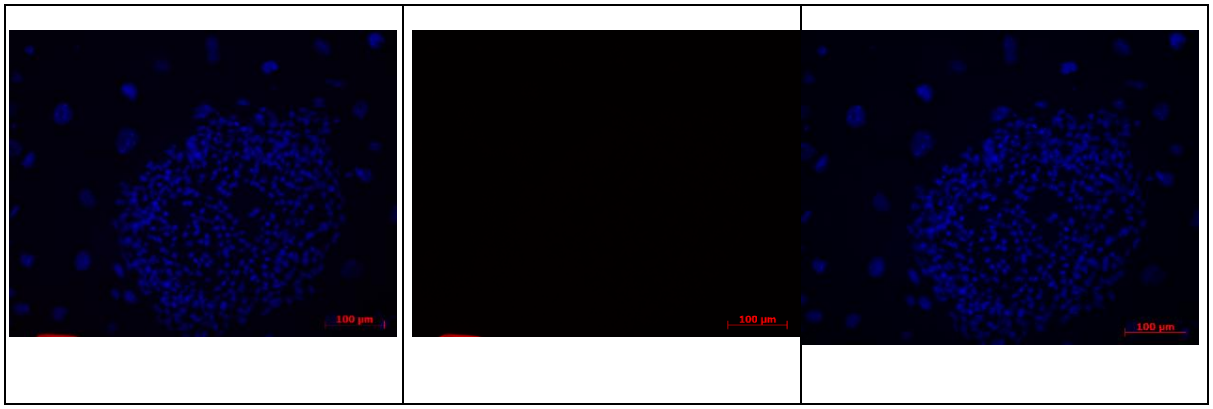

MJD5.3 - Endo Merged, cy3 and DAPI only

Merged **CY3** **Hoechst**

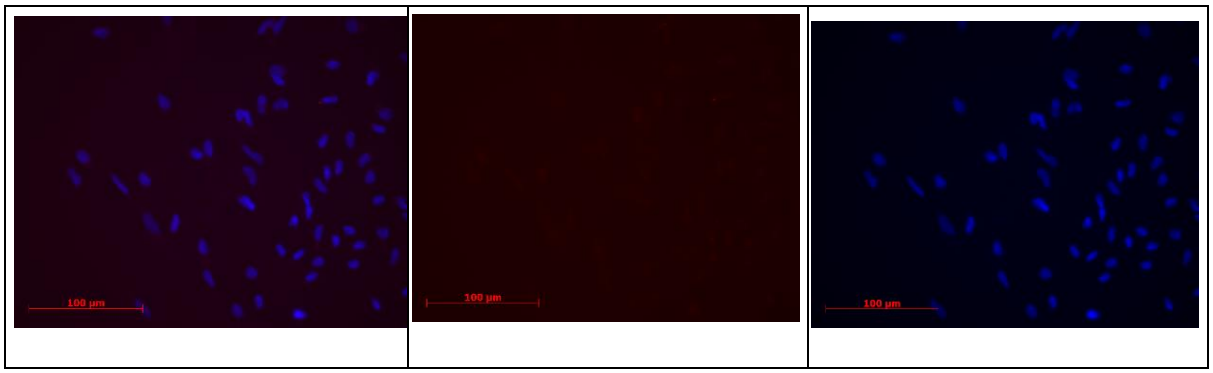

MJD8.5 - Nanog Merged, cy3 and DAPI only

Merged **CY3** **Hoechst**

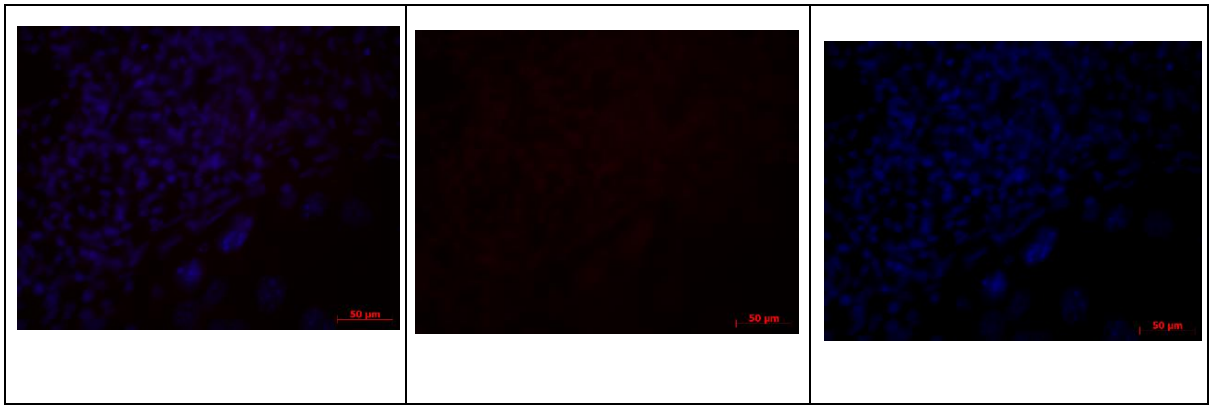

MJD8.5 - OCT Merged, cy3 and DAPI only

Merged **CY3** **Hoechst**

MJD8.5 TRA 1-160 Merged, 488 and DAPI only

Merged **Alexa 488** **Hoechst**

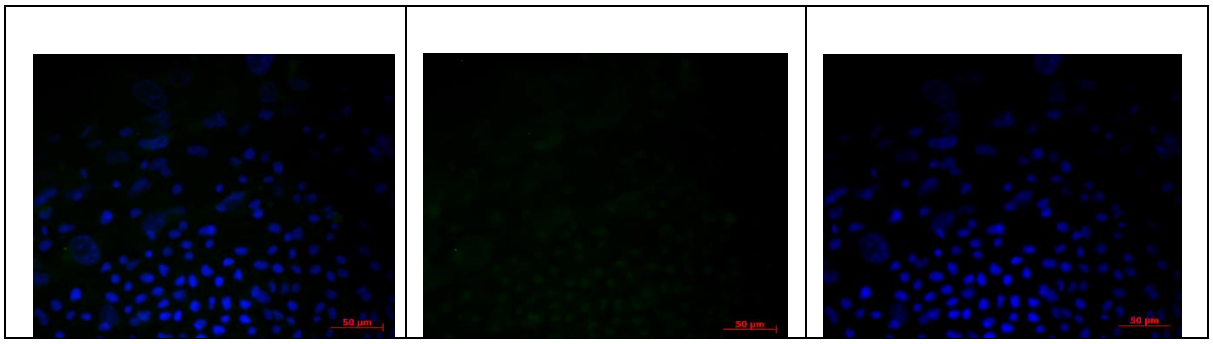

MJD8.5 Mesoderm Merged, 488 and DAPI only

Merged	Alexa 488	Hoechst

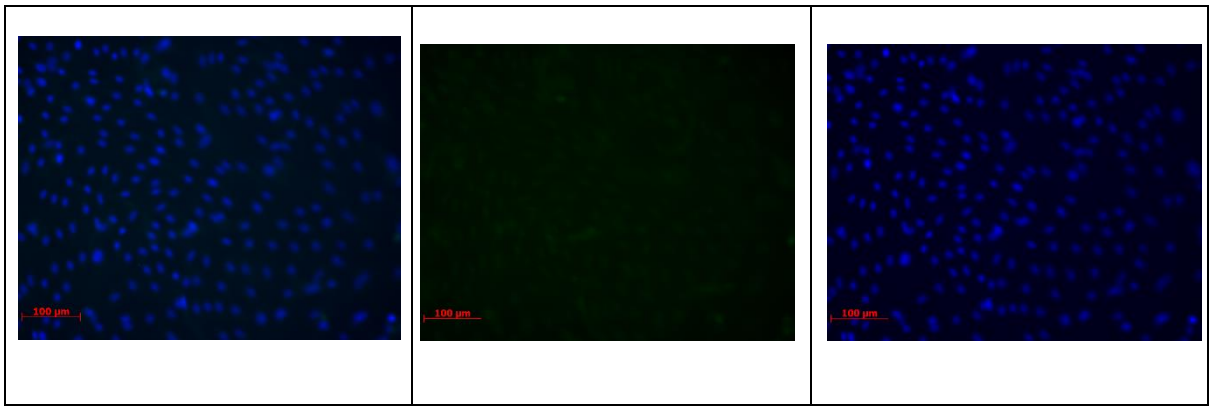

MJD8.5 Ectoderm Merged, 488 and DAPI only

Merged	Alexa 488	Hoechst

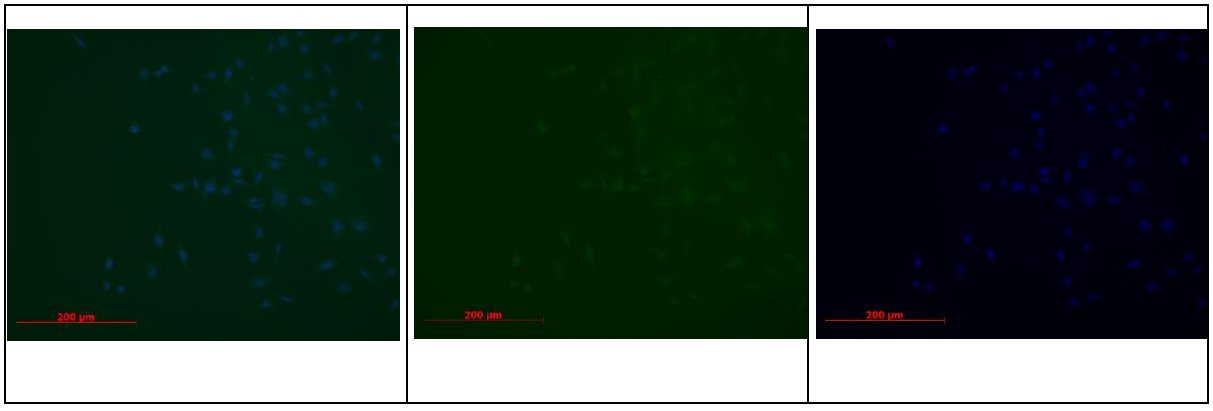

MDC3.4 Tra 1-160 Control Merged, 488 and DAPI only

Merged	CY3	Hoechst
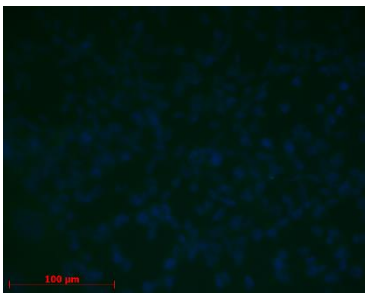	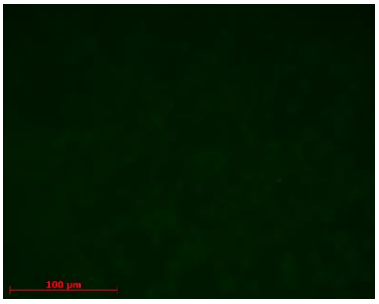	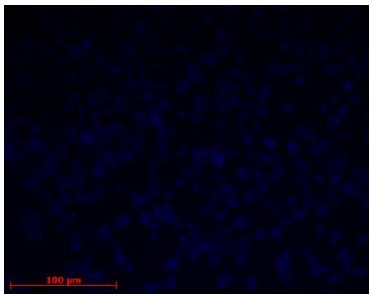

Ct Values

Primer set 1 COL2A1 Band size 122bp

Lane 1: M

Lane 2: CT1,5 ipsc +RT (Old Primer set 1) = ***C_t20,5996***
Lane3: CT1,5 imsc +RT (Old Primer set 1) = ***C_t16.233***

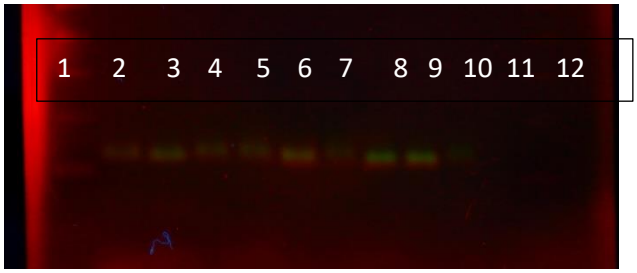

Lane 4: CT1,5 ipsc +RT = ***C_t21,38248***

Lane 5: CT1,5 ipsc -RT= ***C_t 34,45431***

Lane 6: CT1,5 imsc +RT = ***C_t 20,78873***

Lane 7: CT1,5 imsc -RT = ***C_t 36,66483***

Lane 8: CT1,5 imsc +RT DMEM_2 = ***C_t22,365***

Lane 9: MJDC2 FIBS +RT = ***C_t 18,70059***

Lame 10: MJDC2-RT = ***C_t 35,84846***

Lane 11: NTC COL2A1 = ***C_t Undetermined***

Lane 12: M

Lane 1: Marker

Lane 2:MJD5,3 iPSC p6ff + RT (Old Primer set 1) = ***C_t*** 21,38601

Lane 3: MJD5,3 Ipsc p10ff + RT (Old Primer set 1) = ***C_t 14.4045***

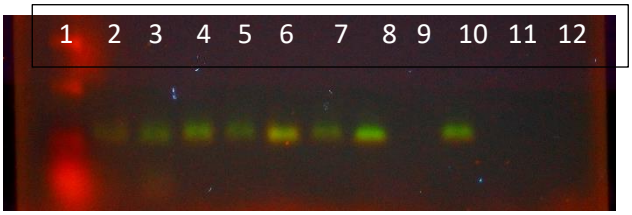

Lane 4: MJD5,3 iPSC p6ff + RT ***= C_t 23,93291***

Lane 5:MJD5,3 iPSC – RT ***= C_t 36,34652***

Lane 6: MJD5,3 iMSC +RT ***= C_t 17,84496***

Lane 7: MJD5,3 iMSC -RT ***= C_t 34,43518***

Lane 8: vvk+RT ***= C_t 17,96139***

Lane 9: VVK -RT ***= C_t Undetermined***

Lane 10: 1,2 imsc +RT = ***C_t 31,12673***

Lane 11: 1,2 imsc -RT ***= C_t Undetermined***

Lane 12: NTC ***= C_t Undetermined***

Appendix D – Clinical definitions

Epiphyseal dysplasia: Is a genetic condition that affects the growth plates (epiphyses) of long bones, causing problems with cartilage and bone development.

Polyarticular osteoarthritis: osteoarthritis (OA) that affects five or more joints at the same time.

Symmetrical *protrusio acetabuli*: A condition where the acetabulum (the socket of the hip joint) protrudes into the pelvic cavity

Multiple epiphyseal dysplasia: is a genetic disorder affecting bone growth, particularly at the ends of long bones (epiphyses), causing joint pain, potential short stature, and early-onset arthritis.

Femoral dysplasia: is also known as hip dysplasia or developmental dysplasia of the hip. This is a condition where the hip joint, specifically the acetabulum, doesn't develop properly, causing the femoral head to be unstable and potentially dislocate.

Appendix E – Ethics Approval

UNIVERSITY OF CAPE TOWN
Faculty of Health Sciences
Human Research Ethics Committee

Room G50- Old Main Building
Groote Schuur Hospital
Observatory 7925
Telephone [021] 406 6492
Email: hrec-enquiries@uct.ac.za
Website: www.health.uct.ac.za/fhs/research/humanethics/forms

06 October 2020

HREC REF: 618/2020

Dr R Ballo
Division of Human Biology
Cellular, Nutritional & Physiological Sciences
Anatomy Building-FHS
Email: Robea.Ballo@uct.ac.za
Student: Thulisa.Mkatazo@uct.ac.za

Dear Dr Ballo

PROJECT TITLE: MODELLING THE EARLY DEVELOPMENT OF CARTILAGE AND BONE IN MSELENI JOINT DISEASE USING INDUCED PLURIPOTENT STEM CELLS-MSC CANDIDATE-MS THULISA MKATAZO SUB-STUDY LINKED TO 822/2015

Thank you for submitting your study to the Faculty of Health Sciences Human Research Ethics Committee (HREC) for review.

It is a pleasure to inform you that the HREC has **formally approved** the above-mentioned study.

This approval is subject to strict adherence to the HREC recommendations regarding research involving human participants during COVID -19, dated 17 March 2020 & 06 July 2020.

Approval is granted for one year until the 30 October 2021.

Please submit a progress form, using the standardised Annual Report Form if the study continues beyond the approval period. Please submit a Standard Closure form if the study is completed within the approval period.
(Forms can be found on our website: www.health.uct.ac.za/fhs/research/humanethics/forms)

The HREC acknowledge that the student: Ms Thulisa Mkatazo will also be involved in this study.

Please quote the HREC REF in all your correspondence.

Please note that the ongoing ethical conduct of the study remains the responsibility of the principal investigator.

Please note that for all studies approved by the HREC, the principal investigator **must** obtain appropriate institutional approval, where necessary, before the research may occur.

HREC/REF:618/2020sa

Yours sincerely

PROFESSOR M BLOCKMAN
CHAIRPERSON, FHS HUMAN RESEARCH ETHICS COMMITTEE

Federal Wide Assurance Number: FWA00001637.
Institutional Review Board (IRB) number: IRB00001938
NHREC-registration number: REC-210208-007

This serves to confirm that the University of Cape Town Human Research Ethics Committee complies to the Ethics Standards for Clinical Research with a new drug in patients, based on the Medical Research Council (MRC-SA), Food and Drug Administration (FDA-USA), International Council for Harmonisation of Technical Requirements for Pharmaceuticals for Human Use: Good Clinical Practice (ICH GCP), South African Good Clinical Practice Guidelines (DoH 2006), based on the Association of the British Pharmaceutical Industry Guidelines (ABPI), and Declaration of Helsinki (2013) guidelines. The Human Research Ethics Committee granting this approval is in compliance with the ICH Harmonised Tripartite Guidelines E6: Note for Guidance on Good Clinical Practice (CPMP/ICH/135/95) and FDA Code Federal Regulation Part 50, 56 and 312.